Abstract of "Driving Forces for Cell Cluster Shape Evolution and Stability " by Asha Nurse, Ph.D., Brown University, May, 2011.

Observation of self assembly of clusters of cells in three dimensions has raised questions about the forces that drive the changes in shape of the cell clusters and the stability of the clusters formed. Cells that self-assemble into a toroidal cluster about the base of a conical pillar have been experimentally observed to spontaneously climb the conical pillar. In other cases, toroidal clusters do not climb the pillar but, instead, they may undergo localized thinning at one or more cross-sections around the circumference of the cluster. Assuming that cell cluster reorganization is due solely to surface diffusion, a mathematical model based on thermodynamics of an isothermal dissipative system is presented. The model shows that the cluster can reduce its surface area by climbing the conical pillar but at the expense of increasing its gravitational potential energy. As a result, the kinetics of the climb is affected by parameters that influence this energy competition such as the slope of the conical pillar or the surface mobility of the diffusing cells. The development of localized deformations in clusters that do not climb the conical pillar is examined by means of a linear stability analysis wherein a nominally uniform toroidal cluster has its shape perturbed by a periodic perturbation in its minor radius. Analysis reveals that the cluster is stable if the surface energy density is spatially uniform. However, if the surface energy density is allowed to vary from point to point around the circumference of the toroid, unstable configurations may develop. The stability of the cluster is observed to depend on its initial minor radius, the radius of the conical pillar and the wave number of the applied sinusoidal perturbation. A stability analysis of nominally cylindrical bodies which evolve in shape due to surface diffusion was then carried out to understand the role of nonlinearity in the stability criteria in such bodies. This analysis may serve

as a basis for a future study of the stability of toroidal clusters or toroidal shapes beyond the range of linear behavior.

Driving Forces for Cell Cluster Shape Evolution and Stability

by

Asha Nurse

Bachelor of Science, Spelman College, 2005

A dissertation submitted in partial fulfillment of the
requirements for the Degree of Doctor of Philosophy
in the School of Engineering at Brown University

Providence, Rhode Island
May, 2011

This dissertation by Asha Nurse is accepted in its present form by the Division of Engineering as satisfying the dissertation requirement for the degree of Doctor of Philosophy.

Date _____ _____

Professor L. Ben Freund, Advisor

Recommended to the Graduate Council

Date _____ _____

Professor Eric Chason, Reader

Date _____ _____

Professor Allan Bower, Reader

Approved by the Graduate Council

Date _____ _____

Professor Peter Weber
Dean of the Graduate School

Vita

Asha Kianga Nurse was born in Trinidad and Tobago. In 1998, she graduated from St. Augustine Girls' High School where she discovered her love for the sciences. She then taught high school Physics for some time in Trinidad while deciding where to continue her education. Her decision to attend Spelman College in Atlanta, GA was invaluable as she was introduced to scientific research. She also became a member of Phi Beta Kappa and earned a Bachelor of Science degree in Physics in 2005. Wanting to continue doing scientific research, she then went on to earn her doctorate degree in the Mechanics of Solids program at the School of Engineering at Brown University.

Acknowledgements

I am indebted to my thesis advisor, Professor L. Ben Freund who has been very supportive through out my time here at Brown University. He is truly an inspiration and a role model and I am honored to have had the opportunity to learn from him how to be both an independent researcher and a balanced individual. I would also like to express my gratitude to the faculty and staff at the School of Engineering and specifically to my committee members Professor Allan Bower and Professor Eric Chason for investing time into my academic career.

I am also grateful to my experimental collaborators Professor Jeffrey Morgan and Jacquelyn Youssef for allowing me to share in their phenomenal scientific journey. To my peers at Brown University both past and present, I thank you for allowing me to learn from you and to thoroughly enjoy my time here.

Finally, to my unfailing support system my mother Stephanie Ferguson, my husband Kavan Clifford and the rest of the Nurse and Clifford family, I am eternally grateful.

Contents

List of Tables

List of Figures

Chapter 1

Introduction

Living systems are an organized, functional ensemble of cells and tissues. Much of the early experimental biology has focused on understanding the factors that influence the spatial reorganization of cells into tissues. A large extent of the experimental work on tissue reorganization involved observation of two dimensional cell cultures. However, the study of cell cultures in three dimensions is relevant as it more closely mimics the environment in living organisms. The advancement of experimental biology to observe three dimensional cell populations, has revealed that cell cultures in three dimensions exhibit more complex behavior than their two dimensional counterparts.

For example, a population of cells observed to self-assemble into a toroidal cluster about the base of a conical pillar exhibits phenomenal behavior. Post self assembly, some toroidal clusters are observed to develop local deformations at various points along its circumference while other clusters are observed to spontaneously climb the conical pillar. These observations were made by Dean et al (2007) while investigating whether three dimensional self assembly could be directed to create structures more complex in shape than that of a sphere. The spherical shape is the three dimensional configuration that has the minimal surface area among all surfaces enclosing a given volume. Based on previous theories, it is the predicted shape for self-assembled

cell clusters with no external forces acting on them. The question posed by these experimental observations is what drives the reorganization of cells in the cluster resulting in the aforementioned observations.

These phenomena provide a basis for a mathematical model aimed at better understanding the factors that drive reorganization of three dimensional cell clusters. Cell cluster reorganization is an important part of processes in developmental biology, tissue engineering, regenerative medicine and cancer biology, to name a few. Along with cell differentiation and multiplication, cluster reorganization accounts for the development of tissue, organs and other features of animal anatomy. Also a main engineering design aspect of tissue engineering and regenerative medicine is tissue growth in three dimensions. Concisely, for these fields the ability to manipulate populations of cells is desired. As a result, it is necessary to understand the driving forces behind cell cluster reorganization.

The behavior of the toroidal clusters post aggregation suggests that the clusters are attempting to reduce their surface to medium interface. The spontaneity of both the climbing process and the development of local deformations indicates that these processes do reduce the free energy of the clusters.

To address the experimental observations, a mathematical model of the climb of the toroidal cluster is first developed. The model proposes that the cluster climbs the conical pillar in order to decrease its surface area and that the upward motion is resisted only by gravity. The free energy of the cluster therefore comprises of a contribution from these two concepts. The proposed process of surface diffusion, by which cells in the cluster reorganize, is however dissipative. The evolution of the morphology of the cluster is then governed by the power balance between the rate of change of the free energy and the energy dissipated.

The development of localized deformations along the circumference of toroidal

clusters that do not climb the conical pillar is viewed to be a result of the unstable growth of surface fluctuations. Small surface fluctuations are present in even the apparently smoothest of surfaces. These fluctuations have been shown to grow, if by doing so the overall free energy of the body is reduced. Therefore, a linear stability analysis of a uniform toroidal shape constrained from contracting its major radius is conducted. The procedure utilizes the effect of an applied perturbation on the change in free energy of the body as it changes from the uniform toroidal configuration of the cluster to determine stability.

To simplify our analysis, the surface properties of the cell cluster, specifically the surface energy density and the surface mobility coefficient, are postulated to be isotropic. The toroidal clusters are taken to have a circular cross section and are also assumed to be initially axisymmetric with respect to the vertical axis. These assumptions are maintained throughout the evolution of the clusters. The formulations of the model are based on the conjecture that cells on the surface of the cluster are loosely bound and can diffuse along the surface. While the occurrence of bulk diffusion within the clusters is acknowledged, the rate of surface diffusion is assumed to be much faster rendering material transport by the process of bulk diffusion to be negligible.

Our goal is to show that surface area reduction is a factor that influences cell cluster reorganization in three dimensions. Clusters with complex geometries wish to reduce their surface areas and would do so once there is an energetically feasible pathway. While others have proposed that clusters of cells evolve so as to reduce their surface area, we also suggest a physical basis of the surface energy density of a cell cluster based on cell to cell adhesions. Both procedures developed here are geometric in nature and can easily translate to other geometries for which the surface area and volume can be determined.

In Chapter 2, relevant historical context is reviewed providing the necessary background for the principles used in the models. The model for the climb of the toroidal cluster up the conical pillar is then outlined in Chapter 3 and the linear stability analysis of the toroidal cluster is presented in Chapter 4. Chapter 5 deals with general issues in linear and non linear stability theory of surfaces of revolution by finding numerical solutions of a classic governing equation for surface diffusion driven shape evolution. The final chapter summarizes the major findings of this body of work and discusses the impact of these results.

Chapter 2

Background to the Study

2.1 Cell Cluster Reorganization

2.1.1 Self-Assembly

Self-assembly is a fundamental process that generates organized structures both in living and in inanimate systems and occurs across many length scales. Processes involving self-assembly are generally fascinating as they create ordered structures out of disordered pre-existing components. The biological process of self-assembly of cells plays an important role in developmental biology such as in morphogenesis and embryology. Much of the early experimental biological studies of self-assembly involved embryonic tissue.

The experimental study of embryonic tissue by Holtfreter (1939) framed the modern analysis of morphogenesis by highlighting the importance of the directed movement of cells. His early experiments revealed that in- vitro amphibian embryonic tissue would round out to form a smooth interface. Taking advantage of an earlier discovery that tissue can be dissociated into a suspension of its constituent cells, he

then began studying self-assembly at the cellular level. Along with his graduate student he discovered that these dissociated cells when placed in suspension both sort out and reassemble in terms of cell type (Townes and Holtfreter 1955).

There have been varied modeling approaches to understanding how cells spatially reorganize themselves within an aggregate; however, three views have dominated the field in the past couple decades. The first, from Turing (1952), suggests that the main features of morphogenesis can be explained by the reaction and diffusion of chemicals, termed morphogens, through a tissue . The Turing reaction diffusion theory proposes that spatial patterning observed in nature is predetermined by the chemical prepattern created by these morphogens. However, the existence of morphogens has not yet been established.

The approach of Oster-Murray differs from the Turing reaction diffusion theory in that pattern formation does not precede morphogenesis but rather both processes act in concert. The mechanochemical models of Oster-Murray (2003), as the name suggests, includes the role of mechanical forces in morphogenesis by including the interactions between each cell and the surrounding extracellular matrix, ECM. Results are obtained by solving a system of coupled nonlinear partial differential equations.

While the two previous models are fundamentally continuum approaches to morphogenesis, Steinberg introduced a discrete, cellular model called the Differential Adhesion Hypothesis, DAH. Noting the similarities between the behavior of dissociated cells and immiscible liquids, the DAH is based on thermodynamics of adhesion. Accordingly, cells reorganize so as to replace weaker cellular adhesions with stronger ones such that cell to cell bonding is maximized and adhesive free energy is reduced (Steinberg 1962). Cell to cell adhesion is energetically favorable due to the lower cohesive energy of a cell-cell interface compared to the adhesive energy of a cell-medium interface (Steinberg 1996). Therefore, when cells in a homotypic suspension

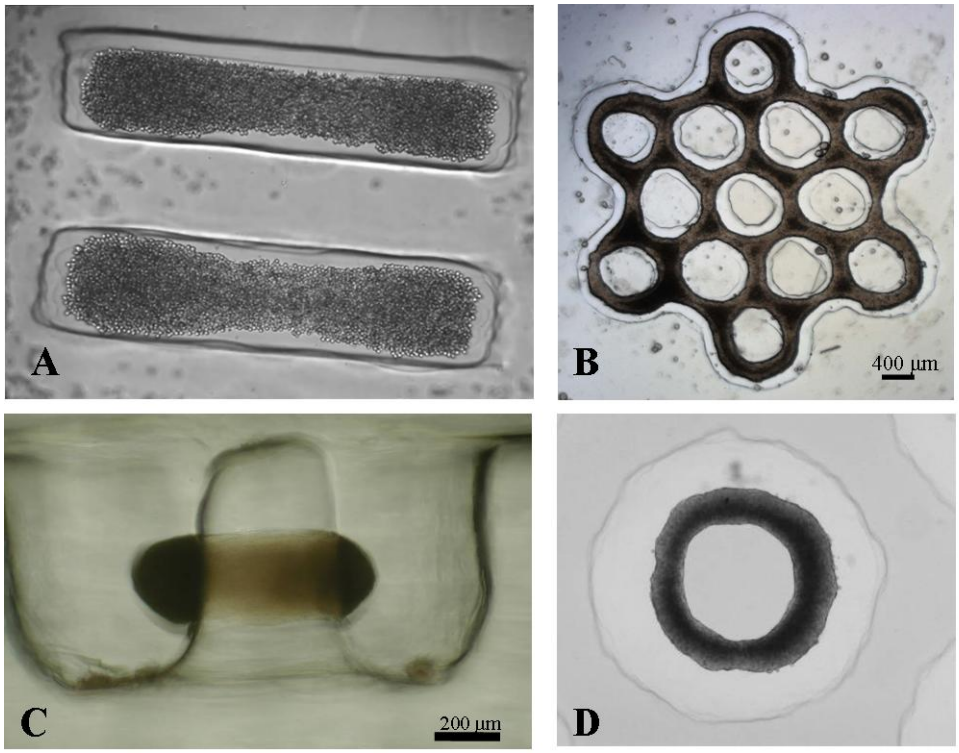

Figure 2.1: Images of the complex three dimensional self-assembled structures formed by (Dean *et al.* 2007). **A** shows the the top view of two rod-like clusters. **B** shows the top view of a honeycomb shaped cluster formed about a series of cylindrical pillars, **C** and **D** show the top and side view respectively of the toroidal cluster formed about a conical pillar.

come into contact, in the absence of external influences, they preferentially adhere to each other resulting in the formation of a spherical aggregate. This adhesion energy difference also explains the formation of the dense self-assembled aggregate, that is, one in which medium has been forced out. The DAH is a widely accepted model and has been successfully implemented in computational methods to show self-assembly and sorting such as the cellular Potts model by Glazier and Graner (1993).

According to the DAH, in the absence of other effects a three dimensional cell suspension would self-assemble into a spherical shape. However, stable non-spherical

shapes have been observed to form in self-assembly experiments in three dimensions (Dean *et al.* 2007). Using novel self designed and fabricated experimental chambers, stable capsular, honeycomb shaped and toroidal clusters can be formed and are shown in Figure 2.1. The experiments involving the toroidal clusters seen in Figures 2.1C-D are of great interest not only because of its geometry but also because of the phenomenal behavior exhibited by these clusters.

2.1.2 Phenomenal behavior of toroidal clusters

The toroidal self-assembled clusters shown in Figures 2.1C-D are of particular interest as they may go on to spontaneously roll up the conical pillar around which it had just self-assembled. In Figure 2.1C, the smooth surface of the self-assembled toroidal cluster in the process of climbing the pillar is captured. This phenomenon, of a self-assembled cluster of cells actively doing work against the force of gravity, brings to question the forces driving this motion.

The simple geometry of the experimental chamber provides a suitable starting point for a model which investigates the source of the mechanical influences that drives configurational changes in the cell cluster. From the rotational symmetry of the chamber, the boundary conditions on the cluster are known with minimal uncertainty. The ascent of the cluster is resisted only by gravity, a well characterized external force whose effects can be modulated by varying the slope of the pillar. As there are no other applied forces, morphological changes in the cluster are thought to be driven only by interactions among the constituent cells.

The DAH has also proposed that clusters of cells evolve in order to reduce their surface area. There has been, however, a lack of biophysical characterizations of the configurational driving force that induces cell cluster reorganization. For this model, a natural origin for the surface energy per unit area of the cell cluster is proposed

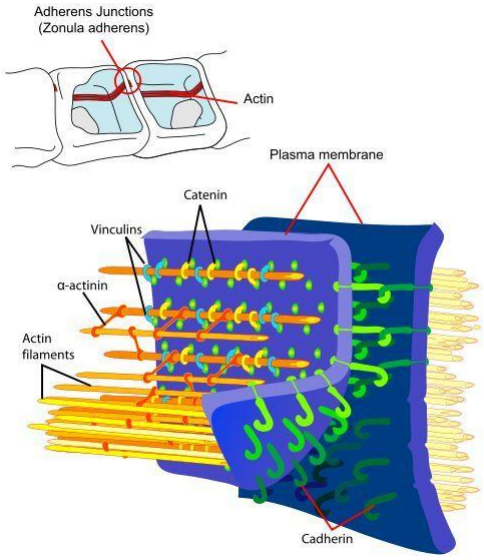

Figure 2.2: An illustration of the adherens junction in epithelial cells showing how the transmembrane proteins, the intracellular anchor proteins and cytoskeletal actin filaments work to interconnect the adhering cells. Image courtesy of Mariana Ruiz

that results from intercellular adhesions.

2.1.3 Cell to Cell Adhesions and Force Generation

When cells come into contact with each other, functional cell junctions are formed that are characterized according to their purpose. There are tight or occluding junctions mainly formed by epithelial cells that form an impermeable barrier between connected cells. There are communicating junctions for cell to cell signaling and interaction. Then, there are the anchoring junctions which are of particular interest as they function to mechanically attach cells and their cytoskeletons either to other cells or to the extracellular matrix.

Anchoring junctions can be further differentiated depending on which cellular cytoskeletal filament is involved in the cell to cell attachment. Of the sub-groups of anchoring junctions, the focus will be on cell to cell junctions, termed adherens

junctions, that connect the actin filaments of contacting cells to each other.

In adherens junctions, cell to cell adhesion on the molecular level begins with the transmembrane adhesion proteins called cadherins, that homotypically bind to the cadherins on an adjacent cell. As illustrated in Figure 2.2the cadherins also attach to the cytoskeletal actin filaments within each cell through intracellular anchor proteins namely α-catenin, β-catenin, vinculin, plakoglobin and α-actinin.

An experimental study by Krendel et al (1999) shows that the spatial organization of the adherens junctions in cultured fibroblast cells differs from that of the more studied cultured epithelial cells. Adherens junctions are aligned perpendicular to the surfaces of the contacting fibroblast cells and are connected to bundles of straight actin filaments. However, adherens junctions in epithelial cells are tangential to the cell to cell boundaries and attach to circumferential actin bundles, known as the adhesion belt, as it encircles each of the connected cells (Alberts *et al.* 2002). Immunofluorescence and confocal imaging have been used to identify the clusters of proteins at intercellular contacts in fibroblasts to be cadherins, β-catenin and connexin -43 which are also recruited into the cytoskeletal network. This confirms that the adherens junctions in fibroblasts also do involve the cytoskeleton (Ko *et al.* 2000).

The attachment of the actin cytoskeletons of the connected cells, at the site of the adherens junction, not only mechanically attaches the cells but also immobilizes the connected cells. Adherens Junctions are cellular structures visible by electron microscopy and are characteristics of mature cell to cell contact. With fibroblasts, these structures begin to form after about fifteen minutes of contact and can continue growing for up to another three hours (Ko *et al.* 2000). In the meantime there is putative non-junctional contact in which the plasma membranes of adjacent cells come close together, on the order of tens of nanometers, allowing interaction between the transmembrane proteins. However, the cells do not become anchored by their

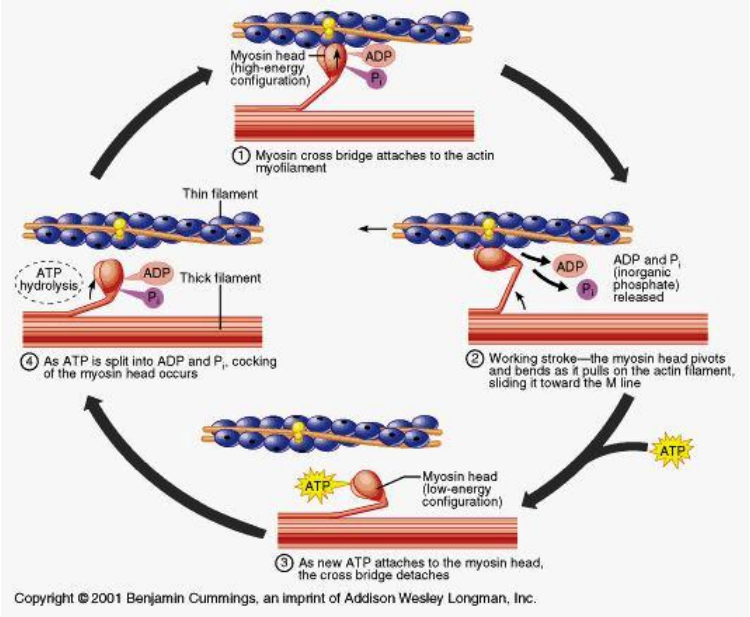

Figure 2.3: Cartoon showing the main components of the actin-myosin cycle and its mechanochemical relationship with the ATP cycle

cytoskeletons and as such retain their mobility. Using electonmicrography, Ko et al (2000) have observed the expansion of cell to cell non junctional contacts into larger junctional plaques in fibroblast cells. The maturation of non junctional contacts has been hypothesized to be due to the diffusion of transmembrane adhesion proteins to the adhesion site causing the enlargement and subsequent stability of the cell junction (Alberts *et al.* 2002).

These mechanical attachments form contractile structures that allow the connected body of cells to provide a mechanical force. The force generation in this mechanical attachment is generated through the relationship of the actin filaments of the cytoskeleton with the motor protein myosin. Lymn and Taylor (1971) linked the rowing motion of the myosin motor proteins to the chemical process of hydrolysis of the phosphorylated nucleotide adenosine triphosphate, ATP.

According to Alberts et al (2002), ATP, which cells both make and consume

repeatedly, is a carrier of free energy for the cell. ATP is also a convenient store of energy within a cell and can be thought of as a cellular potential energy. Within the cell, ATP is synthesized via an energetically unfavorable chemical reaction

$$ADP + P_i \ (inorganic\ phosphate) \underset{\text{Fuel for other cellular processes}}{\overset{\text{Energy Input required}}{\rightleftharpoons}} ATP + H_2O \qquad (2.1)$$

in which a phosphate group is added to the nucleotide adenosine diphosphate, ADP. Conversely, hydrolysis of the phosphate group of ATP is a spontaneous, energy releasing reaction. As a result, ATP hydrolysis is generally coupled with and used to drive other unfavorable cellular processes.

The crystal structure of myosin shows that it comprises of a head or core site where it binds the nucleotide and the actin filament. There is also a converter and lever arm region that rotate relative to the core (Alberts *et al.* 2002). Movement of the myosin motor protein is driven by ATP dependent conformational changes which affects the affinity of the myosin for the actin filament. Each mechanochemical cycle of ATP hydrolysis, as shown in Figure 2.3, produces a power stroke which generates mechanical forces through the cell and its cellular network and propels the myosin protein a single step along the actin filament.

The cycle, begins with the ADP-Pi state in which the myosin core binds weakly to the actin filament causing the release of the phosphate. This release tightens the binding of the core to the actin filament and triggers the rotation of the lever arm forward relative to the core. This is known as the power stroke and is the force generating step of the cycle. During the course of the power stroke, the ADP dissociates from the core. The myosin core lacking a bound nucleotide is firmly attached to the actin filament. However, ATP soon binds to the core and immediately changes the conformation of the domains at the actin binding site of the core reducing the affinity of the myosin for the filament. The core of the motor protein disengages

from the filament allowing the lever arm to be cocked. Hydrolysis of ATP occurs and along with the release of energy, there is a large shape change that displaces the head to a new location along the filament. The protein is now in the ADP-Pi state and the cycle quickly begins again ((Alberts *et al.* 2002), (Vale and Milligan 2000)).

The formation of these contractile structures utilizes ATP and as such lowers the free energy of the connected cells. This concept provides the natural basis for the surface energy of a cluster of cells.

2.1.4 Free Energy and Dissipation

The reorganization of living cells in a self-assembled cluster is a dynamic process as the constituent cells both consume and dissipate energy throughout. The model of the phenomenon exhibited by the toroidal cluster assumes that the most loosely bound cells at the surface of the cluster are mobile and free to diffuse to new locations along the surface with an accompanying surface flux in a direction such that the surface area of the cluster is reduced. The net result is movement up the conical pillar which, however, comes at a cost of increasing the gravitational potential energy of the cluster.

The cluster spontaneously climbs the conical pillar which implies that the process diminishes the free energy of the cluster. However, the proposed process of surface diffusion is a dissipative one. As a result, the rate at which the free energy of the system is reduced depends on the rate at which the energy can be dissipated away from the system according to the power balance

$$\dot{\mathcal{F}}(t) + \mathcal{D}(t) = 0. \tag{2.2}$$

While this expression is useful to determine the configuration of the surface at any given time during the evolution of the cluster, it may not provide the surface configuration that reduces the surface area at that time. The minimal surface configuration

as a function of time is obtained by using calculus of variations.

A variational principle is a mathematical statement used in calculus of variations to seek the extremum of functionals. Many physical principles can be expressed as variational principles. Variational principles are generally stated in an integral form and, therefore, physical principles are sometimes easier to understand in this form. For some physical systems in which the interactions are nontrivial, the variational approach becomes the only method to obtain physically sensible governing equations (Berdichevsky 2009). Once a physical principle can be expressed as a variational principle, all the tools of calculus of variations are available to investigate its behavior.

While formulating a variational approach to surface evolution for a given surface shape, Freund and Suresh (2003) developed a functional of the surface flux field of a diffusing species $\Phi[\boldsymbol{j}]$. Assume that $\boldsymbol{j}$ is the surface flux that minimizes $\Phi[\boldsymbol{j}]$ such that any variation of $\boldsymbol{j}$ leads to an increase in Φ. As $\boldsymbol{j}$ is an element of admissible functions $\mathcal{C}$, then $(\boldsymbol{j} + \epsilon\boldsymbol{j}^*) \in \mathcal{C}$ if ϵ is a scalar and $\boldsymbol{j}^*$ is a continuous surface flux that satisfies the necessary applied boundary conditions (Reddy 2002). Since $\boldsymbol{j}$ is the minimizing flux

$$\Phi[\boldsymbol{j} + \epsilon\boldsymbol{j}^*] \geq \Phi[\boldsymbol{j}], \quad \forall j^* \in \mathcal{C}. \tag{2.3}$$

Stated another way, the surface shape is minimal when $\epsilon = 0$ regardless of the choice of $\boldsymbol{j}^*$ in $\boldsymbol{j} + \epsilon\boldsymbol{j}^*$. Therefore, for the surface shape to be minimum it is necessary that

$$\frac{d}{d\epsilon}\Phi[\boldsymbol{j} + \epsilon\boldsymbol{j}^*]\Big|_{\epsilon=0} = 0 \tag{2.4}$$

The first variation $\delta\Phi$ of the disturbed surface shape $\Phi[\boldsymbol{j} + \epsilon\boldsymbol{j}^*]$ is first order in ϵ. Therefore, (2.4) further leads to the condition that the first variation must vanish that is $\delta\Phi = 0$ for any admissible trial function $\boldsymbol{j}^*$ (Fried 1979).

Freund and Suresh (2003) then implement the extremum principle by using the functional $\Phi[\boldsymbol{j}]$ to analyze the evolution of a surface undergoing a second order perturbation. Each term of the extremum principle was able to be expressed as a function of the amplitudes $a_k(t)$ and their rates $\dot{a}_k(t)$. Differential equations for $a_k(t)$ were then obtained by imposing that the optimal choice of the mode amplitudes maximizes the functional such that

$$\frac{\partial \Phi}{\partial \dot{a}_k}[a_1, a_2] = 0, \quad k = 1, 2. \tag{2.5}$$

The power balance (2.2) that governs the shape evolution of the cluster is the first variation of a functional. Assuming that the functional can be expressed in terms of one or more uncoupled parameters that affect the evolution of the surface, it can be formulated into a similar extremum principle. The configuration of the toroidal cluster at a given time will then be determined by seeking admissible surfaces that minimize the power balance functional.

A mathematical model of the process giving rise to the phenomenal climb of the cluster is presented in Chapter 3. The premise of the model is that the cell cluster climbs the conical pillar to decrease its surface area at the expense of increasing its gravitational potential energy. The power balance (2.2) governs the evolution of the cluster where $\mathcal{F}(t)$ is comprised of both a surface energy and a gravitational potential energy term. A variational approach similar to that of Freund and Suresh will be adopted to determine the morphology of the toroidal cluster. If the hypothesis is valid, it is expected that with time the surface that reduces the extremum principle also corresponds to that of a cluster moving up the conical pillar.

Experimental verification of the results of the model is challenged by the lack of known material properties of the cell cluster, particularly its isotropic surface energy density and the surface mobility coefficient of the cells on the surface. Therefore, instead of seeking an exact match up to the experimental results, the focus in on

capturing the observed trends. The model does, however, allow for the input of the values of these material properties. But presently, the number of unknown properties are either minimized or eliminated through the implementation of nondimensional parameters. The lack of reliable values for these properties is a relevant issue to this field and as such attempts are made to utilize the model to extract these properties.

2.2 Stability of Axisymmetric Bodies

From the results of Dean et al (2007), it is noted that not all of the toroidal clusters spontaneously climb the conical pillar around which it has self-assembled. Some clusters have been observed to remain at the base of the toroidal chamber throughout the duration of the experiment. These clusters may then be observed to undergo local deformations and necking at one or more points along the circumference of the cluster. This behavior while not as dynamic as the climb of the cluster up the conical pillar is relevant to the hypothesis that the reduction of surface area drives reorganization in clusters of cells. The development of deformations may be an alternative process through which the toroidal clusters seek to reduce their surface area. Therefore, the behavior of the surfaces of clusters that remain at the base of the conical pillar will also be analyzed.

2.2.1 Plateau-Rayleigh Type Instability

The deformation behavior exhibited by these clusters is reminiscent of the classic Plateau-Rayleigh instability of cylindrical jets of fluid. Plateau (1873) published his study on the immersion of drops of oil into water whose density is adjusted by the addition of alcohol. Using a spatula, these drops were then formed into cylinders where he noticed that a cylinder became unstable once its length to diameter ratio

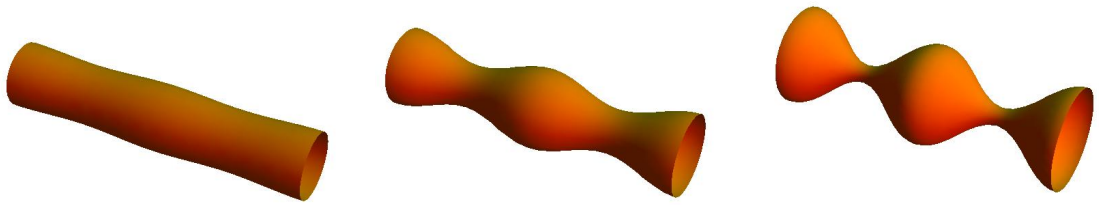

Figure 2.4: An applied axisymmetric sinusoidal perturbation in the radius of the uniform cylinder causes the body to become unstable

was in the range 3.13 to 3.18.

Rayleigh (1878) then conducted a theoretical assessment of cylindrical fluid jets that are bound by surface tension. It was assumed that the Reynolds number of the cylindrical jet is sufficiently high such that the viscosity of the fluid is negligible. Then, he considered the evolution of a cylindrical fluid body to which an infinitesimally small longitudinal perturbation is applied. The continuity equation was linearized to give the resulting conditions for the unstable modes of the cylindrical body of fluid. His analysis revealed that once the length of the cylindrical stream exceeds its circumference, the stream would be unstable.

Nichols and Mullins (1965) then conducted a numerical study of the morphological changes of surfaces of revolution due to capillarity induced surface diffusion. Using a convergent finite difference scheme to solve the governing partial differential equations, they show that phenomena similar to that observed by Plateau can develop in solid bodies. For a cylindrical body with an initial radius r_0 and assuming that both the surface energy density and the surface diffusion coefficient are isotropic, their study shows that similar to the famous Rayleigh result the lateral surface of the cylindrical body becomes unstable once

$$\lambda > 2\pi r_0. \tag{2.6}$$

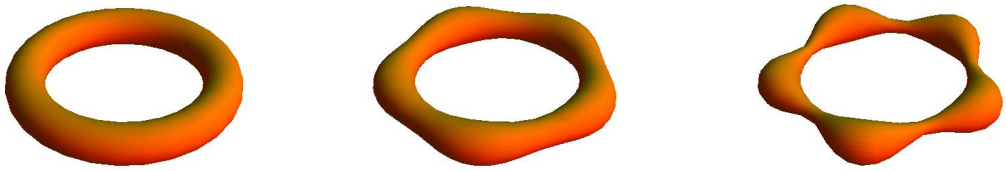

Figure 2.5: An axisymmetric sinusoidal perturbation with wavenumber of 5 is applied to the minor radius of a toroidal body body causing it to become unstable

where λ is the wavelength of the axisymmetric sinusoidal perturbation in the radius of the cylindrical body. They also suggest that the development of an instability can lead to a degeneration of the cylindrical surface into a series of spherical bodies that minimize the surface area while preserving the initial volume of the cylindrical body.

Coleman, Falk and Moakher (1995) also implemented a theoretical analysis of the stability of infinitely long axisymmetric cylindrical bodies considering both infinitesimally small amplitude and finite amplitude longitudinal perturbations. They utilize the finite element method to obtain solutions to the equations that govern the evolution of the bodies. Their numerical solutions show that the Plateau-Rayleigh stability criteria is valid only for small amplitude perturbations. Applied perturbations of finite amplitude are shown to exhibit an initial rapid decay followed by a longer dormant period after which the perturbations begin to grow in amplitude (Coleman *et al.* 1996).

Rings of fluids have also been observed to form in nature such as with the impinging of a droplet onto a superhydrophobic surface, the vortex rings created by dolphins and the fall of droplets into an immiscible fluid ((Renardy *et al.* 2003), (Marten *et al.* 1996), (Baumann *et al.* 1992)). These toroidal shapes, like the cylindrical bodies, may also become unstable and degenerate into spherical droplets. However, these bodies are not as well studied as their cylindrical counterparts due to the experimental difficulties in generating well controlled toroidal shapes.

Recently, Pairam and Fernández-Neives (2009) have developed a novel procedure to generate toroidal fluid droplets by injecting a liquid into a rotating bath containing a viscous fluid. As they can control the ratio of the major radius a of the toroids to its minor radius, they conduct a systematic study of the break up of several toroidal droplets of varying geometries to gauge the dependence of stability on this aspect ratio. They report that only wavelengths which are integer fractions of the length of the torus $2\pi a$ can induce its break up. The number of break up points in the torus n is given by

$$2\pi a = n\lambda \tag{2.7}$$

where λ is the wavelength associated with the mode that induces the breakup.

McGraw et al (2010) have also conducted experiments on the stability of toroidal shapes using solid nano-scale polystyrene toroids. A glassy polystyrene toroid is created from a droplet of solid polystyrene dissolved in toulene that falls from a small needle unto a substrate covered with methanol bath. Spincoating is immediately done to remove the majority of the fluid from the solution, resulting in a solid polystrene toroid left on the substrate. They too are able to control the major and minor radii of the toroids formed and have also investigated the stability of the toroids with respect to its geometry. They too cite the Plateau-Rayleigh instability for the eventual break up of the toroidal body.

For both the solid and liquid toroids, the authors also report a shrinking of the toroidal body towards its center. This is especially observed with sufficiently fat tori. McGraw et al (2010) report that this may be an additional route by which the toroidal shapes reduce its free energy. However, for the toroidal clusters, that do not climb the conical pillar, shrinking toward the center is not allowed due to the presence of the rigid conical pillar.

2.2.2 Shape Evolution due to Surface Diffusion

The evolution processes described in the previous section share some core similarities. Throughout the evolution of both the cylindrical and the toroidal bodies, the volume is conserved while the surface area is being diminished. For the analytical studies, the bodies under consideration are axisymmetric and are assumed to remain as such throughout the evolution process. The surface energy of the body is also assumed to be isotropic and only smoothly curved surfaces are considered. For both the experiments and the analytical models, the only physical driving forces stem from the properties of the surface.

Mullins, in his study of surface grooves at grain boundaries of a heated polycrystal, pioneered a field of study dedicated to surface motion due to surface diffusion. He showed that the flux of material along the surface is proportional to the surface gradient of the chemical potential along the surface (Mullins 1957). Earlier studies were conducted by Herring on the contribution of surface tension to the sintering of powder particles below their melting temperature (Herring 1951). While determining the effect of interfacial energies at triple junctions of grain boundaries, Herring (1953) related the local chemical potential field to the principal curvatures of the surface. The findings of Herring and Mullins have been combined to form a single equation that governs the evolution of surfaces due to the spatial variation of the mean curvature. This equation was implemented in the theoretical study of the stability of surfaces of revolution conducted by Nichols and Mullins (1965).

From a local equilibrium point of view, the observed evolution of the cylindrical and toroidal bodies is a result of variations in the chemical potential over the surface. No matter how smooth the surface of a body appears, perturbations are always present which subsequently affect the local surface curvature. According to Baluffi, Allen and Carter (2005), the diffusion potentials of material at the surface is proportional to

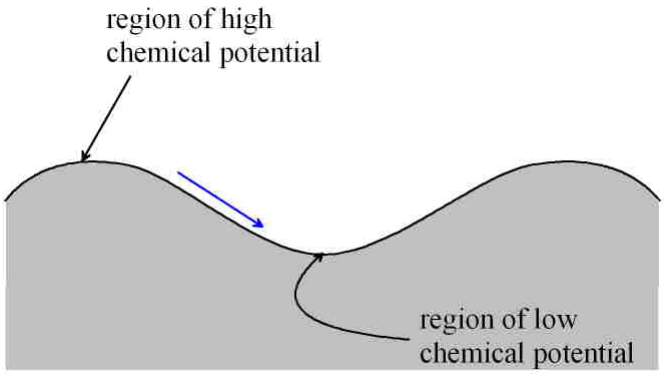

Figure 2.6: A depiction of the surface profile of a section of a perturbed cylindrical surface, S' showing regions of high and low chemical potential. The blue arrow shows the direction of mass transport due to surface diffusion along the surface.

the local curvature of the surface. Therefore, just below a region where the surface is convex, the diffusion potential of the cells is higher than in a region where the surface is concave. As a result of these spatial variations in the diffusion potentials along the surface, there is a net diffusion along the surface from regions of higher surface chemical potential to regions with lower chemical potential as shown in Figure 2.6.

The spatial gradient of the surface chemical potential serves as the driving force for the morphology of the body. In response to this driving force, several processes may act to transport material, apart from surface diffusion, such as volume diffusion, evaporation and condensation. Due to the nature of the subjects being analyzed, the processes of evaporation and condensation can be eliminated as contributing to the material transport process. Also, if the dimensions of the body are small, as is the case with the toroidal clusters, the ratio of surface area of the cluster to its bulk volume is substantial and the effects of surface diffusion can be pronounced. Therefore, while bulk diffusion may still be occurring, it is negligible as surface diffusion proceeds at a much faster rate.

Notedly, Vilenkin and Brokman (1997) have stated that diffusion along the surface

cannot effectively change the shape of the surface unless surface particles are captured or released from a bulk site. However, Cahn and Taylor (1994) have shown that the Herring-Mullins transport equation is an extreme case of a generalized governing equation that includes both surface and bulk diffusion. The Herring-Mullins equation is applicable for situations in which it is easy to incorporate surface particles into the bulk of the material or to detach particles and put them into the surface layer. This ease is considered relative to the rate of at which particles move around in the surface layer and is therefore representative of pure surface diffusion.

In a recent review of his work, Mullins (2001) states that the mass transport equation holds only if there is a local thermodynamic equilibrium. In a sentiment similar to that of Cahn and Taylor, Mullins writes that the assumption of local equilibrium breaks down if the emission of mobile surface particles at sources or the adsorption of particles at sinks requires a driving force comparable to that required by surface diffusion.

2.2.3 Stability Analysis of Axisymmetric Bodies

In a theoretical model of surface stability, the aforementioned ubiquitous perturbations on the surface of a body can be represented as a series of sinusoidal components. As evidenced by the results of the models of stability experiments, the growth or decay of each perturbation component, along with its rate of change, depends on its wavenumber and the initial geometry of the body.

If the only driving force for the evolution of a body is the reduction of its surface area, it should eventually assume the minimum surface area configuration as an equilibrium configuration. Accordingly, from a thermodynamic perspective, the body should evolve into a single sphere. However, experimental results show that such a body evolves into a series of spherical sub-particles. This unpredicted outcome is

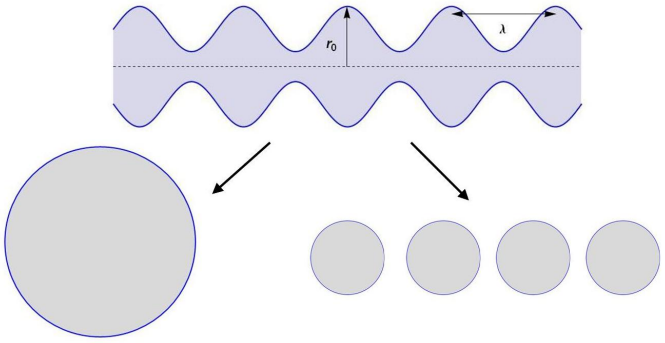

Figure 2.7: A perturbed cylindrical body should evolve into a sphere which is the minimal surface area configuration instead it evolves into a series of discrete spherical particles

explained by the kinetics of the morphology of the body. It takes a much shorter time for a body to evolve into a series of spherical particles than for it to evolve into one large sphere. Furthermore, once the body has progressed into sub-particles, the transport process stops, preventing the system from attaining the global, minimum surface energy configuration.

The study of the stability of an equilibrium configuration, begins with the consideration of another state near the equilibrium state in consideration. This is accomplished in the form of a perturbation. The goal is then to determine whether the perturbed state, in time, will tend toward the equilibrium state. If this occurs, then the equilibrium state is said to be stable. The classic formulation of stability problems is that of an initial value problem. In this respect, stability of an equilibrium state can be determined by the deviation of the amplitude of the perturbation from its starting value. If the amplitude of the perturbation tends to zero from its initial value, then the equilibrium state is said to be stable. However, if the amplitude of the perturbation increases from its initial value, then the equilibrium state being probed is deemed unstable.

While the initial value of a perturbation can be freely chosen, the selection should

be based on the physical system under consideration, if one exists. Therefore, the nature and intensity of the applied perturbations should reflect the unavoidable fluctuations present in the experimental apparatus (Eckhaus 1965). Admittedly, it is impossible to account for all the possible fluctuations that may occur during an experiment as perturbations may be introduced on a continuous or intermittent basis.

Eckhaus (1965) conducted a mathematical study of stability theory on the use of periodic and aperiodic applied perturbations and the effect on the solutions obtained. In summary, for proper formulation of stability problems, aperiodic perturbations must be applied. Periodic initial value problems allow only for periodic solutions, severely limiting the arbitrariness of the formulation. Considering the case of a weak instability, he shows that in the linear theory the amplitude of the applied perturbations grow when the wavenumber is in some interval. This is in agreement with the works of Nichols and Mullins, Plateau and Rayleigh. He then shows that in the non-linear theory, the wavenumbers that fall within the interval of instability remain bounded and tend to a harmonic solution in the limit $t \to \infty$. This mathematical analysis is in agreement with the results of Coleman, Falk and Moakher (1996).

Traditional linear stability analysis involves the use of a single harmonic perturbing function that has an infinitesimally small amplitude. The small amplitudes of the perturbations justifies the linearization of the governing transport equations generally done in linear stability theory. However, if one were to consider all of the possible sinusoidal components of a perturbation and each is given the same initial small amplitude, then the component that grows fastest eventually dominates the evolution of the body. Therefore, the consideration of a single harmonic perturbing function for a linear analysis is warranted once as the dominating mode is generally considered. Furthermore, for linear analysis, superposition of solutions is valid. Therefore, solutions for multiple wavelengths are simply additive.

Due to the simplifications implemented in linear stability analysis, the results obtained are only valid for short times and cannot be used to predict the evolution of the perturbed shape. This is especially pertinent for studying instabilities. As the amplitude of the perturbation grows, the assumption of small amplitude and the subsequent linearization of the governing equations for the morphology of the body are no longer valid. Despite the simplifications, as demonstrated by Plateau and Rayleigh and by Nichols and Mullins, linear stability theory has had considerable success in defining critical condition for perturbation growth that have been experimentally verified. But, the study by Coleman, Falk and Moakher reinforces that the results of a linear stability analysis is only valid for very short times.

Nonlinear stability problems arise when perturbations can no longer be assumed to have infinitesimal amplitudes. As such, in a theoretical study of nonlinear stability analysis the applied perturbation is commonly multiple, finite amplitude, periodic functions. In accord with the works of Eckhaus, a multi-harmonic perturbing function is used to simulate aperiodicity (Choy *et al.* 1995). The results of a nonlinear stability analysis give a more reliable determination of the long term behavior of the perturbed shape.

2.2.4 Implementation

Given, the experimentally observed deformations of clusters that do not climb the conical peg, a stability analysis of a toroidal shape is conducted using a novel approach. The free energy function of a toroidal cluster that does not climb the conical pillar has only a surface energy component. If the surface energy density of the cluster is constant, reduction of its surface area is equivalent to reduction of the free energy of the cluster. If the surface energy density is a function of position along the surface, then reduction of the free energy then becomes equivalent to reduction

of the surface energy of the cluster. As noted by Carter and Glaeser (1987), in their thermodynamic analysis of the morphological stability of continuous intergranular phases, perturbations that reduce the free energy of the body increase in amplitude without thermodynamic barrier in amplitude.

The relationship between the free energy, the surface energy of a cluster and the growth or decay of the perturbation can be utilized to determine the effect of small amplitude perturbations on the stability of the cluster. Such a linear stability theory rationalizes how the toroidal cluster leaves from its uniform equilibrium configuration.

The equilibrium shape being considered is that of a uniform toroidal cluster. Analysis begins with the application of an infinitesimally small amplitude periodic perturbing function. If the surface energy density is constant over the surface of the cluster, stability is instead ascertained by observing the effect of the perturbation on the surface area of the cluster. If the perturbation causes the surface area of the cluster to increase from its initial value, then the perturbation decays and the uniform toroidal configuration is a stable equilibrium state. However, if the perturbation decreases the surface area from its initial value, the perturbation spontaneously grows in amplitude as the uniform toroidal cluster is not a local equilibrium state.

However, if the surface energy density is a function of position over the surface, stability is set by observing the effect of the perturbation on the surface energy term of the cluster. Similar to the previous concept, if the perturbation causes the surface energy of the body to increase from the uniform configuration value, then the perturbation decays and the uniform toroidal configuration is stable. This rationale is implemented in Chapter 4 to determine the critical parameters that define stable and unstable configurations of the toroidal clusters. The aim is to establish some linear stability criteria for the stability of the toroidal clusters based on its geometry and the dimensions of the constricting conical pillar. These stability criteria can then

later be experimentally verified.

For a scenario with constant surface energy density, the stability criteria can be experimentally verified as the dimensions of the cluster are recorded throughout its shape evolution. Therefore, the changes in the surface area and the volume of the cluster are known with a relative degree of certainty. However, for a scenario in which the surface energy density is a function of position, experimental verification becomes difficult at best.

In Chapter 5 the Herring-Mullins equations will be solved to observe the evolution of a perturbed cylindrical body for both a linear and nonlinear analysis. For the linear analysis, a small amplitude single harmonic perturbing function is applied to a uniform cylindrical surface. The governing equations are linearized and an analytical solution obtained. For the nonlinear analysis, following the rationale of Eckhaus, multi-harmonic finite amplitude functions are implemented as the initial cylindrical surface. The governing partial differential equations will be solved numerically and a function will be fit to the solution in order to visualize the solution at various times. Coleman, Falk and Moakher (1996) solve the Herring-Mullins governing equation to obtain the evolution of the axisymmetric cylindrical body using a space-time finite element method. Our method of solving the governing equations is more robust than the finite element approximation method. As such, their reported initial and boundary conditions will be implemented into our numerical scheme and the numerical solutions to the governing equations obtained will be compared.

Chapter 3

The Model

Studies aimed at understanding the processes that control the formation of spatial patterns of living cells during anatomical development have been ongoing for decades. Shape evolution, termed morphogenesis, along with cell proliferation and cell differentiation are fundamental in the development of tissues, organs and other features of organisms. The processes involved in morphogenesis rely on still obscure chemical or electrical signaling mechanisms and mechanical influences, or an interplay of all of these, that account for the reorganization of clusters of cells.

Experimental work in the laboratory of Professor Jeffrey Morgan at Brown University shows that dissociated cells, in three dimensions, can self-assemble into a variety of shapes depending on the constraints and external forces imposed. Stable aggregates in capsule, toroid and even honeycomb shapes were formed (Dean *et al.* 2007). In this context, the process of self-assembly refers to the organization of existing components into a larger structure and is distinct from formation by limiting the process to be reversible and to involve only pre existing components (Whitesides and Grzybowski 2002). For the present case, the existing components are the dissociated cells and the larger structures formed will be referred to as either aggregates

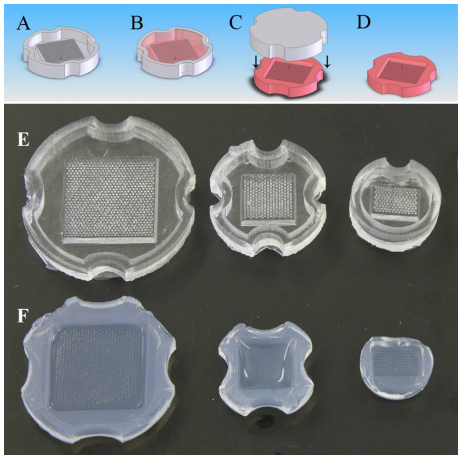

Figure 3.1: Figures **A** − **D** illustrate the making of wax molds. Figure **E** wax molds with decreasing amounts of experimental chambers from left to right. The resulting block of experimental chambers are shown in **F**

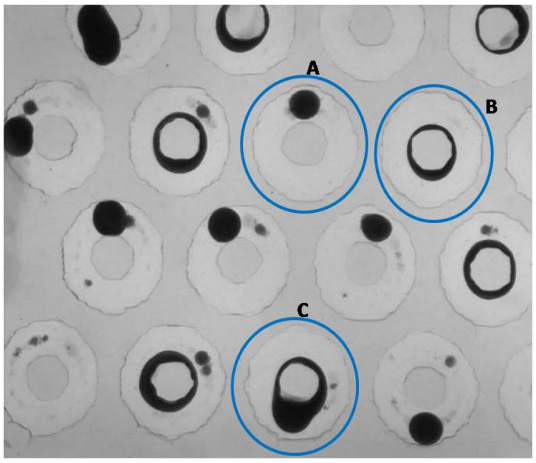

Figure 3.2: Magnified overhead view of experimental chambers in which the toroidal clusters are formed. Clusters are seen to display varied behavior

or clusters. Self-assembly mimics natural biological processes such as embryogenesis, morphogenesis and tumor formation. Therefore, the drive to understand the mechanisms of self-assembly is evident.

Mainly, it is the precise nature of the forces driving the reorganization of the cells in a cluster that remains obscure. The adhesion of the surface molecules may be strong enough or it may be that the cytoskeleton has the major role in the process of the cluster formation and evolution. In an attempt to gain clearer understanding of the origin and magnitude of the forces that drive the morphology of a cell cluster, Professor Morgan and his students have conducted a series of experiments in which cell suspensions are placed into experimental chambers designed for the purpose. The cells contact each other and self-assemble into micro-tissue structures that are observed over time in the presence of an applied force, usually gravity. Rather than evolving into the minimum surface area configuration, the behavior of the clusters was found to be more complex.

The role of mathematical modeling in studying such a process should not be simply descriptive but should attempt to provide a plausible explanation for the occurrence of the phenomena. Therefore, the aim here is not to find a mathematical expression that fits the experimental data. Rather, using physical laws, a simplified representation that captures the essential features of the phenomenon is presented. Arguably, when dealing with living matter such as cells, there is added complexity regarding the uncertainty of which natural laws are pertinent. Therefore, a key element to modeling is to start simple. Analysis of the results of the model reveals whether the parameters included are adequate and may also determine their importance. Unimportant details can be excluded and finer details or secondary phenomena can be taken into account as necessary. The eventual result is a refined model which is not yet complete until it can accurately predict an outcome of an experiment which was not used in developing its features. Hence it is also useful to develop the model in terms of measurable quantities to allow for the very important interplay between model and experiment. If done correctly, models will suggest experiments and in turn experiments will guide model building. This, according to Murray (2003), proves to be a more efficient research tool than either one working alone.

3.1 Experimental Background

The published manuscript by Dean et al (2007) contains the full details of the three dimensional self-assembly experiments. Here details are provided for only the aspects of the experiments on the toroidal clusters that are relevant to this work. As shown in Figure 3.1, submillimeter experimental chambers are made by setting gels into wax molds. The shape of the mold is specified in a computer aided design program, and then produced by rapid prototyping. Polyacrylamide gel is used to create the mold because its non-adhesive properties suppresses the interaction between the cells and

the experimental chambers. After the gels are removed from the wax molds, they are transferred to a culture plate, rinsed with fresh culture medium and then equilibrated with the medium overnight. The chambers are then rinsed with fresh medium and the cell suspension is added.

The vertically oriented experimental chambers of interest to us are cylindrical in shape and have conical pillars extending upward from their bases. The slope of the conical pillar is 65° from the horizontal. The diameter of the chamber is 1400μm and the diameter of the conical pillar at its base is 650μm. The base of each chamber was also filleted with a radius of 200μm. For clarity, dimensions are shown in Figure 3.3.

Two cell types are used in the self-assembly experiments, normal human fibroblasts, NHFs, and rat hepatoma cells, H35s. The H35s are a rodent cell line derived from liver tumors and, as such, it is a cancerous cell line. It may have been an original intention of the experimentalists to compare the self-assembly behavior of a cancerous cell line to a healthy cell line. The NHFs are derived from neonatal foreskins. Fibroblasts, being members of the connective-tissue family, are responsible for secretion of ECM. However, over the time interval within which the experiments are conducted, ECM production is negligible.

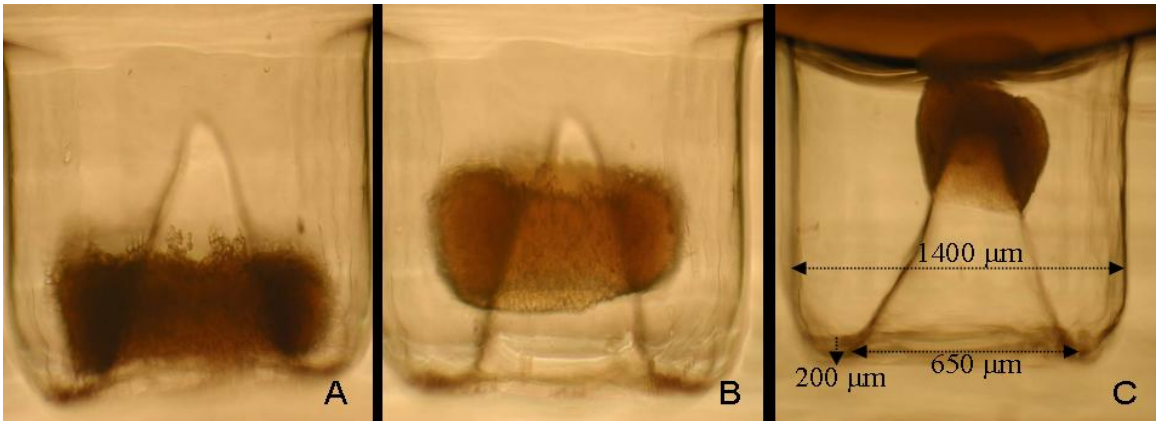

Figure 3.3: Side view images of the experimental chambers showing the toroidal cluster at various stages of climb

A 70μL volume of cell suspension of a single cell type is introduced into each cylindrical chamber. The cells, being slightly more dense than the solvent, gradually settle in the annular region at the bottom of each chamber. Here, the cells almost immediately begin to self-assemble. If a sufficient number of cells is introduced into each chamber, a compact toroidal cluster is formed at the base of the conical pillar.

The cells, having formed a compact toroid at the base of the chamber as shown in Figure 3.3A, have then been observed to climb the conical pillar at varying rates. Some clusters make it to the top of the pillar, where they go on to form a near spherical shape as shown in Figure 3.3C. These clusters may then roll down the pillar to form a more compact spherical shape to one side of the base of the chamber as shown in Figure 3.2A. Other clusters, at least within the duration of the experiment, appear to stall in their ascent along the pillar.

The time lapse images of the toroids, such as those shown in Figure 3.3, are acquired by a microscope modified to lie horizontally and further equipped with a camera. Side view images of the experimental chambers are obtained with the use of a right angled prism used to reflect the images into the lens of the camera. Image analysis to determine the changes in morphology of the cell clusters is done using the public domain image processing and analysis software ImageJ (Rasband 1997–2010). Cell toxicity testing was also done to ensure that the cells in the cluster are viable; cells sometimes observed at the base of the chamber that are not part of the cluster, as seen in Figure 3.3B, are not alive.

3.2 The Model

In this section a mathematical model is described that captures the observed features of the self-assembly experiments. The model presumes that cells in the cluster are reorganizing through surface diffusion in such a way that the shape of

the evolving cluster is continuously reducing its surface area while keeping its volume constant. Surface diffusion refers to movement of the most loosely bound cells on the surface of the cluster. For simplification, it is assumed that throughout the evolution of the cluster its azimuthal cross-section is always circular and that its shape is axially symmetric with respect to the vertical axis of the conical pillar.

Principal geometric features of the model are represented by the diagram in Figure 3.4. The conical pillar extending upward from the base of the chamber is represented by a right circular cone with α being the slope with respect to the horizontal plane. The toroidal cluster of cells initially has its center of mass at a vertical distance $z(0)$ below the apex of the cone, with an initial major radius $a(0)$ and initial minor radius $b(0)$ characterizing its shape. It has been shown that, throughout the experiments, changes in the volume of the cluster are not statistically significant (Youssef *et al.* 2010). Consequently, the volume is assumed to remain constant at the value

$$v_0 = 2\pi^2 a(0)b(0)^2 = 2\pi^2 a(t)b(t)^2. \tag{3.1}$$

The total surface area of the cluster $S(t)$ can then be expressed in terms of the minor radius $b(t)$ by

$$S(t) = 4\pi^2 a(t)b(t) = 2v_0/b(t) \tag{3.2}$$

where the major radius $a(t)$ has been eliminated by means of (3.1). Note that, for the surface area $S(t)$ to decrease, $b(t)$ has to increase in magnitude. As the volume is constant, this implies that $a(t)$ decreases in magnitude which corresponds to movement up the conical pillar.

At time t, the distance of the center of mass of the cluster from the apex is

$$\overline{z}(t) = a(t)\tan\alpha - b(t)\sec\alpha. \tag{3.3}$$

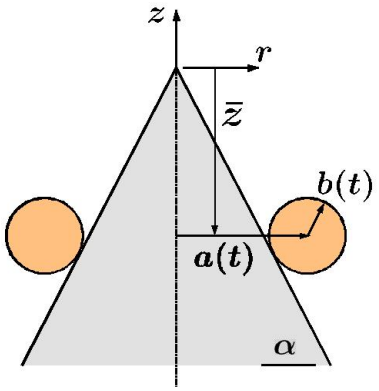

Figure 3.4: Diagram showing physical parameters of the model

Letting ρ denote the mass density of the cells relative to the density of the medium and letting g denote the gravitational acceleration, the gravitational potential energy of the cluster is $-v_0\rho g\bar{z}(t)$. This is one of the contributions to the free energy of this system. The other main contributor is the surface energy of the cluster.

3.2.1 Origin of Surface Energy

The surface energy of the cluster is the free energy increase when the surface area of the cluster is increased by unit area and therefore has units of energy per unit area. Surface energy is a characteristic material property that arises due to the disruption of intermolecular bonds when a free surface is created. It is proposed that the origin of the surface energy is similarly due to the disruption of intercellular bonds within the cluster.

When cells come into contact with each other, functional cell junctions are formed that are characterized according to their purpose. Our focus is on a sub-group of anchoring junctions, termed adherens junctions, that connect the actin filaments of contacting cells to each other. The attachment of the actin cytoskeletons of the connected cells, at the site of the adherens junction, not only mechanically attaches

the cells but also immobilizes the connected cells.

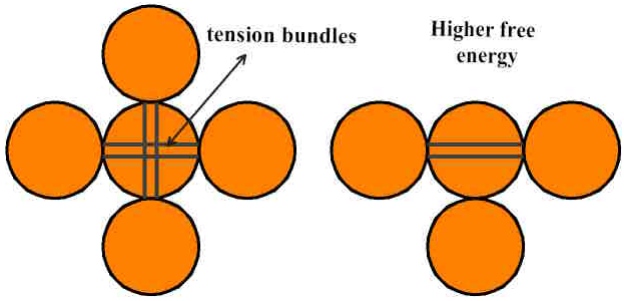

Figure 3.5: An illustration of the origin of surface energy

With the aid of transmembrane adhesion proteins and the intracellular anchor proteins, the cluster becomes a vast network of connected cells. This network can contract through the relationship of the cytoskeletal actin filaments with the motor protein myosin. Myosin is a cytoskeletal motor protein that uses the mechanical changes caused by the hydrolysis of adenosine-5'-triphosphate (ATP) to propel itself along the actin filament. Hence, the hydrolysis of ATP provides the energy for the contraction process.

Presumably, the cells in the cluster have readily accessible chemical energy in the form of ATP. Generation of contraction in these tension bundles within the cells requires hydrolysis of ATP and, as such, utilizes some of this surplus background chemical energy. Therefore by forming these tension bundles the free energy of the interacting cells is lowered. Cells at the surface of clusters are unable to bond with other cells to the same degree as cells embedded in the cluster as illustrated in Figure 3.5. Consequently, cells on the surface of the cluster will have a higher free energy compared to cells within the cluster. This resulting excess free energy is a possible origin of surface energy of the cluster.

Let γ be defined as the excess free energy of cells on the surface of the cluster relative to those cells that are fully embedded within the cluster, measured per unit

area of the surface of the cluster. Then, the net free energy associated with the surface is $\gamma S(t)$ and the system free energy of the cluster is

$$\mathcal{F}(t) = -v_0 \rho g \overline{z}(t) + \gamma 2 v_0 / b(t). \tag{3.4}$$

From a thermodynamic perspective, it is known that a system will spontaneously seek to reduce its free energy. Therefore, it is hypothesized that the cells on the surface of the cluster reorganize themselves to configurations with lower surface area. The tendency to lower surface energy, and consequently system free energy, results in a configurational force on the toroidal cluster that pulls the cluster up the conical pillar. It is assumed that this rearrangement of cells on the surface of the cluster is a result of surface diffusion only and the local flux of material along the surface is given by the surface flux $\boldsymbol{j}$. From a continuum perspective, when considering configurational changes due to continuous surface diffusion, the flux is a measure of the volume flow rate of material per unit surface distance perpendicular to the flux. The flux is therefore a vector tangent to the surface and has physical dimensions of volume per unit length per unit time. Due to the toroidal shape of the cluster, $\boldsymbol{j}$ is most readily found by using the fundamental concepts of Riemannian geometry.

3.2.2 Riemannian Geometry

If a two-dimensional surface is described in terms of two curvilinear surface coordinates (u^1, u^2), a parametric representation of the two dimensional surface in three dimensional space is given by the vector

$$\boldsymbol{r}(u^1, u^2) = x(u^1, u^2)\, \boldsymbol{e}_x + y(u^1, u^2)\, \boldsymbol{e}_y + z(u^1, u^2)\, \boldsymbol{e}_z. \tag{3.5}$$

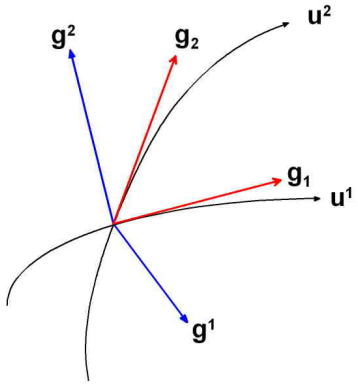

Figure 3.6: Diagram showing the covariant (red) and reciprocal (blue) base vectors to the surface defined by surface coordinates (u^1, u^2)

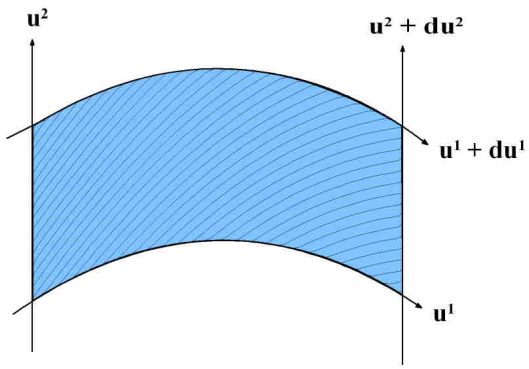

Figure 3.7: Illustration showing area element of the surface bounded by the surface coordinates (u^1, u^2)

The unit vectors $\boldsymbol{e}_x$, $\boldsymbol{e}_y$ and $\boldsymbol{e}_z$ define a fixed Cartesian basis that has its origin at the center of the toroidal cluster, shown in Figure 3.8, and $x = x(u^1, u^2)$, $y = y(u^1, u^2)$ and $z = z(u^1, u^2)$ are the rectangular coordinates of a surface point with curvilinear surface coordinates (u^1, u^2).

At any point on the surface,

$$\boldsymbol{g}_\lambda = \frac{\partial \boldsymbol{r}}{\partial u^\lambda}, \quad \lambda = 1, 2 \tag{3.6}$$

are vectors tangent to the coordinate curves $u^\lambda = \text{constant}$. These vectors, shown in red in Figure 3.6, are the covariant base vectors with their directions being tangent to the grid lines along which the corresponding coordinates vary. The covariant base vectors along with the normal vector to the surface form a local vector basis at any point on the surface. Here the normal vector $\boldsymbol{n}$ is the outward normal to the surface so that a right handed basis is formed. The unit vector normal to the surface is

$$\boldsymbol{n} = \frac{\boldsymbol{g}_1 \times \boldsymbol{g}_2}{|\boldsymbol{g}_1 \times \boldsymbol{g}_2|}. \tag{3.7}$$

Therefore, a surface vector $\boldsymbol{a}$ can be represented as $\boldsymbol{a} = \sum_{1}^{2} a_\lambda \boldsymbol{g}_\lambda + a_{(n)}\boldsymbol{n}$. Alternatively a vector can be represented using the contravariant or reciprocal base vectors $\boldsymbol{g}^\lambda$. While the covariant base vectors are tangent to the coordinate lines, the contravariant base vectors, shown in blue in Figure 3.6, are orthogonal to them. For an orthogonal curvilinear coordinate system, the contravariant or reciprocal base vectors are

$$\boldsymbol{g}^\lambda = \frac{\boldsymbol{g}_\lambda}{|\boldsymbol{g}_\lambda|^2}. \tag{3.8}$$

The normal vector that completes the right handed basis with the reciprocal base vectors is the same normal vector as for the covariant basis.

For a surface described by curvilinear coordinates $\boldsymbol{r}(u^1, u^2)$ such as in equation (3.5), the square of the linear element ds^2 is given by a quadratic form in the differentials of the surface coordinates

$$ds^2 = \left|\frac{\partial \boldsymbol{r}}{\partial u^1}\right|^2 (du^1)^2 + 2\frac{\partial \boldsymbol{r}}{\partial u^1} \cdot \frac{\partial \boldsymbol{r}}{\partial u^2} du^1 du^2 + \left|\frac{\partial \boldsymbol{r}}{\partial u^2}\right|^2 (du^2)^2 \tag{3.9}$$

where the absolute value denotes the length of the vector in Euclidean space. From equation (3.6), the coefficients of the differentials can be written in terms of the covariant base vectors to give

$$ds^2 = (\boldsymbol{g}_1 \cdot \boldsymbol{g}_1)\,(du^1)^2 + 2(\boldsymbol{g}_1 \cdot \boldsymbol{g}_2)\,du^1 du^2 + (\boldsymbol{g}_2 \cdot \boldsymbol{g}_2)\,(du^2)^2. \tag{3.10}$$

Riemann defined the infinitesimal distance ds between adjacent points in n dimensional space, whose coordinates in any system are given by u^i, by the relation

$$ds^2 = G_{ij}\, du^i du^j, \quad (i, j = 1, 2, \ldots, n) \tag{3.11}$$

where the coefficients G_{ij} form what is called the Riemannian metric tensor (Weatherburn 1938). Any space which is characterized by such a metric is termed a Riemannian space and geometry based on a Riemannian metric is known as Riemannian geometry. The metric tensor of the surface allows for computation of the length of paths in the space. As can be seen from equations (3.10) and (3.11), the components of the metric tensor are formed by the covariant base vectors according to

$$G_{\lambda\delta} = \boldsymbol{g}_\lambda \cdot \boldsymbol{g}_\delta = \frac{\partial \boldsymbol{r}}{\partial u^\lambda} \cdot \frac{\partial \boldsymbol{r}}{\partial u^\delta}. \tag{3.12}$$

The area element of a surface is calculated by summing over the differential areas spanned by the covariant base vectors. As shown in Figure 3.7, the area of an element of surface bounded by coordinate curves u^1, $u^1 + du^1$, u^2 and $u^2 + du^2$, is given by

$$dS = \sqrt{\det\left[G_{ij}\right]}\ du^1 du^2 \quad = \sqrt{G_{11}G_{22} - G_{12}^2}\ du^1 du^2 \tag{3.13}$$

where det refers to the determinant of the matrix.

Differential operations on vector fields in Riemannian space are also possible and have the same physical meaning as in Euclidean space. The surface divergence at a point in curvilinear coordinates is still a measure of the spreading out or the convergence of the vector field at that point. For a surface vector field $\boldsymbol{v}$, the surface divergence at a point in the Riemannian manifold is given by

$$\nabla_s \cdot \boldsymbol{v} = \boldsymbol{g}^\lambda \cdot (\partial_\lambda \boldsymbol{v}). \tag{3.14}$$

Some of the basic formulations of Riemannian geometry that are required to understand the model for the climb of the toroidal clusters up the conical pillar are presented here. Subsequent chapters will build on this formalism, introducing other

aspects of Riemannian geometry that are pertinent to this body of work.

3.3 Analysis of the Model

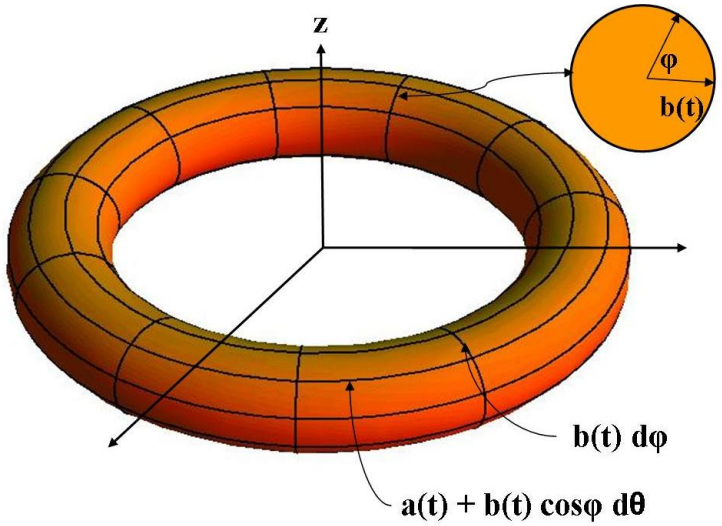

Figure 3.8: Diagram showing the parameters that define the element of surface area of the toroidal cluster

For the points on the surface of a torus, $u^1 \rightarrow \theta$ and $u^2 \rightarrow \phi$. Substituting the parametric equations for x, y and z into (3.5) gives the following surface equation

$$\boldsymbol{r}(\theta,\phi,t) = \Big(a(t)+b(t)\cos\phi\Big)\cos\theta\boldsymbol{e}_x+\Big(a(t)+b(t)\cos\phi\Big)\sin\theta\boldsymbol{e}_y+b(t)\sin\phi\boldsymbol{e}_z \quad (3.15)$$

where the major radius $a(t)$ is always greater than the minor radius $b(t)$. The angle ϕ has a range $-\pi \leq \phi < \pi$ and sweeps out the circular azimuthal cross-section of the torus. The other angle θ has the range $0 \leq \theta < 2\pi$ and gives the angular position of this circular cross-section about the vertical z axis.

As the configuration is axially symmetric, it is assumed that the surface flux is also axially symmetric and therefore has the form $\boldsymbol{j} = f(\phi)\boldsymbol{g}_\phi$. The conservation

equation, in the reference configuration, requires that

$$v_n + \nabla_s \cdot \boldsymbol{j} = 0 \tag{3.16}$$

where v_n is the normal speed of the surface relative to material points currently on the surface. This says that if cells move out of an infinitesimal region on the surface, that is, the divergence of flux in that region is positive, then the number of cells within that region has decreased and the surface retracts in the normal direction. The net rate of material accumulation or depletion determines the surface speed v_n. To determine $f(\phi)$ in terms of the geometric features of the model, the conservation of mass equation is solved for $f(\phi)$ for a given v_n.

As there are no other modes of transport other than surface diffusion, the divergence in (3.16) is the surface divergence. According to equation (3.14), the surface divergence of the surface flux is

$$\nabla_s \cdot \boldsymbol{j} = \boldsymbol{g}^{\lambda} \cdot (\partial_{\lambda} \boldsymbol{j}) = \boldsymbol{g}^{\theta} \cdot (\partial_{\theta} \boldsymbol{j}) + \boldsymbol{g}^{\phi} \cdot (\partial_{\phi} \boldsymbol{j}) \tag{3.17}$$

To find $\boldsymbol{j}$ specific to the cells on the surface of the cluster in the experimental setup, the normal speed specific to the model must be known. Therefore, the position of points on the surface of the torus (3.15) have to be reconfigured to agree with the parameters of the model. The position of surface points on an azimuthal section of the toroidal cluster with respect to the apex of the conical pillar is given by

$$\boldsymbol{r}(\theta, \phi) = \{a(t) + b(t)\cos\phi, \overline{z}(t) + b(t)\sin\phi\}. \tag{3.18}$$

The outward normal speed of the surface is the inner product of the outward normal to the surface and the rate of change of points on the surface, that is $v_n =$

$\boldsymbol{n} \cdot \partial_t \boldsymbol{r}(\theta, \phi)$. The normal speed necessarily has to be zero at the lines of contact between the cluster and the conical pillar. The conservation equation can now be solved for the term $f(\phi)$. The resulting constant of integration represents flow of material around a θ = constant section with no shape change. As this term would contribute to the dissipation but does not affect change in the shape of the torus, it is necessarily set to zero.

The premise of the model is the spontaneous reduction of the free energy of the cluster. The system, being isothermal, has to dissipate the free energy that is lost in the process of evolution. As such, surface diffusion is a dissipative process. If the surface mobility of the diffusing cells is represented by the parameter m_s then the total dissipation at any time t is given by

$$\mathcal{D}(t) = \frac{1}{m_s} \int_{S(t)} \boldsymbol{j} \cdot \boldsymbol{j} \, dS \tag{3.19}$$

where dS is an element of surface area and $S(t)$ is the total surface area. The element of surface area for the torus as dictated by equation (3.13) becomes

$$dS = b(t)\big[a(t) + b(t)\cos\phi\big] \, d\phi \, d\theta. \tag{3.20}$$

The parameter m_s, known as the surface mobility coefficient, represents the mass flow per unit gradient in surface chemical potential (Freund and Suresh 2003). It is a material property that is always positive in value and is based on the random movement of the diffusing species. While m_s is assumed here to be constant, it may depend on temperature, concentration and binding energy of the diffusing species (Dill and Bromberg (2003), Porter and Easterling (2000)).

The integrand of (3.19), the inner product of the surface flux with itself, is a function of $b(t)$, α and ϕ only. Therefore, the dissipation integral can be represented

as

$$\mathcal{D}(t) = \frac{1}{m_s} 2\pi \int_0^{2\pi} f(b(t), \alpha, \phi) b(t) \big(a(t) + b(t) \cos\phi\big)\, d\phi. \tag{3.21}$$

While complicated, the dissipation integral can be evaluated by a change of variables to complex variables. The introduction of the special polar exponential $e^{i\phi} = \cos\phi + i\sin\phi$ allows the complex number z to be expressed in the polar form $z = re^{i\phi}$. Along the unit circle, $r = 1$ and the trigonometric functions $\sin\phi$ and $\cos\phi$ are expressed in terms of the complex variable z by

$$\cos\phi = \frac{1}{2}\left(z + \frac{1}{z}\right), \quad \sin\phi = \frac{1}{2i}\left(z - \frac{1}{z}\right). \tag{3.22}$$

Using these trigonometric expressions, along with $d\phi = \frac{-i}{z} dz$, a change of variables from ϕ to z converts the integral given by (3.21) to the form

$$\mathcal{D}(t) = \frac{-2\pi i}{m_s} \int_0^{2\pi} \frac{F(b(t), \alpha, z)}{z}\, dz. \tag{3.23}$$

The form of the integrand allows evaluation by means of the Cauchy Residue Theorem. Full analysis of the denominator of the integrand in (3.23) reveals that there are two simple poles. Hence the evaluation of the dissipation integral is reduced to finding the residues at these two poles.

Using the constant volume expression (3.1) all system variables can be completely characterized by the single time dependent variable $b(t)$. Energy conservation tells us that the total free energy lost from the system must equal the total energy dissipated from the system. However, this is not very useful in finding the evolution of $b(t)$ that minimizes the surface over time. Thermodynamics of dissipative systems at constant temperatures, as is demonstrated in (Freund and Suresh 2003), indicates that isothermal systems evolve in such a way that the quantity $\mathcal{F}'(t) + \frac{1}{2}\mathcal{D}(t)$ is stationary under variations in the parameters that characterize the rate of change of

configuration. In the present case, there is only one such parameter, namely $b'(t)$. Therefore, a differential equation governing the evolution of $b(t)$ that minimizes the surface is established by the condition that

$$\frac{\partial}{\partial b'(t)}\left[\mathcal{F}'(t)+\frac{1}{2}\mathcal{D}(t)\right]=0. \tag{3.24}$$

The resulting ordinary differential equation is algebraically complicated. Consequently, the equation is integrated numerically utilizing the initial condition $b(0)=b_0$.

It is general practice to present results, whenever possible, in terms of nondimensional quantities. As such, the minor radius $b(t)$ and the time t are normalized with respect to system parameters according to

$$\tau=\frac{m_s\rho g t}{b_0^2},\qquad \beta(\tau)=\frac{b(t)}{b_0}. \tag{3.25}$$

In doing this, two nondimensional ratios have been identified which influence the resulting ordinary differential equation for $\beta(\tau)$. The two ratios

$$\omega=\frac{v_0}{b_0^3},\qquad \kappa=\frac{\gamma}{\rho g b_0^2} \tag{3.26}$$

provide analytic insight into interdependencies between parameters especially, since parameters such as γ and m_s are not easily measured. The first of the ratios, the parameter ω, is a geometrical constant established by the initial configuration of the system. The second ratio κ characterizes the relative influence of the surface energy of the cluster to its gravitational potential energy. This parameter also provides a basis for deductions to be made about γ.

Scrutiny of the details of the ordinary differential equation in (3.24) reveals that

the first term, the rate of change of the free energy, is a function of $\beta(\tau)$ only. Meanwhile the derivative of the dissipation is a function of both $\beta(\tau)$ and $\beta'(\tau)$. Hence, the differential equation can be represented as

$$f(\beta(\tau)) + g(\beta(\tau)) + h(\beta'(\tau)) = 0 \tag{3.27}$$

where $f(\beta(\tau))$, $g(\beta(\tau))$ and $h(\beta'(\tau))$ are complicated algebraic functions. An expression for $\beta'(\tau)$ can be easily isolated. Several quadrature methods can be employed to numerically solve a first order ordinary differential equation such as (3.27). The second order Runge-Kutta method is chosen as it requires no other function to be calculated apart from the expression for $\beta'(\tau)$. Also, no initial starting values are necessary besides $\beta(0)$. The Runge-Kutta method is easy to implement numerically and runs quickly, allowing the use of small time steps over a large time interval. Results of the numerical integration of the differential equation are illustrated in the next section.

3.4 Results and Discussion

To obtain a numerical solution to equation (3.24), values have to be input for various parameters. From experimental data, values for α, b_0 and v_0 are readily obtained. In the process of isolating $\beta'(\tau)$ in (3.27), the ρg terms from the free energy and from the dissipation expressions cancel each other. Because precise values for m_s and γ are not available, these parameters are eliminated from the differential equation by substituting the dimensionless ratios (3.25). From the first of these dimensionless ratios, if τ and t are both set to the same value of one this implies that m_s has an inherent value of $b_0^2/\rho g$.

Figure 3.9 shows the results of the numerical integration of (3.24) for $\beta(\tau)$ at

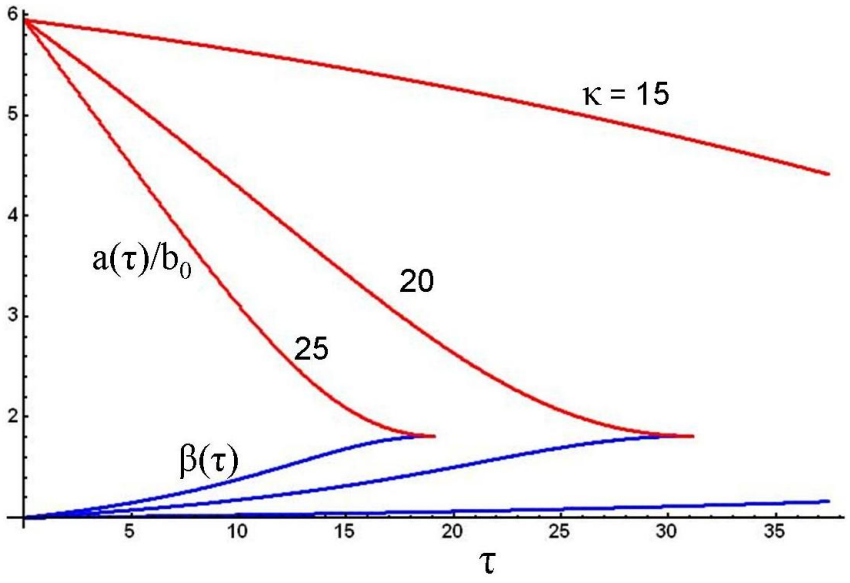

Figure 3.9: Graph showing numerical results of (3.24) at varying values of κ using initial data from NHF cluster experiments

three values of κ for which the cluster tends to climb up the conical pillar. At each time point, using volume conservation, the normalized major radius $a(\tau)/b_0$ is also calculated and this result is depicted by the red curve. As predicted, the minor radius of the cluster increases while its major radius decreases. This is in direct correlation to motion up the conical pillar. Note also from the surface energy equation (3.2) that, as the minor radius increases, the surface area of the cluster decreases, and consequently the surface energy of the cluster decreases. The convergence of the radii to a common point indicates that the cluster has reached the top of the pillar and the 'hole' of the toroidal cluster no longer exists. Similar trends exist for toroidal cluster comrpised of H35 cells. However, comparing Figures 3.9 and 3.10, it is clear that H35 clusters have a slower rate of climb than NHF cell clusters.

From Figures 3.9 and 3.10, it is seen that increasing the value of κ reduces the time the cluster takes to reach the top of the conical pillar. All other things being equal, this means that increasing κ increases the rate of climb of the cluster. This is

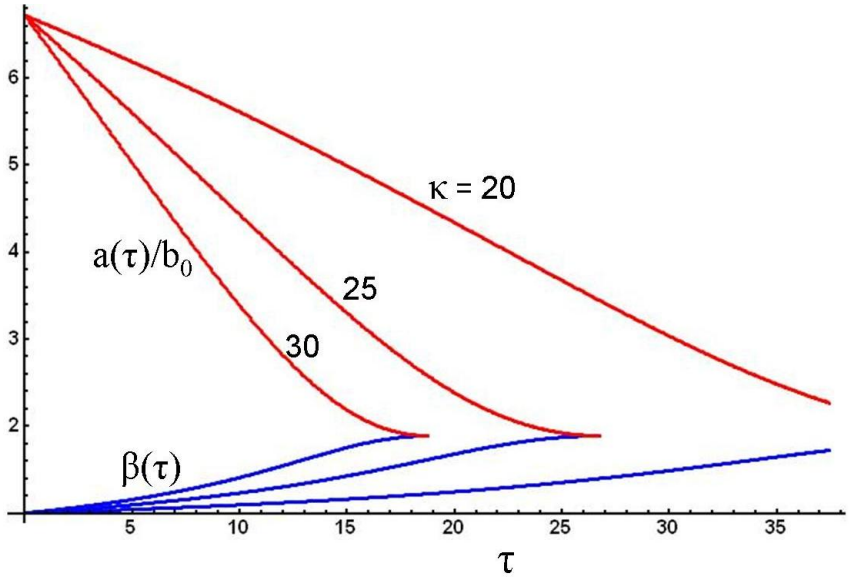

Figure 3.10: Graph showing results for numerical integration of (3.24) at varying values of κ using initial data from H35 cluster experiments

to be expected because for κ to increase, either the influence of the surface energy of the cluster increases or the influence of the gravitational potential decreases. Either of these scenarios results in a larger driving force to move the cluster up the conical pillar. Likewise, reducing the value of κ slows the rate of climb. This proves a likely explanation as to why some clusters do not reach the top of the pillar within the time interval of experimental observation. These clusters have an inherent κ value that results in such a slow rate of climb that they do not make it to the top of the pillar in the duration of the experiment. For a conical pillar with a slope of 65°, the rate of climb of a NHF cluster decreases until $\kappa = 13.93$ and for a H35 cluster until about $\kappa = 15.59$. At these values, an equilibrium is reached in which the tendency to decrease surface area of the cluster is just balanced by resistance to increasing gravitational energy. Clusters having this κ ratio have nothing to gain energetically by climbing the conical pillar and as such will remain at the base of the chamber throughout the experiment.

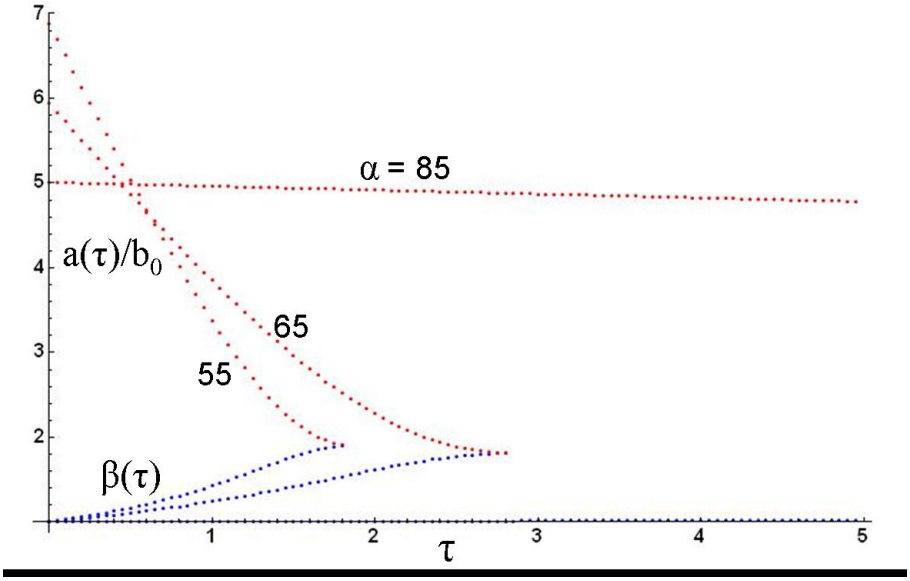

Figure 3.11: Results of ODE (3.24) for κ =100 showing the influence of varying the value of α on the rate of climb of the cluster

The trends observed by varying κ suggest that there should be a similar trend by varying α. As mentioned earlier, the force of gravity can be modulated by changing α. For steeper slopes, that is larger α values, there is a larger resistance from the gravitational potential energy. As such, the rate of climb should decrease as α increases. Chambers with conical pillars of slope 55° and 85° were created and the self-assembly experiments were conducted for both cell types. While the diameter of the chamber remains at 1400 μm, the diameter of the base of the conical pillar varies with its slope. For slopes 55° and 85°, the diameter of the base of the conical pillar is 780 and 600 μm respectively. The base of each chamber was also filleted with a radius of 200 μm. As only physical dimensions have been changed, the numerical scheme to find the minor radius, as previously described, is still applicable.

The numerical result for a NHF cluster with a fixed value of $\kappa = 100$ for different conical pillar slopes is shown in Figure 3.11. Consistent with experimental observations, with all other parameters held constant, the rate of climb of the cluster is

faster on conical pillars that have a lower slope. Similar trends are observed for H35 clusters, but at slower rates of climb in comparison to the rates of the NHF clusters.

For all the results presented so far the value of m_s has been unchanged at $b_0^2/\rho g$. Increasing the value of m_s increases the mobility of the cells on the surface and should increase the rate at which the cluster evolves. The effective value of m_s is altered by varying the input values of τ and t. If the value of the ratio of t to τ is increased to 2, then the value of m_s now becomes $b_0^2/2\rho g$, one half of its previous value. Conversely, a ratio of t to τ of 1/2, doubles the original value of m_s such that $m_s = 2b_0^2/\rho g$. The results of the numerical solution of equation (3.24) for $\kappa = 20$, $\alpha = 55°$ at each of these three values of m_s are shown in Figure 3.12. The results validate that the rate of climb of the cluster is faster at larger values of m_s.

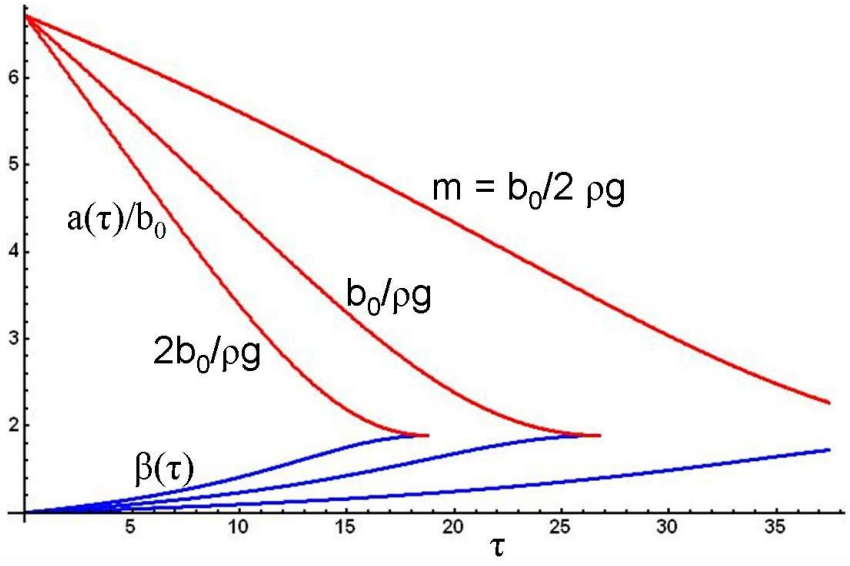

Figure 3.12: Results of (3.24) for $\kappa = 20$, $\alpha = 55°$ at three different values of m_s. The graphs show the effect of increasing the value of m_s on the rate of climb of the cluster.

3.4.1 Extraction of Values for the Surface Energy Density

The equilibrium condition at low κ values provides an opportunity to find an approximate value of surface energy density. At this κ_{eq} value, the decrease in the surface energy of the cluster if it were to climb the pillar just balances its increase in gravitational potential energy $W(t)$ such that it is not energetically favorable for the cluster to climb the conical pillar. Letting the rate of change of a variable with respect to time be represented by a dot over the symbol for the variable,

$$\kappa_{eq} = \frac{\dot{S}(t)}{\dot{W}(t)}. \tag{3.28}$$

This energy balance can be used to calculate γ by substituting the corresponding formulae for $S(t)$ and $W(t)$ and computing the necessary time dependent derivatives. Rearranging the energy balance experienced by the cluster, results in

$$\gamma = \kappa_{eq} \frac{\rho g b_0^2}{2\pi^2} \left(\omega \tan\alpha - 2\pi^2 \sec\alpha\right) \tag{3.29}$$

which can be used to extract a value for γ from κ_{eq}.

However, to obtain a numeric value of γ, the relative density ρ has to be known. As a prerequisite, the density of the cell suspension, ρ_c, for each cell type must be known. To determine ρ_c, a sedimentation experiment was suggested which measures the rate at which individual cells settle under the influence of gravity.

To do this, monodispersed cells are pipetted into the experimental chambers containing medium and side view imaging is done to measure the settling rate. Initially, the cells settle with a given acceleration. However, steady state fall is soon reached and the cells settle at a constant velocity v. Assuming a cell to be spherical in shape

with radius r and volume V, Newton's second law requires

$$V\rho_c\frac{dv}{dt} = V\rho_c g - V\rho_m g - 6\pi\mu v a. \tag{3.30}$$

The terms on the right hand side are the forces acting on a cell as it settles. The first term is the gravitational force acting on a cell. The second represents the upward buoyant force on a cell based on the weight of the displaced medium and the last term is the drag force on a cell based on Stoke's law where μ is the viscosity of medium. As the settling velocity of the cells is constant at steady state fall, the left hand side of equation (3.30) is zero. With the density of the medium ρ_m known to be similar to that of water, results from the sedimentation experiment puts the density of NHF and H35 cells at 1.05 g/cm^3 and 1.08 g/cm^3 respectively.

Revisiting the equilibrium condition that exists for the NHF cluster at $\kappa_{eq} = 13.93$, equation (3.29) gives a resulting γ value of 0.821 mJ/m^2. This calculated value of γ is the surface energy per unit area of the cell clusters. However, this determined value of γ may also apply to the individual cell, if it is assumed that the binding sites on the surface of a cell are evenly spaced and are fixed spatially, meaning that the sites are not allowed to preferentially crowd certain areas of the cell surface. Within these constraints, the surface energy per unit area of the cluster of a given cell type is the same as that for the given cell.

For each different slope of the conical pillar, an equilibrium κ value can be found at which the cluster does not climb the conical pillar. Using the experimental data γ can be determined from (3.29). The surface energy values obtained from experimental chambers with slopes $\alpha = 55°, 65°$ are tabulated and presented in Table 3.1. The γ value for the cluster formed by the cancerous H35 cell line is higher than the γ value of the NHF cluster which may account for its slower rate of climb on the conical pillar. For a given change in configuration, an H35 cluster can greater reduce its surface

Angle	NHF		H35	
α	κ_{eq}	γ	κ_{eq}	γ
55	10.70	0.427	13.26	1.106
65	13.93	0.821	15.59	1.608
average		0.624		1.357

Table 3.1: Values of γ in mJ/m^2 obtained from the equilibrium condition at $\kappa = \kappa_{eq}$ using Eq (3.29)

time	γ (mJ/m^2)	m_s $10^{-14}(m^4hr/g)$
2	0.0580	0.5432
4	0.0638	0.9196
6	0.0667	1.238
8	0.0693	1.386
average	0.06364	1.022

Table 3.2: Values of γ and m_s of NHF clusters determined using Eq (3.38) and experimental data from conical pillars with slopes 55° and 65°.

energy, and consequently its free energy, in comparison to an NHF cluster. Therefore an H35 cluster may not need to change its configuration as often as an NHF cluster, resulting in its slower rate of climb.

Using the essential features of the model, another procedure that allows the determination of both the surface energy density γ and the surface mobility m_s is developed. From equation (3.4), the surface energy and the gravitational potential energy are the two principal contributing factors to the free energy of the toroidal cluster. Letting $\dot{W}$ denote the rate of change of gravitational potential energy and $\dot{S}$ be the rate of change of surface energy, the rate of change of the free energy becomes

$$\dot{\mathcal{F}}(t) = \dot{W} + \dot{S} \;\; = -v_0\rho g\left(\sec(\alpha) + \frac{v_0\tan(\alpha)}{\pi^2 b(t)^3}\right)\dot{b}(t) + \gamma 2v_0\frac{\dot{b}(t)}{b(t)^2} \tag{3.31}$$

where (3.3) has been utilized to determine $\dot{\bar{z}}(t)$. Implementing the dimensionless time τ, the dimensionless minor radius $\beta(\tau)$ from (3.25) and the first of the nondimensional ratios ω from (3.26), $\dot{W}$ can also be written in a dimensionless form

$$\frac{\dot{W}}{\rho g b_0^3\dot{b}(t)} = \omega\left(\sec(\alpha) + \frac{\omega\tan(\alpha)}{\pi^2\beta(\tau)^3}\right). \tag{3.32}$$

Similarly, with the aid of the second nondimensional ratio κ from (3.26) $\dot{S}$ can also

be written in a dimensionless form

$$\frac{\dot{S}}{\rho g b_0^3 \dot{b}(t)} = -2\frac{\gamma}{\rho g b_0^2}\frac{\omega}{\beta(\tau)^2} = \frac{-2\kappa\omega}{\beta(\tau)^2} \tag{3.33}$$

As mentioned earlier, the dissipation has been found to be a function of $b(t)$ and $\dot{b}(t)$ along with other system parameters such that

$$\mathcal{D}(t) = \frac{1}{m_s} f\left(\alpha, \frac{b(t)}{b_0}\right)\dot{b}(t). \tag{3.34}$$

From the normalization of time in equation (3.25), the dimensionless time τ can also be stated as the ratio $\tau = t/t_0$ where, t_0 is given by

$$t_0 = \frac{b_0^2}{m_s \rho g} \tag{3.35}$$

and is a unit of time determined by the initial conditions of the system. Accordingly, the dimensionless form of the dissipation can be written as

$$\frac{\mathcal{D}(t)}{\rho g b_0^3 \dot{b}(t)} = t_0 f\big(\alpha, \beta(\tau)\big)\dot{\beta}(\tau). \tag{3.36}$$

Energy conservation requires that the free energy lost from the system equals the energy dissipated from the system, that is $\dot{\mathcal{F}}(t) + \mathcal{D}(t) = 0$. Rewriting the energy balance in terms of the dimensionless quantities gives

$$\omega\left(\sec(\alpha) + \frac{\omega\tan(\alpha)}{\pi^2\beta(\tau)^3}\right) - \frac{2\kappa\omega}{\beta(\tau)^2} + t_0 f\big(\alpha, \beta(\tau)\big)\dot{\beta}(\tau) = 0. \tag{3.37}$$

The rearrangement of equation (3.37) reveals that a linear relationship exists

between t_0 and κ

$$t_0 = \frac{-2\omega}{\beta(\tau)^2 f\big(\alpha, \beta(\tau)\big)\dot{\beta}(\tau)}\kappa - \frac{\omega\left(\sec(\alpha) + \frac{\omega\tan(\alpha)}{\pi^2\beta(\tau)^3}\right)}{f\big(\alpha, \beta(\tau)\big)\dot{\beta}(\tau)}. \tag{3.38}$$

The data for each experimental time point can be used to generate its a separate curve using (3.38). The values presented in each line of Table 3.2 are obtained from the intersection point of two curves generated using data from experiments conducted using conical pillars with slopes 55° and 65°.

The γ values from the extraction method are comparatively smaller than the γ values obtained from κ_{eq}. The κ_{eq} method is derived from the energy balance of the surface energy and the gravitational potential energy experienced by clusters that do not climb the pillar. Therefore, it is important to note that the κ_{eq} values are void of dissipative effects. Clusters for which $\kappa = \kappa_{eq}$, according to the model are not reducing their free energy and, as such, there is no energy to be dissipated from the system. Hence, from the results of the model, the κ_{eq} values are independent of the input value of m_s. The extraction method, however, is based on the energy balance between the free energy lost and the energy dissipated as the cluster climbs the conical pillar and is dependent of the surface mobility m_s.

The extension of the model to extract values for surface energy differs from traditional methods such as optical trapping, atomic force microscopy and micropipette aspiration methods in that the values obtained do not rely on the method used to probe the cells and the conditions under which the experiments are done. However, the extraction method is very sensitive to errors in the input values. In the extraction method, for the $t = 2$ data set, if the input values are changed to its value plus that of the data error bar, the newly calculated values are $\gamma = 0.04805\ mJ/m^2$ and $m_s = 31.310^{-14}\ m^4hr/g$. In comparison to the first line of Table 3.2, the γ values are not affected nearly as much as the m_s values. The inconsistency of the m_s results may

arise from the small magnitude of the values which require a more sensitive method.

3.5 Conclusions from the Basic Model

The formation of stable non-spheroid, self-assembled structures in three dimensions may seem to contradict the Steinberg DAH which has been used to explain the commonly observed spherical shape of aggregates as the shape that reduces its surface area in the absence of external forces. However, the results of the mathematical model of the experiments reinforces the reduction of surface area process of self-assembled structures. Evidently, the clusters self-assemble into an initial shape determined by the configuration of the experimental chamber, in this case a toroidal shape is formed. The model then shows that clusters attempt to decrease their surface area by climbing the conical pillar. The results of the model highlight the extent to which a cluster would go to reduce its surface area. Meanwhile, from experiments the clusters do not further evolve once they have become spherical.

Thermodynamics states that isothermal systems seek to minimize their free energy. From (3.4), the cluster also reduces its free energy as it reduces its surface area. This provides an explanation for the spontaneous climb of the cluster up the conical pillar. However, not all clusters spontaneously climb the pillar nor do the clusters climb the pillar at the same rate. As implied by the model, this is due to the energy penalty, in the form of gravitational potential energy, that must now be paid for reduction of the surface area of the cluster.

The energy struggle of the cluster is evidenced by the dimensionless ratio κ defined in equation (3.25). The solution of the differential equation (3.24) at different κ values shows that for larger values of κ there is an increase in the relative effect of the surface energy in comparison to the gravitational potential energy, resulting in an increase in the rate of climb of the cluster. The model shows that for some cluster configurations

with κ_{eq}, the energy penalty is too great and it is energetically favorable for the the cluster not to climb the pillar. Accordingly, the kinetics of the climb are also affected by the slope of the conical pillar. At steeper slopes, the energy penalty for configurational changes that decrease surface area is increased and, as such, slows the rate of climb of the cluster.

The current model is limited in that it assumes the cluster to be a uniform, axially symmetric shape. The model can be easily extended to other uniform shapes. However, using volume and surface area integrals to characterize the cluster, the model can also be extended to nonuniform shapes. The resulting expressions and the manipulation of these expressions would undoubtedly be cumbersome but it is possible. As was done here, the constant volume expression can be used to reduce the number of dependent variables.

The model presented here is also limited in that it is only valid for clusters that climb the conical pillar. The model cannot determine the behavior of the cluster after $a(t) = b(t)$, indicating that the cluster has reached the top of the conical pillar. The model also cannot provide any explanations for the subsequent evolution of clusters that do not spontaneously climb the conical pillar. A new method for this is necessary and will be presented in the next chapter.

Chapter 4

Linear Stability of a Toroidal Cluster

The model outlined in the preceding chapter dealt solely with the climb of the toroidal cluster up the conical pillar. However, experimental observation reveals that not all toroidal clusters which form at the base of the conical pillar go on to spontaneously climb the pillar. Some clusters have been observed to remain in the annular trough at the base of the chamber for the duration of the experiment. As captured in Figure 4.1, these clusters are often observed to undergo localized thinning, or 'necking', at one or more cross-sections around the circumference. This localized deformation may eventually result in the break-up of a cluster into one or more discrete segments. The aforementioned model provides no insight into the reasons underlying such behavior of these clusters. However, observations based on the results of the former model are useful toward gaining some understanding as to why these clusters do not spontaneously climb the conical pillar.

The dimensionless ratio κ, defined by (3.26), characterizes the influence of the surface energy of the cluster relative to the gravitational potential energy. From the results obtained in the preceding chapter, it was noted that for clusters with a

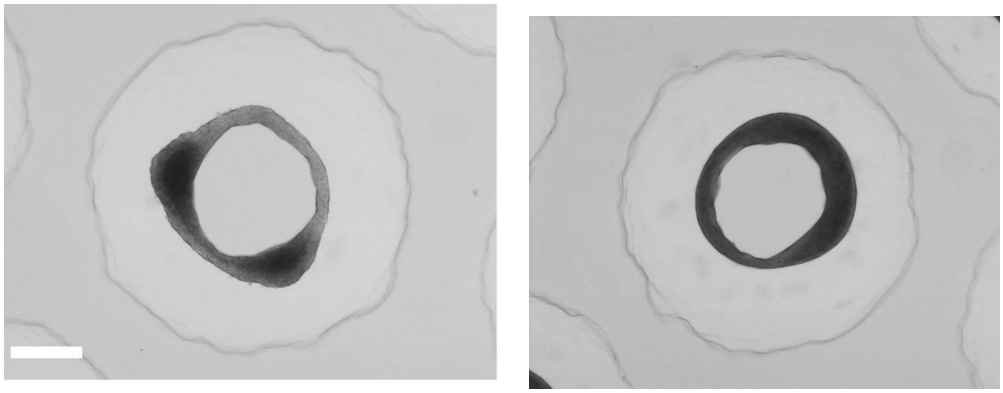

Figure 4.1: Overhead view images of toroidal clusters that do not spontaneously climb the conical pillar showing the localized necking that may develop along its circumference. The scale bar represents 200 μm.

particular value of κ denoted by κ_{eq}, the rate of change of the gravitational potential energy of the cluster is just balanced by the rate of change of the surface energy of the cluster in a virtual increment of upward motion. Therefore, it is not favorable for the cluster to climb the conical pillar because the energetic driving force for that motion is too weak. The finding of an equilibrium κ value indicates that the behavior of clusters that do not spontaneously climb the conical pillar is not the result of a random statistical process but, more likely, is related to the initial dimensions of the cluster. Therefore, a different approach is necessary to understand the change in morphology observed for a self-assembled cluster which remains in the annular trough at the base of the chamber over time.

It has been verified by direct experimental observation that the volume of the clusters that climb the conical pillar remain constant throughout their evolution (Youssef *et al.* 2010). Consequently, for clusters that remain at the base of the chamber, it will also be assumed that the volume is conserved. As was the case for the previous model, the surface properties of the cluster are again assumed to be isotropic and

to not depend on the deformation of the cluster itself. The behavior of the clusters evidenced in Figure 4.1 is reminiscent of the classic Plateau-Rayleigh instability by which an observed cylindrical body of fluid acted on by capillary forces becomes unstable through thinning of its cross-section at points along its length.

The driving force for processes that exhibit Rayleigh-like instability stems from a chemical potential gradient along the surface which, in turn, arises as a result of variations in surface shape with position. Gradients in the chemical potential along the surface then drive transport of material along the surface of the body, resulting in changes in shape of the body as the system tends to restore balance in the chemical potential from point to point. In this work, the dominant mass transport process is assumed to be surface diffusion. Cells on the surface of the cluster are able to diffuse, as a consequence of thermal activation, from regions of the surface with higher chemical potential to regions with lower chemical potential in order to result in a configuration with a uniform chemical potential and possibly a lower net surface energy.

For axially symmetric deformations, the classical result of Rayleigh states that perturbations in the cross-sectional radius with wavelengths that exceed the cross-sectional circumference of the body will reduce the specific surface energy of the body. Nichols and Mullins (1965) show that, similar to the famous Rayleigh result, the lateral surface of a solid cylindrical body becomes unstable once the wavelength of a sinusoidal longitudinal perturbation is greater than the initial circumference of the cylinder. They suggest that the development of an instability can lead to a degeneration of the initially cylindrical surface into a series of unconnected spherical bodies that reduce the surface area while preserving the initial volume of the cylindrical body, a phenomenon that has since been observed experimentally.

According to Eggers (1997), if the body is not under the action of any external

forces initially or if the time scale of the surface induced mechanism is much shorter than the time scale of any other process at work on the body, then the problem of stability is purely geometrical. Therefore, there should also exist geometric dimensions for a toroidal body that influence whether or not it is stable against small perturbations in shape. Recent experimental work to investigate the stability of both solid and liquid toroids has shown that stability of a toroidal droplet is influenced by its geometry (Pairam and Fernandez-Nieves (2009), McGraw *et al.* (2010)). Authors of both studies cite the Plateau-Rayleigh instability for the eventual break up of the toroidal body. They also note a shrinking of the major radius of the toroidal body throughout its evolution in shape. However, due to the presence of the rigid conical pillar in the present case, the toroidal clusters of cells under investigation are constrained from decreasing their major radii.

Therefore, in this chapter, the aim is to apply the concepts of linear stability analysis to establish the geometrical features of the toroidal cluster under the specified constraints which determine whether or not the cluster is stable against the growth of initially small amplitude nonuniform deformations. This way, in addition to determination of whether or not a cluster will climb the pillar, the configurational stability of the cluster can also be determined.

Stability will be ascertained by examining the behavior of a small amplitude spatial perturbation in the minor radius of the initially uniform torus configuration, with that amplitude depending on angular position θ. The following sections discuss general issues of stability analysis. Section 4.2 describes the procedure used in the present stability analysis of the toroidal clusters with constant surface energy density where the main objective is the calculation of the surface area and the volume of the perturbed clusters. Section 4.3 addresses instances in which the surface energy density of the toroidal cluster is not constant over the surface. The objective in such

a case is to determine the effect of the perturbation on the free energy of the cluster.

4.1 Stability Analysis

To analyze the stability of a particular equilibrium state of a physical system, one considers a state near equilibrium, defined by perturbing the values of whatever coordinates have been used in describing the configuration in a manner consistent with constraints. Then, one examines whether or not the system, upon release from that perturbed state, will tend toward the equilibrium state in time . In general stability problems, the initial value of the perturbation is specified, and stability is determined by the behavior of the magnitude of the perturbation over time. If, starting from its initial prescribed value, the magnitude tends to zero then the equilibrium state is said to be stable. However, if the magnitude of the perturbation tends to increase from its initial value, the equilibrium state being analyzed is deemed unstable.

While the initial magnitude of a perturbation is arbitrary, the spatial distribution of the perturbation must be consistent with any constraints imposed on the physical system under consideration. For the constant room temperature experimental set up which has motivated this study, a small amplitude fluctuation that is periodic in the circumferential direction is a likely choice for the starting value of the stability analysis.

As described above, the central idea of linear stability analysis is to determine whether or not a physical system in equilibrium will spontaneously return to that equilibrium configuration if the configuration is slightly perturbed. Expounding on this, when a perturbation is imposed on a system starting from equilibrium, the forces involved become unbalanced so that nonzero residual forces arise. If these forces tend to restore the system to the starting configuration then the system is stable in that starting configuration, and otherwise it is not. Stated in this way, it becomes clear

that stability can be examined by determining the nature of the unbalanced forces which arise due to the applied perturbation. If they tend to restore the starting configuration, the system is stable whereas, if they tend to drive the system further from equilibrium, then the starting configuration is unstable.

Therefore, beginning with the uniform torus as the equilibrium state, the cluster is presumed to explore configurations near to this state through the small amplitude perturbations in surface shape. Whether the cluster will return to its uniform torus configuration or not depends on the way in which the free energy of the body changes in the course of that perturbation. According to Carter and Glaeser (1987), perturbations which decrease the free energy of the body increase in amplitude without thermodynamic barrier. As such, if the perturbation decreases the free energy of the body, the body will not return to its equilibrium state and the equilibrium state is linearly unstable. However, if the perturbation increases the free energy of the body, the perturbation will decay in order to return the body to its stable equilibrium state. This is the central idea of the stability concept applied in this work.

4.2 Formulation of the Model

This chapter deals with the stability of clusters that do not climb the conical pillar. For the time being, the term cluster will refer only to the toroidal clusters that remain in the annular trough at the base of the chamber; in particular, it excludes those clusters that are observed to climb up the pillar. The equilibrium state for which stability is being examined is that of the uniform torus shown in Figures 4.2 and 4.3.

As indicated in Figure 4.3, the uniform torus has a circular azimuthal cross-section of radius b_0. The axis of rotational symmetry of the cluster coincides with $\boldsymbol{e}_z$ and the underlying rectangular vector basis has its origin at the center of the torus. The

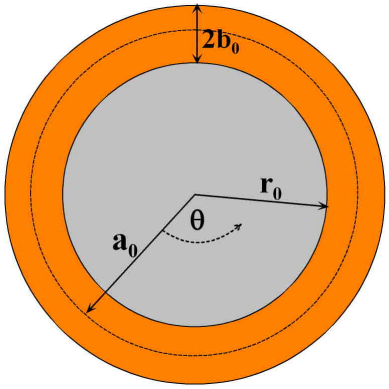

Figure 4.2: Diagram showing a overhead view of the conical pillar with radius r_0 and uniform toroidal cluster with major radius a_0 and minor radius b_0.

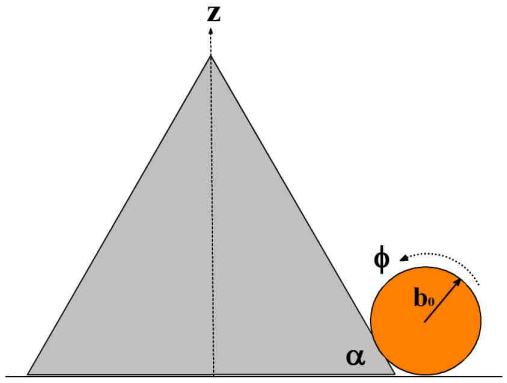

Figure 4.3: Diagram showing the side view of the conical pillar and the circular cross-section of the toroidal cluster.

unperturbed cluster, as shown in Figure 4.2, has major radius a_0 and minor radius b_0. The cluster is constrained from contracting its major radius by the rigid conical pillar of radius $r_0 = a_0 - b_0$.

The model presented in this chapter aims to determine a linear stability criterion for the cluster by examining the departure of the cluster from its uniform toroidal configuration as a result of a small amplitude sinusoidal perturbation in the minor radius about the z-axis. As was noted above, the rate of change of the free energy of the cluster as it departs from its equilibrium configuration determines the linear stability of the equilibrium state.

The toroidal clusters cannot change their gravitational potential significantly so the free energy is the total surface energy associated with the surface of area $S(t)$, that is

$$\mathcal{F}(t) = \gamma S(t) \tag{4.1}$$

where γ is the isotropic surface energy per unit area. From equation (4.1), if γ is spatially constant over the surface, then the perturbation that decreases $\mathcal{F}(t)$ simultaneously decreases the surface area of the cluster. Therefore, a perturbation that

results in a decrease in the surface area of the cluster also indicates a potential path for unstable deformation. On the contrary, a cluster is stable against any perturbation that causes an increase in its surface area as it changes from its uniform torus shape. The stability of the cluster can be determined from the change in its surface area as it departs from its uniform configuration, and a method for determining this change is outlined in the following section. It is important to note that this view of stability is based on the idea of a spatially constant surface energy density.

4.2.1 Calculating the Surface Area and Volume of the Perturbed Shape

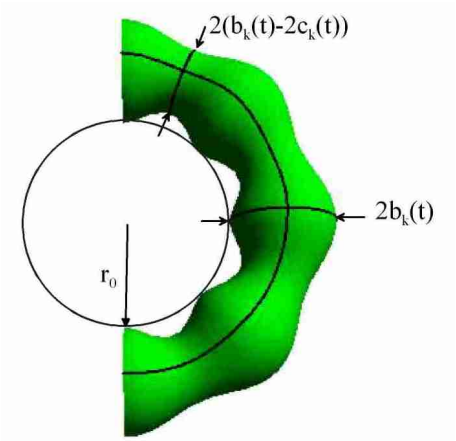

Figure 4.4: Diagram of the perturbed toroidal cluster formed by applying the sinusoidal fluctuation in the minor radius given by (4.2) to the uniform torus defined by (4.3).

Suppose that the current surface profile of the toroidal cluster is a macroscopically smooth surface. It is then assumed that the surface profile of the torus changes by the development of a periodic fluctuation in the minor radius which results in a slight

deviation of the surface from its original shape according to

$$b(\theta, t) = b_k(t) - c_k(t)(1 - \cos k\theta). \tag{4.2}$$

The wave number of the sinusoidal fluctuation k and the parameter $c_k(t)$ is the amplitude of the surface fluctuation. As the focus will be on the linear stability of the uniform torus, only cases where $|c_k(t)|/b_0 \ll 1$ are considered.

The perturbed clusters are also assumed to maintain 2π periodicity with respect to angular position around the z axis. Using Riemannian geometry with surface coordinates $(\theta,\ \phi)$, points on the surface of the perturbed shape are identified by means of the vector

$$\begin{aligned} \boldsymbol{r}(\theta, \phi) \quad &= \quad \big(a(t) + b(\theta, t)\cos\phi\big)\cos\theta\, \boldsymbol{e}_x + \big(a(t) + b(\theta, t)\cos\phi\big)\sin\theta\, \boldsymbol{e}_y \\ &\quad + b(\theta, t)\sin\phi\, \boldsymbol{e}_z \end{aligned} \tag{4.3}$$

for $0 \leq \theta < 2\pi$ and $-\pi \leq \phi < \pi$. The change in the surface of the torus due to the surface fluctuation is illustrated in Figure 4.4 where the major radius of the perturbed cluster is $a(t) = r_0 + b_k(t)$.

From the surface fluctuation expression given by (4.2), it is evident that if $|c_k(t)|$ were negative then the maximum amplitude of the fluctuation, which occurs at $k\theta \to \pi$, would be $b_k(t) + 2|c_k(t)|$. From Figure 4.4, this is not physically possible as the radius of the rigid conical pillar is fixed at r_0. Therefore, $c_k(t)$ must have a small positive value. The diagram also indicates the largest and the smallest cross-sectional areas of the perturbed cluster are determined by the minor radii $b_k(t)$ and $b_k(t) - 2c_k(t)$, respectively.

For spatially constant γ, variations in the free energy of the cluster correlate to variations in its surface area. Therefore, the tendency for growth or decay of an

applied perturbation will be determined by the change in the surface area as the cluster changes from its uniform toroidal shape. As discussed in Section 3.2.2, the area element of the surface corresponding to increments in surface coordinates (ϕ, θ) is given in terms of the Riemannian metric tensor of the surface $G_{\phi\theta}$. The metric tensor in turn is determined by the covariant base vectors of the surface in accordance with (3.12). According to the surface area expression given by (3.2), the surface area of the torus is

$$S(t) = \int_0^{2\pi} \int_{-\pi}^{\pi} \sqrt{\det\left[G_{\phi\theta}\right]}\, d\phi\, d\theta. \tag{4.4}$$

Next, the rate of change of the surface area $\dot{S}(t)$ for any integer value of k is determined. As the limits of the integral defining $S(t)$ are independent of time, $\dot{S}(t)$ can be computed by differentiation with respect to time under the integral sign in equation (4.4). Subsequently, the rate of change of the surface area as the cluster tends to depart from the uniform configuration $\dot{S}(0)$ is determined by letting the fluctuation parameters in the expression for $\dot{S}(t)$ relax to their initial values

$$b_k(0) \to b_0, \quad c_k(0) \to 0. \tag{4.5}$$

Furthermore, the fluctuation parameters $b_k(t)$ and $c_k(t)$ cannot vary independently. Rather, the relationship between the variation of the two parameters is constrained by the fact that the volume is conserved. To determine this relationship, the volume is calculated by integration of the volume element dV over the full ranges in the coordinates. For curvilinear coordinates in three dimensional space, the volume element can be computed by means of the determinant of the Jacobian matrix of the parametric equations of the toroidal body, relating the underlying Cartesian coordinates (x, y, z) to the curvilinear coordinates (u^1, u^2, u^3) chosen to describe the shape.

The Jacobian in this case is

$$dV = \left| \frac{\partial(x, y, z)}{\partial(u^1, u^2, u^3)} \right|. \tag{4.6}$$

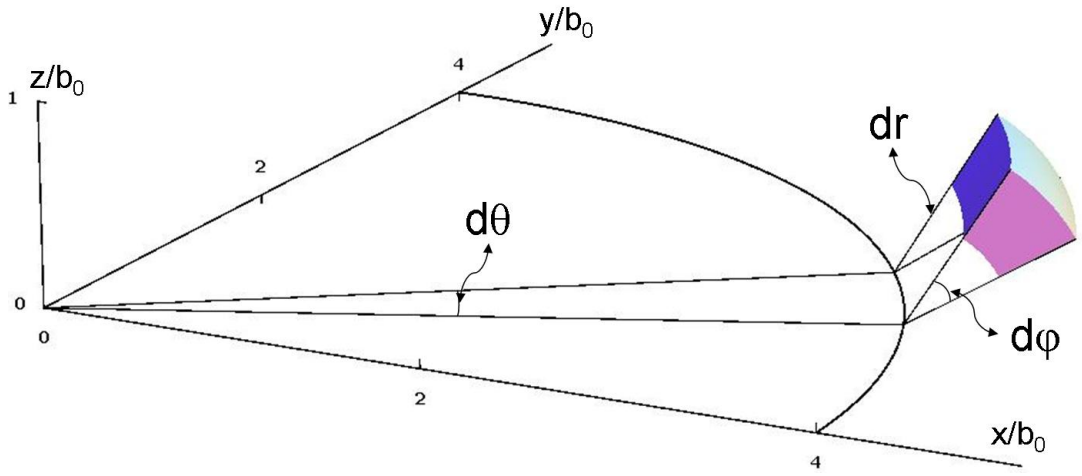

Figure 4.5: An illustration of the volume element dV which is integrated over the full ranges of the coordinates to determine the volume integral

According to the parametric representation of the perturbed surface given by (4.3), $(u^1, u^2) \rightarrow (\theta, \phi)$. The shape of the bounding surface is expressed in terms of these coordinates. From Figure 4.2, in order to span the volume, these coordinates are augmented by a radial coordinate in the azimuthal cross-section, say r, specifying the radial distance of a point from the circle of radius a_0 in any section specified by a value of θ. The range of this radial coordinate within the section is $0 < r < b(\theta, t)$. The Cartesian coordinates (x, y, z) are then expressed in terms of $(u^1, u^2, u^3) = (\theta, \phi, r)$

by

$$\begin{aligned} x &= (a(t) + r\cos\phi)\cos\theta \\ y &= (a(t) + r\cos\phi)\sin\theta \\ z &= r\sin\phi. \end{aligned} \tag{4.7}$$

It follows that the volume of the perturbed cluster is determined by evaluating the integral expression

$$V(t) = \int_0^{2\pi}\int_{-\pi}^{\pi}\int_0^{b(\theta,t)} \big(a(t) + r'\cos\phi\big) r'\, dr' d\phi\, d\theta. \tag{4.8}$$

The condition that the volume must be conserved as the perturbation grows then requires that $V(t) = V(0)$ which, in turn, implies that $\dot{V}(0) = 0$. This requirement leads to a relationship between $\dot{b}_k(0)$ and $\dot{c}_k(0)$ which must be enforced in examining the change in surface area due to the perturbation. If $\dot{V}(0)$ is determined under these conditions, and if the limiting values of $b_k(0)$ and $c_k(0)$ identified in (4.5) are introduced, it is found that the initial rates $\dot{b}_k(0)$ and $\dot{c}_k(0)$ must be related according to

$$\dot{b}_k(0) = \frac{2(b_0 + r_0)\dot{c}_k(0)}{3b_0 + 2r_0}. \tag{4.9}$$

After incorporating this relationship, $\dot{S}(0)$ can be expressed in terms of $\dot{c}_k(0)$ only. The resulting expression for $\dot{S}(0)$, which determines the linear stability of the uniform torus against the small amplitude perturbation (4.2), will be discussed in the Section 4.4.

4.2.2 An Alternate Perturbed Shape

From the illustration of the perturbed surface in Figure 4.4, it is evident that the inner surface of the perturbed cluster is not everywhere in contact with the conical

pillar. Therefore, a second equation for points on the surface of the perturbed shape is adopted for which the inner surface of the cluster does conform to the pillar. This is done by modifying the equation to insure that contact with the pillar at the inner edge is everywhere maintained. In this case, the perturbation defining $b(\theta, t)$ given in (4.2) is substituted into the expression

$$\begin{aligned} \boldsymbol{r} &= \big(r_0 + b(\theta,t)(1+\cos\phi)\big)\cos\theta\,\boldsymbol{e}_x + \big(r_0 + b(\theta,t)(1+\cos\phi)\big)\sin\theta\,\boldsymbol{e}_y \\ &+ b(\theta,t)\sin\phi\,\boldsymbol{e}_z. \end{aligned} \tag{4.10}$$

This perturbed cluster shape is shown in Figure 4.6. The diagram also identifies the azimuthal sections with the largest and smallest diameters of the cluster, determined by the radii $b_k(t)$ and $b_k(t) - 2c_k(t)$ respectively.

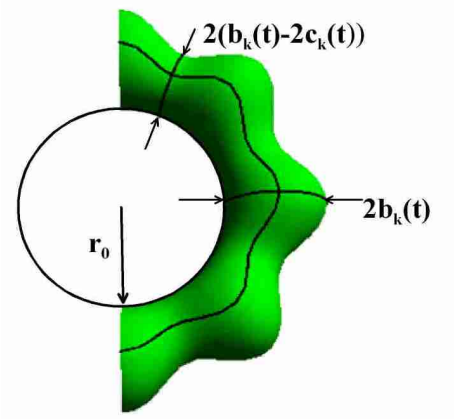

Figure 4.6: Diagram of the perturbed toroidal cluster formed by applying the sinusoidal fluctuation in the minor radius given by (4.2) to the alternate uniform torus defined by (4.10). Note that the innre surface remains conformed to the conical pillar.

Unlike the case of the first perturbed shape considered, in the present case it is not necessary to restrict the parameter $c_k(t)$ to take on only positive values.

Because the surface specifying the shape of the perturbed cluster has changed

from the previous case, the metric tensor has to be redefined and the area and volume elements of the surface must be modified accordingly. The calculation generally proceeds as outlined in the previous section. Using equation (4.6), the volume integral for the perturbed cluster, shown in Figure 4.6, is

$$V(t) = \int_0^{2\pi} \int_{-\pi}^{\pi} \int_0^{b(\theta,t)} (1+\cos\phi)\left(r_0 + r'(1+\cos\phi)\right) r'\, dr' d\phi d\theta. \tag{4.11}$$

Then, conservation of volume requires that $\dot{V}(0) = 0$ which, for this perturbation, requires that

$$\dot{b}_k(0) = \dot{c}_k(0). \tag{4.12}$$

This constraint must then be imposed on the corresponding expression for $\dot{S}(0)$. The expression obtained for $\dot{S}(0)$ which determines the linear stability of the uniform torus defined by (4.10) against the small amplitude perturbation (4.2) is presented in Section 4.4.

4.3 Non-constant Surface Energy Density

Up to this point, all analysis has been conducted under the assumption that the surface energy density is spatially constant over the surface of the cluster. However, as surface energy is proposed to derive from cell to cell adhesions, γ is initially zero and essentially begins to grow in value at local regions until it is everywhere the same. Therefore, due to the fact that the surface energy actually evolves in time as the cluster forms, γ may not necessarily be constant. For example, as the suspension of cells is introduced into the experimental chamber, it is possible for cells to settle nonuniformly about the base of the chamber giving rise to spatially nonuniform intercellular adhesion. As a result, mature adherens junctions can likely develop at one or more specific sites within the cluster while the rest of the cluster is still undergoing putative

non-junctional contact. Consequently, this can cause the surface energy density to vary with position over the surface as well as to vary with time.

If γ varies with time and with position over the surface, however, the change in free energy of the body is not equivalent to the change in the surface area of the body. Consequently, the stability of the cluster cannot be determined from the change in its surface area only. That approach is only applicable if γ is spatially constant.

Therefore, in this section an approach is formulated for instances in which γ is not constant over the surface. As was done for instances in which γ is spatially constant, analysis begins with a uniform toroidal cluster and examines its departure from that uniform configuration as a result of an applied small amplitude sinusoidal perturbation in the minor radius given by (4.2). However, presently, considering the determination of the surface area of the toroidal cluster given by (4.4), the free energy of the body takes the form

$$\mathcal{F}(t) = \int_0^{2\pi} \left[\gamma(\theta) \int_{-\pi}^{\pi} \sqrt{\det\left[G_{\phi\theta}\right]}\, d\phi \right] d\theta. \tag{4.13}$$

To simplify the analysis, the study will focus on a surface energy density that is a function of angular positions θ only, that is, for $\gamma(\theta)$. Therefore, at one or more sites along the circumference of the cluster, functional adherens junctions are formed and begins to exert contractile forces in the azimuthal cross-section of the cluster while the rest of the cluster is still in the non-junctional contact stage. This results in the surface energy density being essentially zero at the surface of the cluster except for those regions where ATP is being consumed in the contractile structures.

Beginning with the uniform torus defined by (4.3), the surface energy density is assumed to have the form

$$\gamma(\theta) = 0.1\,\mathrm{sign}\left(\theta - \frac{7\pi}{8}\right) - 0.1\,\mathrm{sign}\left(\theta - \frac{9\pi}{8}\right) \tag{4.14}$$

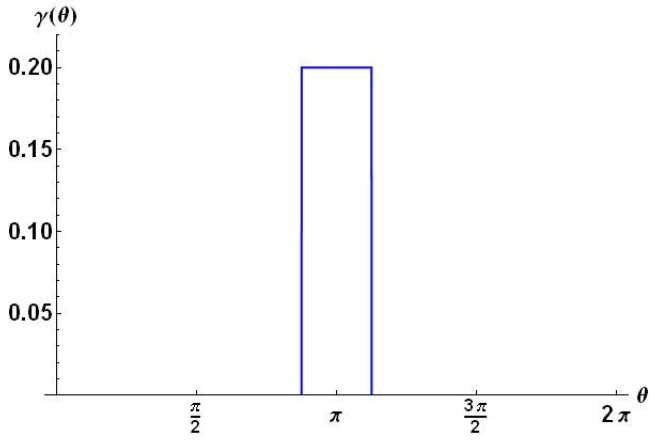

Figure 4.7: The simple surface energy density function $\gamma(\theta)$ used in the linear stability analysis of the toroidal cluster.

and is illustrated in Figure 4.7. The stability of the cluster is then determined by $\dot{\mathcal{F}}(t)$ as $t \to 0$ where the derivative with respect to time can be taken under the integral sign. Once again, the expression obtained from the constant volume constraint (4.9) is used to express the change in free energy as the cluster departs from its uniform configuration in terms of only one of the fluctuation parameters $\dot{c}_k(0)$.

As noted in Section 4.1, if the perturbation decreases the free energy of the body, the perturbation can grow in amplitude spontaneously and the equilibrium state is linearly unstable. However, if the perturbation increases the free energy of the body, the amplitude of the perturbation will tend to decay and the equilibrium state is stable.

Using the alternate uniform toroidal shape defined by (4.10), the analysis is then repeated to determine $\dot{\mathcal{F}}(0)$ for the surface fluctuation given by (4.2). The results of these stability analyses for both uniform toroidal shapes with $\gamma(\theta)$ are also presented in Section 4.4.

4.4 Results

An approach to examination of the linear stability of a uniform self-assembled toroidal cluster upon perturbation of its surface shape was outlined in the preceding sections. In order to be admissible, a perturbation must preserve the total volume of the cluster and, additionally, it must be consistent with the constraints imposed by the geometry of the chamber on the surface of the cluster. For cell clusters in which γ is assumed to be constant over the entire surface of the cluster, stability of the initial rotationally symmetric toroidal cluster shape is studied by considering the change in surface area associated with perturbations in surface shape.

According to this reasoning, stability is determined by the algebraic sign of $\dot{S}(0)$ as the cluster departs from its uniform configuration. If $\dot{S}(0) > 0$ then the cluster is stable under the assumed perturbation in shape whereas, if $\dot{S}(0) < 0$, the system can spontaneously lower its free energy by perturbing in that way and is therefore unstable. In the foregoing section, this idea was implemented for a particular perturbation of the form (4.2) applied to an initially uniform toroidal cluster. The perturbation in each case consisted of making the radius of the azimuthal cross-section $b(\theta, t)$ of the toroid vary periodically with angular position θ around the z-axis, resulting in the perturbed toroidal cluster surface shapes shown in Figures 4.4 and 4.6.

For the first of these perturbed toroidal clusters shown in Figure 4.4, the rate of change of the surface area $\dot{S}(0)$ as it departs from the reference shape is found to be

$$\dot{S}(0) = 4\pi^2\big((2b_0 + r_0)\dot{b}_k(0) - (b_0 + r_0)\dot{c}_k(0)\big). \tag{4.15}$$

Notably, there is lack of dependence on the wavenumber k. Using equation (4.9) as implied by the requirement of zero volume change, the dependence of $\dot{S}(0)$ on the

variation of the surface fluctuation parameter $\dot{c}_k(0)$ is given by

$$\dot{S}(0) = 4\pi^2 b_0 \frac{b_0 + r_0}{3b_0 + r_0} \dot{c}_k(0). \tag{4.16}$$

Since b_0, r_0 and π are all positive constants, the sign of $\dot{S}(0)$ is determined by the sign of $\dot{c}_k(0)$.

From the limiting values of the fluctuation parameters as $t \to 0$, $c_k(0) = 0$. Furthermore, the constraint of the rigid pillar constrains values of $c_k(t)$ for $t > 0$ to be positive. Together, these features imply that $\dot{c}_k(0)$ is necessarily positive. it then follows from (4.15) that $\dot{S}(0)$ is also positive. Consequently, a uniform toroidal cluster is linearly stable under this particular family of applied perturbations. Knowing from experiments that instabilities do develop in the toroidal clusters, the case of a second perturbation which is somewhat richer in detail is examined.

For the alternate perturbed shape, the initial rate of change of surface area was found to depend on the initial values of the perturbation according to

$$\dot{S}(0) = 4\pi^2(2b_0 + r_0)(\dot{b}_k(0) - \dot{c}_k(0)). \tag{4.17}$$

However, the additional requirement that the volume be conserved as the shape changes given in (4.12) implies that $\dot{S}(0) = 0$ for this perturbation. Therefore, the rate of change of surface area upon application of this particular perturbation provides no indication of whether the area increases or decreases as t increases from zero.

The inability to form unstable configurations from these uniform toroidal shapes suggests that the surface energy density of the cluster may not be constant over the surface of the cluster. This led to the analysis of stability for instances in which γ is a function of position over the surface. For purposes of a very simple illustration the

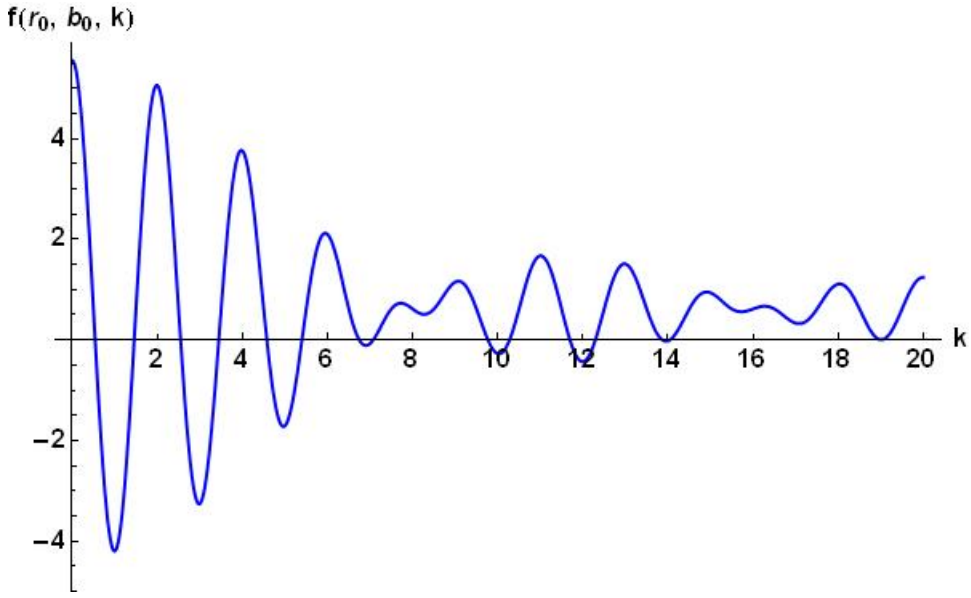

Figure 4.8: For analysis with $\gamma(\theta)$, a plot of $f(r_0, b_0, k)$ from the expression (4.18) varying with wavenumber k for $b_0 = 1$ and $r_0 = 4$.

non-constant surface energy density $\gamma(\theta)$ is defined by (4.14).

An expression for $\dot{\mathcal{F}}(0)$ is found as the cluster departs from its uniform toroidal configuration due to the fluctuation in the minor radius $b(\theta, t)$ defined by (4.2). The first of the uniform toroidal clusters defined by (4.3) departs its equilibrium configuration in such a way that

$$\dot{\mathcal{F}}(0) = f(r_0, b_0, k)\, \dot{c}_k(0) \tag{4.18}$$

where the relationship between the variation of the fluctuation parameters imposed by the constant volume throughout the shape evolution (4.9) is used. As was discussed previously, $\dot{c}_k(t)$ is necessarily positive for all t. Therefore, the outcome of the stability depends on the algebraic sign of the coefficient function $f(r_0, b_0, k)$.

Assuming $b_0 = 1$, the geometric dimensions of the experimental chambers gives $r_0 = 4$. Using these values $f(r_0, b_0, k)$ is plotted as a function of k and is shown in Figure 4.8. Applying the stability concept that perturbations which decrease the free

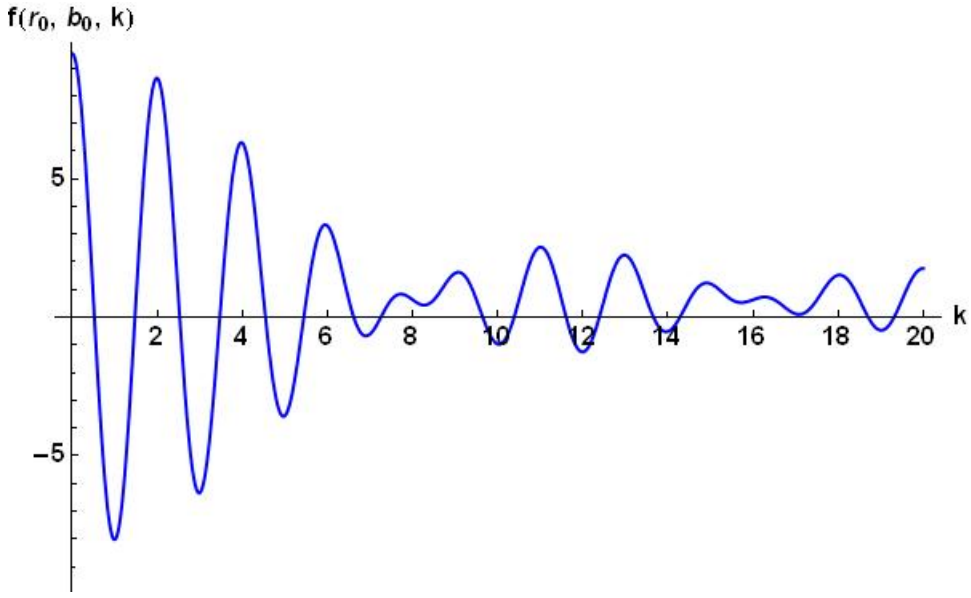

Figure 4.9: For the analysis with $\gamma(\theta)$, $f(r_0, b_0, k)$ of the $\dot{\mathcal{F}}(0)$ expression plotted as a function of wavenumber k at an increased ratio of $r_0/b_0 = 8$.

energy render the body unstable, there are three distinct regions of this plot. The first is defined for $k \leq 8$, where the uniform toroidal cluster is unstable for odd wave numbers and stable for even wave numbers . Next in the interval $9 \leq k < 14$, the reverse is true in that the uniform toroidal cluster is stable for odd wave numbers and unstable for even wave numbers. For the final region, $k > 14$, the uniform torus configuration is always stable under the applied perturbation (4.2).

For the alternate uniform toroidal shape defined by (4.10), the rate of change of the free energy as the shape departs its uniform configuration is found to be

$$\dot{\mathcal{F}}(0) = g(k, r_0, b_0)\, \dot{c}_k(0) \tag{4.19}$$

where equation (4.9) as implied by the requirement of zero volume change has been substituted. However, for this alternate perturbed shape whose inner surface conforms to the conical pillar, there are no restrictions for the algebraic sign of the parameter

$c_k(t)$ and furthermore for the parameter $\dot{c}_k(0)$.

Inputting $b_0 = 1$ and $r_0 = 4$, $g(r_0, b_0, k)$ is plotted as a function of k and shown in Figure 4.10. In this plot $\dot{\mathcal{F}}(0) = 0$ for $k = 1$ and for multiples of $k = 8$. Within these intervals, the uniform toroidal configuration alternates from stable to unstable depending on whether k is even or odd. The dependence of the stability on whether k is even or odd is also inverted from interval to interval.

It should be noted that the positioning of the sign function in the expression for $\gamma(\theta)$, the amplitude of the sign function and the width of the non-zero region are arbitrarily chosen. While changing these parameters affects the plots shown in Figures 4.8 and 4.10 in both simple and complicated ways, stable and unstable toroidal configurations are still obtained that vary with the wave number.

For example, altering the intensity of $\gamma(\theta)$, changes the values on the y-axis for both $f(r_0, b_0, k)$ and $g(r_0, b_0, k)$ but has no bearing on the wave numbers that define the aforementioned regions of interest. Adjusting the position and width of the non-zero region of $\gamma(\theta)$ has a more complicated influence on the functions $f(r_0, b_0, k)$ and $g(r_0, b_0, k)$ as it affects the wave numbers that define stable and unstable configurations.

Of more interest to this work is the effect of changing the ratio of r_0 to b_0. The function $f(r_0, b_0, k)$ is plotted for the ratio of $r_0/b_0 = 8$ and is shown in Figure 4.9. An increased ratio of r_0/b_0, implies a toroid with a smaller cross-sectional area. Doubling this ratio increases the magnitude of $\dot{\mathcal{F}}(0)$ for any given wavenumber. This suggests that toroids with smaller cross-sectional areas have a faster response to the surface fluctuation than toroids with larger cross-sectional areas. Increasing the r_0/b_0 ratio also increases the k above which the toroidal configuration is always stable allowing for more wave numbers that cause the uniform torus to become unstable.

A plot of $g(r_0, b_0, k)$ for $r_0/b_0 = 8$ is shown in Figure 4.11. At this increased ratio,

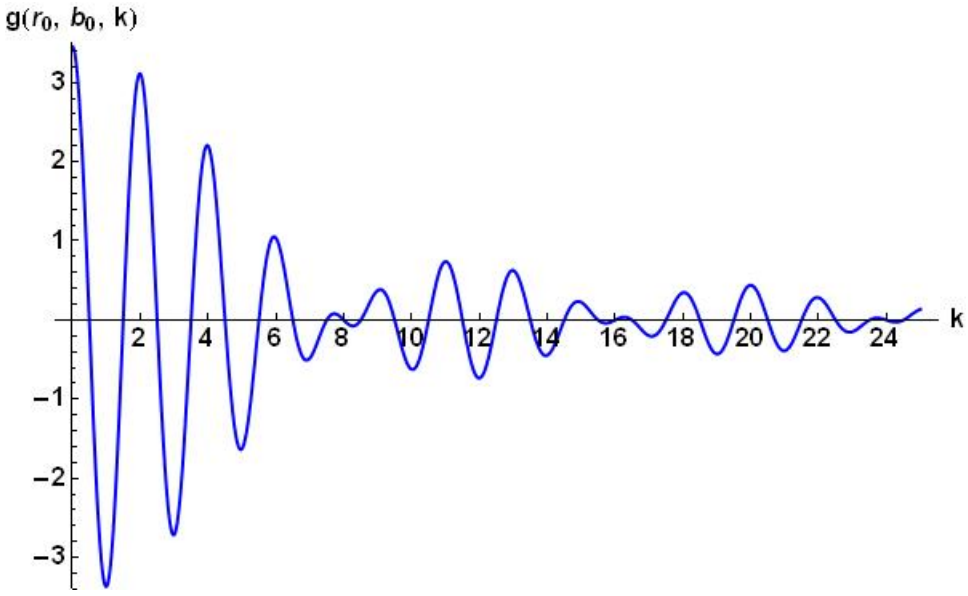

Figure 4.10: For $\gamma(\theta)$, the coefficient function $g(r_0, b_0, k)$ in (4.19) is plotted against the wavenumber k of the surface fluctuation for $b_0 = 1$ and $r_0 = 4$.

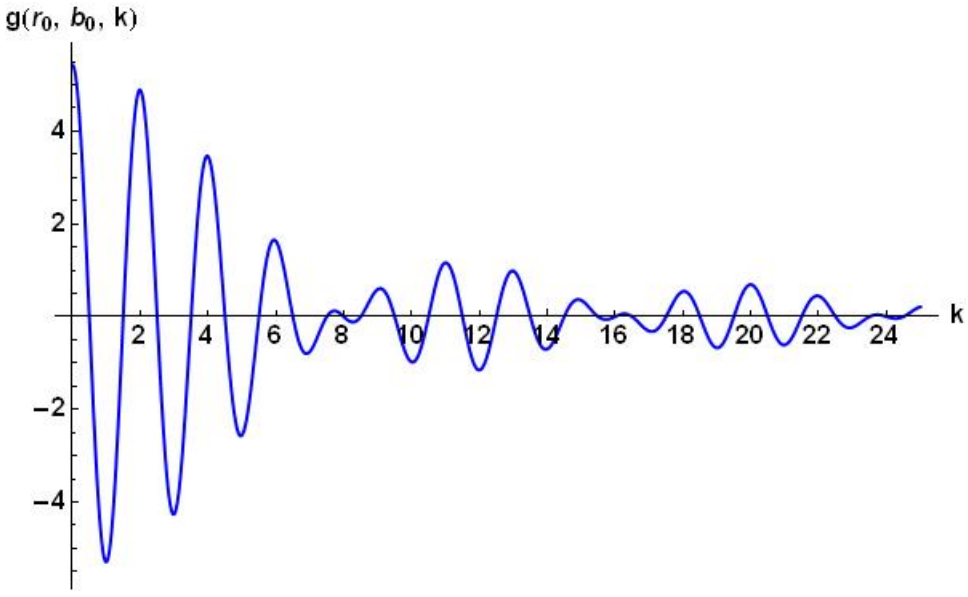

Figure 4.11: For $\gamma(\theta)$, $g(r_0, b_0, k)$ from (4.19) plotted as a function of wavenumber k at a ratio of $r_0/b_0 = 8$.

there is also an increase in the magnitude of $\dot{\mathcal{F}}(0)$ for any given wave number. This, however, is the only noticeable change as the ratio of r_0/b_0 is doubled. This suggests that for the alternate perturbed toroidal shape (4.10), the ratio influences the kinetics of the response to the applied surface fluctuation but not the thermodynamics.

4.5 *Conclusions on Linear Toroidal Stability*

The effect of a small amplitude periodic perturbation in the minor radius of the toroid on the stability of two uniform toroidal clusters has been investigated for instances in which γ is either spatially constant or is a function of circumferential angle θ. With regards to the spatially constant γ, the stability is determined by the sign of $\dot{S}(0)$ as the cluster leaves its uniform configuration. The first of the uniform toroidal shapes defined by (4.3) was found to be always stable against the applied perturbation given by (4.2). On the other hand, the alternate uniform toroidal shape (4.10) gave no conclusive stability information for the applied perturbation. The conclusion of stability under one particular perturbation is by no means exhaustive and there are many other perturbation choices for which the question of stability can be examined.

However, experimental observations as shown in Figure 4.1 indicate that some of the toroidal clusters may become unstable. Therefore, a likely reason for the lack of development of an unstable configuration from the perturbation of the uniform toroidal state is that for these clusters γ is not spatially constant. As a result, a stability analysis for which $\gamma(\theta)$ is not spatially constant is developed. For $\gamma(\theta)$, stability is determined by the sign of $\dot{\mathcal{F}}(0)$ as the cluster leaves its uniform configuration.

For both uniform toroidal configurations, instabilities are observed to develop depending on the value of k and the ratio of r_0 to b_0. The influence of the geometry of the cluster on the its stability is expected based on the toroidal stability experiments of Pairam and Fernández-Neives (2009) and McGraw et al (2010). Both of these authors

also report a contraction of the toroids towards their center. McGraw et al (2010) even state that this may be an additional pathway by which the toroids reduce their free energy. However, the cellular clusters being analyzed are constrained from shrinking in the major radius due to the presence of the rigid conical pillar. Therefore, it is to be expected that the dimensions of the conical pillar relative to the dimensions of the toroidal cluster would affect the stability of the cluster.

It should be clarified that this analysis does not take away from the model presented in Chapter 3 in which the surface energy density is assumed to be spatially constant. For the clusters that go on to climb the conical pillar, it is believed the intercellular adhesion is the same in all directions. As a result, contraction of the intercellular network generates forces equally in each direction of the cluster and results in the entire cluster moving up the conical pillar. This constant tension that is formed uniformly within the cluster before the climb remains unchanged during the process of climbing the conical pillar.

However, for the clusters that remain in the annular trough at the base of the conical pillar, perhaps due to the uneven deposition of cells, intercellular adhesion is not yet maximal in all directions within the cluster. Therefore, contraction of the cellular network does not generate an evenly distributed force within the cluster. Regarding the proposed origin of surface energy for the cellular cluster, this results in regions on the surface having an unevenly distributed surface energy density.

To help determine whether the observed localized thinning at one or more cross-sections around the circumference is a result of uneven deposition of cells into the experimental chambers, it may be of interest to experimentally observe the behavior of clusters formed using a cell deposition process that is even both spatially and with respect to time.

Admittedly, $\gamma(\theta)$ is only a very simple example of surface energy density being

a function of position along the surface. However, the purpose of the analysis was more to show that, for a variable surface energy density, unstable configurations may develop for small amplitude surface fluctuations. Therefore, more complicated functions of γ involving the azimuthal cross-sectional angle ϕ or involving functions of time, should also result in the formation of unstable configurations for small amplitude surface perturbations.

As discussed in Section 2.2, linear stability analysis is only valid for a finite time interval. However, the aim of this stability analysis, as is generally the case, is to define a boundary between a stable and unstable state by the critical value of a measurable parameter which can then be verified by experimental work. A linear stability analysis is therefore sufficient and the results suggest that the ratio of r_0/b_0 on the stability of the toroidal clusters should now be experimentally investigated.

Naturally, the next step would be a nonlinear stability analysis of the toroidal clusters. However, such an analysis will be complicated due to the large number of time dependent parameters involved in the calculations.

Chapter 5

General Problems in Configurational Stability

Cylindrical geometry and its resulting morphological instability arises in the synthesis and application of many materials. The formation of rod shaped precipitates in many eutectic structures, the development of cylindrical pore channels during crack healing, the occurrence of fibers with cylindrical geometry in reinforced composites, the stability of pore phases during the sintering of powder compacts are just a few examples for which cylindrical stability plays an important role in material performance.

Much of the work done on the stability of axisymmetric bodies involves cylindrical surfaces. A study by Nichols and Mullins (1965) on the evolution of surfaces of rotation, due to surface diffusion, showed the existence of a Rayleigh-type instability for solid cylindrical bodies. They show that a cylindrical body is stable under applied longitudinal perturbations that have wavelengths less than the initial circumference of the cylinder. However, the cylindrical body is unstable for perturbations whose wavelengths exceed the initial circumference. This has become a familiar, and generally accepted result for the stability of a cylindrical body under small amplitude

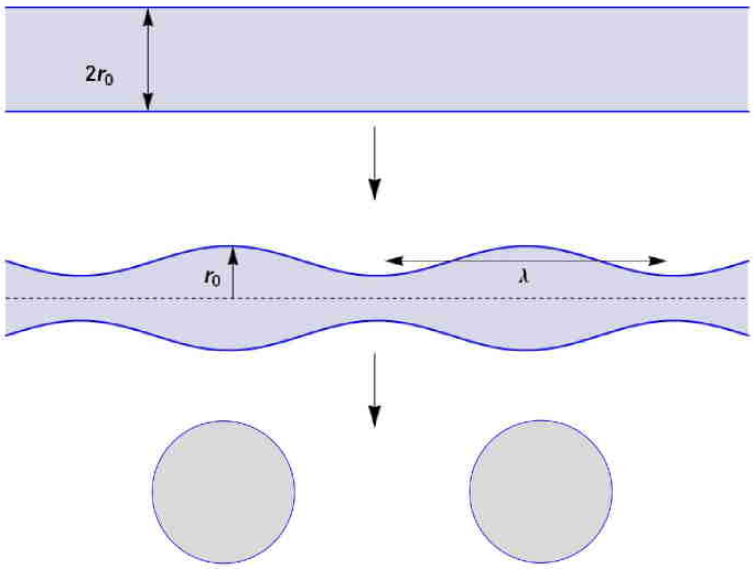

Figure 5.1: An illustration of the evolving cylindrical body

longitudinal perturbations.

In the absence of external forces acting on the cylindrical body, the only energy in the system that changes with the surface morphology is its surface energy. Therefore, provided that the surface energy is isotropic, the free energy of the body can be decreased by the reduction of the surface energy of the cylinder. Applied perturbations that grow in amplitude over time decrease the surface energy of the body (Carter and Glaeser 1987). Hence, as illustrated in Figure 5.1, the spontaneous growth of a perturbation may eventually result in the break up of the cylindrical body into discrete spherical particles. The driving force for such a process arises from the gradient in the chemical potential along the surface due to the variation of the local surface curvature induced by the applied perturbation. In response to the surface chemical potential gradient, there is diffusion of particles along the surface that results in changes in the morphology of the cylindrical body.

Coleman, Falk and Moakher (1995) have demonstrated that the Plateau-Rayleigh

stability criterion for the small amplitude perturbation of a cylindrical body is no longer valid once the amplitude of the perturbation becomes sufficiently large. By solving the nonlinear differential equation that governs the evolution in shape of the body, they observe that an applied finite amplitude longitudinal perturbation decays rapidly and then, after an incubation period, the perturbation grows in amplitude (Coleman *et al.* 1996).

In this chapter, the works of Coleman, Falk and Moakher (1995, 1996) are used as a basis for the study of the stability of axisymmetric surfaces. The goal is to reproduce the stability criteria for an axially symmetric cylindrical body using both linear and nonlinear perturbation analysis. Unlike the previous chapter, these stability problems do not necessarily correspond to any specific physical situations. Rather, they are mathematical models aimed at better understanding linear and non linear stability. The following section outlines the procedure for determining the mean curvature of the axially symmetric surface and the resulting differential equation that governs the shape evolution of the cylindrical body. In section 5.2, this governing differential equation will be linearized to determine the stability criterion for a cylindrical body under a small amplitude perturbation. The full nonlinear differential equation will then be solved numerically, in section 5.3, to determine the long term behavior of these cylindrical bodies. The results of these analyses will be presented and discussed in section 5.4.

5.1 Curvature Driven Diffusion

Mullins (1957), while studying surface grooves at grain boundaries of a heated polycrystal, pioneered a field of study focussed on surface motion due to surface diffusion. While determining the profile of the surface grooves along the traces of grain boundaries on the surface of a polycrystalline due to surface diffusion, Mullins

derived a classical transport equation with isotropic surface energy density in the form

$$\boldsymbol{j} = -m_s \nabla_s \chi. \tag{5.1}$$

The parameter $\boldsymbol{j}$ represents the flux of particles along the surface, m_s is the surface mobility coefficient of the diffusing surface particles, the operator ∇_s is the surface gradient operator and χ is the surface chemical potential. The surface gradient of the chemical potential is a vector lying on the tangent plane of the surface which has the component form

$$\nabla_s \chi = \partial_z \chi \, \boldsymbol{g}^z + \partial_\theta \chi \, \boldsymbol{g}^\theta \tag{5.2}$$

where $\boldsymbol{g}^z$ and $\boldsymbol{g}^\theta$ are the contravariant base vectors at a point on the surface.

Chemical potential is a widely used but often misunderstood term. The general concept of the chemical potential, denoted here by μ, was introduced by Gibbs (1875,1876) for his study of homogeneous bodies in contact, in which it is defined as the change in free energy for each particle added to or removed from a homogeneous, collective body of particles with the entropy and volume held fixed. As such it has come to be broadly defined as the partial molar Gibbs free energy. This is a somewhat limiting definition of μ.

From its name- the chemical potential- Gibbs may have intended μ to be an analogue to other potentials such as the gravitational potential and the electric potential which characterize the tendency for mass or charge to move from one point to another. For example, if two points are at the same electric or gravitational potential then no charge or mass can flow between them. However if point A has a higher potential than point B, then charge or mass would move from point A to B. A more intuitive definition of μ, articulated by Job and Herrmann (2006), is "the tendency of substances to change their location, chemical composition or state of aggregation". For a spontaneous chemical reaction, phase change or migration from state A to state

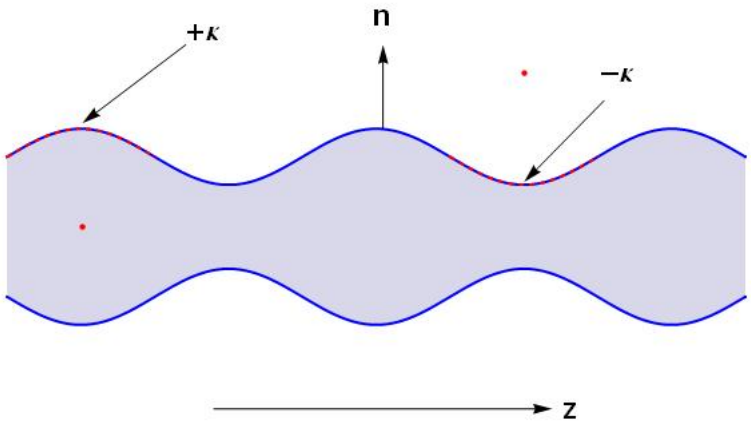

Figure 5.2: An illustration of the perturbed cylindrical surface showing the adopted sign convention. The red dot shows the center of curvature for the highlighted portion of the surface.

B, it is a necessary but not sufficient condition that the chemical potential of state A has to be higher than that of state B.

As with the gravitational and electric potential, the absolute value of the chemical potential at a point has little significance. Rather, it is the difference in chemical potential between neighboring points, or locally the spatial gradient of μ, that is significant. The spatial gradient of μ represents the thermodynamic driving force in any process that changes or causes migration from A to B.

In a similar manner, the surface chemical potential χ is a thermodynamic driving force for the movement of particles along the surface. As evidenced by (5.1), if χ varies along the surface of a body, then particles experiencing thermal activation on the surface will diffuse from regions of higher χ to regions of lower χ. The surface chemical potential is also a measure of the change in free energy per unit volume of material added to the surface of a body at fixed temperature and strain. From this definition, if the volume per particle is represented by Ω, then the relationship between chemical potential and surface chemical potential is $\mu = \Omega\ \chi$.

Assuming the surface energy per unit area γ to be isotropic and assuming the cylinder is not acted on by any external forces, the free energy of the body is

$$\mathcal{F}(t) = \int_{S'} \gamma \, dS \ . \tag{5.3}$$

Where S' refers to regions of the surface S that are unrestrained and can change in configuration with respect to the material over time. Therefore, the free energy change of the body with respect to time depends on the rate of change of the surface.

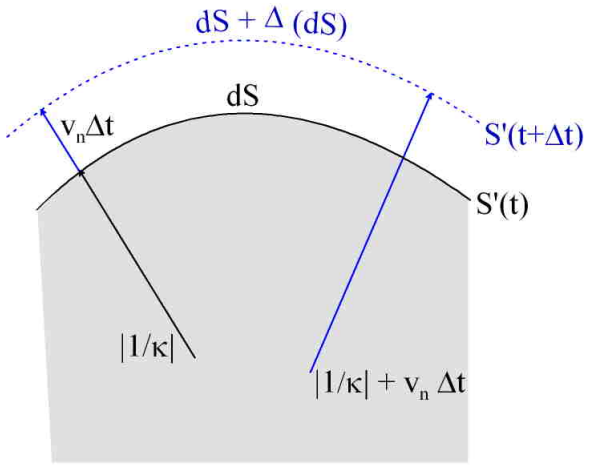

Figure 5.3: An illustration of how $\Delta(dS)/\Delta t$ is computed for an advancing surface that is $for v_n > 0$

The normal speed of the surface v_n is a function of position over the surface and determines the net rate of particle accumulation at a point on the surface. If v_n is positive then material is being added to the surface at that point and if it is negative then material is being removed from that point on the surface. The mean curvature of the surface κ is an indicator of how much the surface is curved in three dimensional space. The adopted sign convention, from Freund and Suresh (2003), states that for positive κ, the center of curvature of a point on the surface lies in the same direction

as the outward normal to the surface at that point. This sign convention is visualized in Figure 5.2.

For the surface illustrated in Figure 5.3, at time t, the magnitude of the mean curvature of the surface is given by $-\kappa$, where the negative sign arises due to the sign convention for curvature, and the mean radius of curvature of the surface is $|1/\kappa|$. At a later time $t+\Delta t$, due to material accumulation at a rate of v_n, the surface will have advanced a distance given by $v_n \Delta t$. The mean radius of curvature of the surface has now increased to $|1/\kappa| + v_n \Delta t$. The change in the area of surface element dS per unit time, $\Delta(dS)/\Delta t = -v_n \kappa dS$. Therefore, the rate of change of free energy is

$$\dot{\mathcal{F}}(t) = -\int_{S'} \gamma \, \kappa \, v_n \, dS \ . \tag{5.4}$$

The expression $v_n dS$ gives a measure of the rate at which material volume is being added to or removed from the free surface. As a result, the surface chemical potential, which is the free energy per unit volume of material added or removed from the surface, is determined by

$$\chi = -\gamma \, \kappa. \tag{5.5}$$

This expression for χ is in agreement with work by Herring (1953) in the study of the effect of interfacial energies at triple junctions of grain boundaries. In this study, Herring found the driving force for curvature driven motion to be $(\Lambda + \Lambda'')\kappa$. The specific surface free energy Λ as defined by Herring is the increase in free energy per unit increase in crystal face area and is therefore equivalent to γ. The second derivative Λ'' is taken with respect to the inclination of the surface. Having assumed that the properties of the surface are isotropic, $\Lambda'' = 0$ and the surface chemical potential given by equation (5.5) is identical to the chemical potential given by Herring.

As γ is isotropic and independent of orientation, the expression for the chemical

potential (5.5) can be incorporated into the transport equation (5.1) to give

$$\boldsymbol{j} = \gamma\, m_s\, \nabla_s \kappa. \tag{5.6}$$

The surface gradient vector $\nabla_s \kappa$ points in the direction in which κ increases most rapidly. Therefore the transport equation implies that the surface flux is in the direction from crests on the surface to troughs.

The volume of the evolving cylindrical body is conserved, so that, at any infinitesimal region on the surface, local volume conservation requires that $v_n + \nabla_s \cdot \boldsymbol{j}$. As a result, the transport equation for surface flux (5.6) can be further combined with this conservation equation to arrive at the single equation that provides the basis for the study of surface motion due to the spatial variation of the mean curvature,

$$v_n = \gamma\, m_s \nabla_s^2 \kappa. \tag{5.7}$$

The symbol ∇_s^2 represents the surface Laplacian operator, $\nabla_s \cdot \nabla_s$.

The parameter κ is twice the mean curvature at a point on the surface which is determined from the principal curvatures σ_1 and σ_2 such that

$$\kappa = (\sigma_1 + \sigma_2)\,. \tag{5.8}$$

At each point on the surface σ_1 and σ_2 represent the maximum and minimum curvatures at that given point. These principal curvatures are the eigenvalues of the characteristic equation for the curvature tensor $\boldsymbol{B}$ with respect to the metric tensor $\boldsymbol{G}$ given by

$$\det[B_{ij} - \sigma G_{ij}] = 0. \tag{5.9}$$

The metric tensor to the cylindrical surface is found by (3.12). At a point on the

surface, B_{ij} is calculated as the variation of the surface normal vector with respect to distance along coordinate lines in the surface. From equation (3.6), the covariant base vectors of the surface $\boldsymbol{g}_z$ and $\boldsymbol{g}_\theta$ represent the variation of the surface vector with respect to the surface coordinates (z, θ). Therefore the components of the tensor B_{ij} are determined to be

$$B_{ij} = -\partial_i \boldsymbol{n} \cdot \boldsymbol{g}_j, \tag{5.10}$$

where the outward unit normal to the surface $\boldsymbol{n}$ is determined by equation (3.7).

According to Cahn and Taylor (1994), the transport equation (5.7) governs situations in which both the surface energy and the surface mobility are isotropic and surface motion is controlled solely by surface diffusion. Consequently, it corresponds to situations for which the surface mobility coefficient m_s is large and the diffusion coefficient, by comparison, is not large. Therefore, this transport equation (5.7) is applicable to the study of the evolution of the axisymmetric cylindrical bodies. According to Elliott and Garcke (1997), for quite the opposite situation in which the diffusion coefficient is comparatively larger than m_s, surface motion is governed by the transport equation $v_n = m_s(\kappa - \kappa_{av})$ where κ_{av} is the average mean curvature on S.

In this section, the equation (5.7) that governs the transport of material along the surface due to the spatial variation of κ has been derived. The mean curvature, which induces the surface chemical potential gradient, can be determined by the local geometry of the surface from equation (5.8). The subsequent section deals with the application of the linearized transport equation to an initially slightly perturbed cylindrical surface to determine its stability.

5.2 Linear Perturbation Analysis

Linear perturbation analysis is a starting point into the investigation of the dynamics of the cylindrical body. To study the stability of the cylindrical body, the shape must be perturbed to allow it to explore configurations about its current shape. In this section, the Herring-Mullins transport equation (5.7) will be used to study the effect of a small amplitude perturbation on the surface of a cylindrical body, defined in Riemannian geometry, in order to reproduce the thermodynamic minimal perturbation wavelength for which the surface will be stable.

To begin, a small amplitude longitudinal perturbation is applied to a uniform cylindrical body with radius r_0 as in Figure 5.4. As is done by Nichols and Mullins (1965), the cylindrical body is taken to have isotropic surface properties and it is assumed that surface diffusion is the primary mechanism for material transport. Then, based on the initial circumference of the cylindrical body $2\pi r_0$ in relation to the wavelength λ of the applied perturbation, the perturbation can either grow in amplitude or decay away. The accepted linear perturbation result states that there is a minimum wavelength $\lambda_{min} = 2\pi r_0$ above which an infinitesimal periodic perturbation applied to the surface grows in amplitude. For $\lambda > \lambda_{min}$, the perturbation decreases the free energy of the cylindrical body in comparison to that of an unperturbed cylinder having nominally the same dimensions and therefore grows in amplitude. For $\lambda < \lambda_{min}$, the perturbation increases the free energy of the body and consequently its amplitude decays in time.

As shown in Figure 5.4, the cylindrical body is oriented such that the horizontal z axis coincides with the axis of symmetry of the cylinder. The body is assumed to remain axisymmetric throughout its evolution and it is assumed to be infinitely long such that surface fluxes to and from the lateral edges of the cylinder do not have to be taken into account. Instead there is a representative length $L \gg r_0$ over which the

solution will be obtained. With the origin of the underlying rectangular basis at the center of the cylindrical face at $z = 0$ where $0 \leq z \geq L$, the points on the surface of the cylinder are identified by means of the coordinates z and θ by the vector

$$\boldsymbol{f}(z,\theta) = r(z,t)\cos\theta\,\boldsymbol{e}_x + r(z,t)\sin\theta\,\boldsymbol{e}_y + z\,\boldsymbol{e}_z \tag{5.11}$$

where $r(z,t)$ is the radius of the cross-section at axial position z. The vector components are referred to a fixed Cartesian basis.

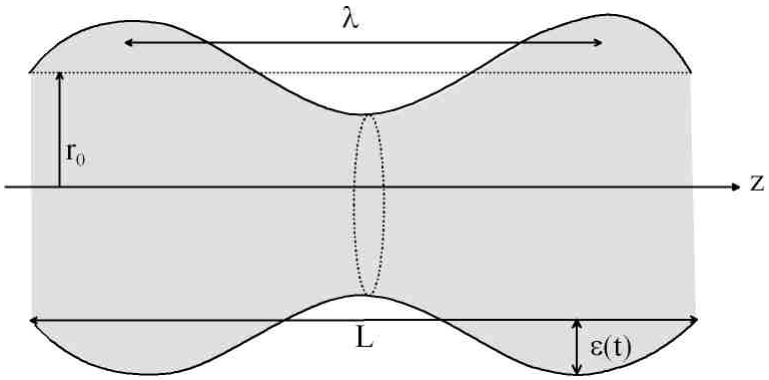

Figure 5.4: Diagram showing the physical parameters of the perturbed cylindrical body. Note that the body retains its circular cross-section throughout its shape evolution.

Suppose that a longitudinal perturbation of the form

$$r(z,t) = r_0 - c\,\epsilon(t)\cos\left(\frac{2\pi z}{L}\right) \tag{5.12}$$

is applied to the cylindrical surface where $c \ll 1$ such that the amplitude of the perturbing function is infinitesimally small. The introduction of a perturbation changes the local mean curvature κ which can be determined from the Riemannian geometry of the body according to equation (5.8). For linear stability theory, the surface slopes are small as $\epsilon(t)/L \ll 1$ and the normal speed of the surface at a point can be

approximated by

$$v_n = \frac{\partial r(z,t)}{\partial t} = c\,\dot{\epsilon}(t)\cos\left(\frac{2\pi z}{L}\right). \tag{5.13}$$

Substitution of the expressions for v_n and κ into the transport equation (5.7) yields, as expected, a nonlinear fourth order partial differential equation in the radial coordinate $r(z,t)$. This differential equation governs the morphology of the cylindrical body.

Beginning with the work of Mullins (1957) on the study of small amplitude perturbations of a cylinder, it has become customary to reduce the governing equation to a linear equation in the perturbation amplitude $\epsilon(t)$. Here, a series expansion in powers of $\epsilon(t)$ is formed and only terms linear in $\epsilon(t)$ are retained. The transport equation is now an ordinary differential equation in the perturbation amplitude $\epsilon(t)$. Regarding the initial cylindrical surface to be slightly perturbed such that $\epsilon(0) = 1$, this ordinary differential equation can be solved to give an expression for $\epsilon(t)$ that dictates the algebraic sign of the rate of change of the amplitude of the applied perturbation.

From the expression (5.12), the time dependent expression for $r(z,t)$ is known. Therefore, the evolution of the surface shape can be observed by plotting $r(z,t)$ at various intervals of time. At each time interval, the volume of the perturbed shape over the length L is calculated to ensure that the volume remains constant. The volume is that swept out as the curve $r(z,t)$ revolves about the z-axis,

$$V(t) = \pi \int_0^L r(z,t)^2\,dz\,. \tag{5.14}$$

A small value of the amplitude constant c is necessary for the volume of the cylindrical body to be constant. As the boundary conditions are independent of time, it is expected that the linearized differential equation admits exponential time dependent solutions (Eckhaus 1965). The solution of the linearized ordinary differential equation for $\epsilon(t)$ and graphs of the time evolution of $r(z,t)$ at varying ratios of r_0/L are

presented and discussed in section 5.4.

5.3 Nonlinear Stability Analysis

The previous section dealt with the stability criteria obtained from the linearization of the transport equation (5.7) that governs the evolution of the shape of the bodies due to the Laplacian of the mean curvature of the surface. However, the linear analysis is no longer considered valid once the amplitude of the perturbation has become a significant fraction of the wavelength. Also, for some physical systems, the stability must be studied for perturbations whose amplitudes cannot be assumed to be infinitesimally small.

In this section, the goal is to develop a satisfactory method for solving the governing equation and analyzing the subsequent behavior of the perturbations. The works of Coleman, Falk and Moakher (1996) will be used as a point of departure for the study of the time dependent behavior of an initially uniform cylindrical surface to which a finite amplitude longitudinal perturbation is applied. However, instead of approximating the differential equation itself, the nonlinear partial differential equation governing the radial coordinate will be solved numerically.

For the nonlinear analysis, a more convenient variable of the form

$$R(z,t) = \frac{1}{2}r^2(z,t) \tag{5.15}$$

is introduced. This modification is done in order to simplify the variational formulation needed as a basis for the finite element scheme utilized to numerically solve the transport equation (Coleman *et al.* 1996). To enable direct comparison with the reported results and to simplify the manipulation of the resulting equations, a similar modification is adopted. Therefore, the equation for points on the cylindrical surface

in terms of this modified radial coordinate $R(z,t)$ becomes

$$\boldsymbol{F}(z,\theta) = \sqrt{2R(z,t)}\cos\theta\,\boldsymbol{e}_x + \sqrt{2R(z,t)}\sin\theta\,\boldsymbol{e}_y + z\,\boldsymbol{e}_z. \tag{5.16}$$

As the surface slope is no longer restricted to be small, equation (5.13) cannot be used to determine the normal speed of the surface. Therefore, as is done in Section 3.3, v_n is found by taking the inner product of the outward normal to the surface with the rate of change of points on the surface, that is,

$$v_n = \boldsymbol{n}\cdot\partial_t\boldsymbol{F}(z,\theta) \;\; = \frac{\partial_t\boldsymbol{F}(z,\theta)}{\sqrt{\det\left[G_{ij}\right]}}, \tag{5.17}$$

where G_{ij} is the metric tensor of the distorted surface defined by equation (5.16).

The shape of the surface remains rotationally symmetric with respect to the z-axis. Consequently, the chemical potential χ is also rotationally symmetric and is independent of θ as shown in Figure 5.5. As a result, the surface flux has no circumferential component and can be represented by $\boldsymbol{j} = q\,\boldsymbol{g}_z$ where q is the component of the flux in the surface along the θ = constant direction. The surface divergence of $\boldsymbol{j}$ in terms q assumes the form

$$\nabla_s\cdot\boldsymbol{j} = \partial_z(q\,\boldsymbol{g}_z)\cdot\boldsymbol{g}^z + \partial_\theta(q\,\boldsymbol{g}_z)\cdot\boldsymbol{g}^\theta. \tag{5.18}$$

The partial differentiation is complicated by the fact that the contravariant and covariant base vectors are functions of position. However, the use of Christoffel symbols of the second kind simplifies the manipulation of the expression. The Christoffel symbol $\Gamma^k_{ij} = \partial_j\boldsymbol{g}_i\cdot\boldsymbol{g}^k$ represents the rate of change of the i^{th} base vector with respect to the j^{th} coordinate resolved in the k^{th} coordinate direction. Utilizing the Christoffel

symbols, the surface divergence of the surface flux assumes the form

$$\nabla_s \cdot \boldsymbol{j} = \partial_z q + q\,(\Gamma^z_{zz} + \Gamma^\theta_{z\theta}). \tag{5.19}$$

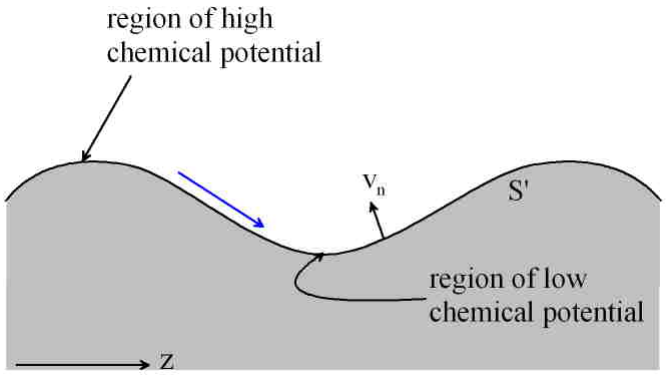

Figure 5.5: An illustration of the perturbed cylindrical surface, S'. Due to the direction of mass transport along the surface shown by the blue arrow, the normal speed at that point on the surface is given by v_n.

The covariant and contravariant base vectors have an inverse relationship such that $\boldsymbol{g}^\alpha \cdot \boldsymbol{g}_\lambda = \delta^\alpha_\beta$. Accordingly,

$$q = \boldsymbol{j} \cdot \boldsymbol{g}^z. \tag{5.20}$$

Due to the nature of the applied perturbation, as shown in Figure 5.5, the axial curvature of the surface varies spatially in the z direction. However, the cross-section at any point along z is that of a circle and as such the azimuthal curvature is constant. As a result, the component of the surface gradient of κ in the θ-direction is $\partial_\theta \kappa = 0$. Therefore, the axial component of $\boldsymbol{j}$ can be expressed as

$$q = \partial_z \kappa\, \boldsymbol{g}^z \cdot \boldsymbol{g}^z. \tag{5.21}$$

As expressions for both v_n and $\nabla_s \cdot \boldsymbol{j}$ are known, the conservation equation can be

readily enforced to obtain a time dependent partial differential equation of the form

$$\partial_t R(z,t) = \sqrt{\det\left[G_{ij}\right]}\left(-\partial_z q - q(\Gamma^z_{zz} + \Gamma^\theta_{z\theta})\right). \tag{5.22}$$

This differential equation can be solved for the modified radial coordinate $R(z,t)$ and the result can be used to determine the evolution of the surface. It should be noted that the Herring-Mullins transport equation (5.7) would also result in equation (5.22) if the surface flux is taken to be of the form $\boldsymbol{j} = q\,\boldsymbol{g}^z$.

The initial condition for the partial differential equation is a periodic fluctuation of $R(z,t)$ along the axis of symmetry of the form

$$R(z,0) = 1 + c_1 \cos nz, \tag{5.23}$$

where c_1 is a small constant and n is real number. As with the linear perturbation analysis, the cylindrical body is assumed to be infinitely long and the geometry is assumed to be periodic in z with period L. Therefore, for the numerical solution, the body can be assumed to have a finite length L and the following periodic boundary conditions are applied

$$\begin{aligned} R_z(0,t) = 0 \qquad R_z(L,t) = 0 \\ R_{zzz}(0,t) = 0 \qquad R_{zzz}(L,t) = 0. \end{aligned} \tag{5.24}$$

The value for L is at least the length of one wavelength of the applied perturbing function.

Using these initial and boundary conditions, the partial differential equation (5.22) is numerically integrated with Wolfram Mathematica® software to obtain a solution for $R(z,t)$. A continuous and analytic function is then fit to the numerical solution to

enable the visualization of the radial coordinate $\sqrt{R(z,t)}$ at varying values of time. As a check of volume conservation, the initial and final volumes of the cylindrical body over L are calculated from the revolution of the curve defined by $\sqrt{R(z,t)}$ about the $z-$axis according to equation (5.14).

The initial surface conditions and lengths L reported by Coleman, Falk and Moakher are used to obtain solutions to the partial differential equation for $R(z,t)$. These solutions are presented and compared to the reported solutions in the following section.

5.4 Results

For the linear perturbation analysis, expressions for v_n and κ obtained from the geometry of the slightly perturbed cylindrical surface are substituted into the transport equation given by (5.7). The resulting partial differential equation is linearized to become an ordinary differential equation in $\epsilon(t)$. This ordinary differential equation is then solved using the initial condition $\epsilon(0) = 1$ to give

$$\epsilon(t) = \exp\left(\frac{4cm_s\pi^2\gamma(L^2 - 4\pi^2 r_0^2)}{L^4 r_0^2}t\right). \tag{5.25}$$

For a general analysis such as this, values of the parameters m_s and γ influence the time scale but not the general nature of behavior. Therefore, to examine stability the values of m_s and γ can be set to equal 1. As the expression for $\epsilon(t)$ has been determined, the complete time dependent expression for the radial coordinate of the cylinder is known. This expression for $r(z,t)$ given by (5.12) is then graphed as a function of z at various times. The radial coordinate at $r(0,t)$ is also plot as a function of t.

Figure 5.6 shows plots of $r(z,t)$ versus z at various times for a cylinder with an

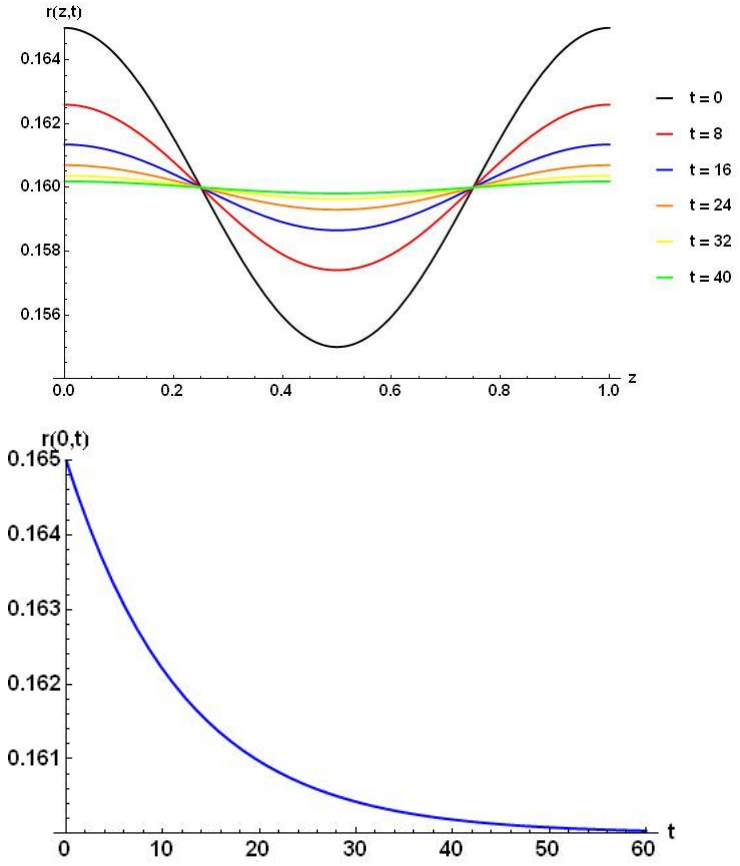

Figure 5.6: Both graphs show the decay of applied perturbation (5.12) on a cylindrical body with $r_0 = 0.16$ and $L = 1$. The Figure on the left shows $r(z,t)$ versus z at various t while the curve on the right shows $r(0,t)$ versus t.

initial radius $r_0 = 0.16$ and with length $L = 1$. The curve represented by $t = 0$ indicates the initial configuration of the perturbed surface. Subsequent plots for $r(z,t)$ versus z are shown at increasing time values and captures the decay of the perturbation. By the last time shown, the surface has returned to its unperturbed configuration with radius $r_0 = 0.16$.

The familiar result for small amplitude perturbations of a long cylinder states that for the cylinder to be stable the applied perturbation wavelength must have a value such that $\lambda \leq 2\pi r_0$. For the applied perturbation given by (5.12), the wavenumber is $k = 2\pi/L$ and hence $\lambda = L$. As $\lambda = 1$, the stability criteria can be more simply

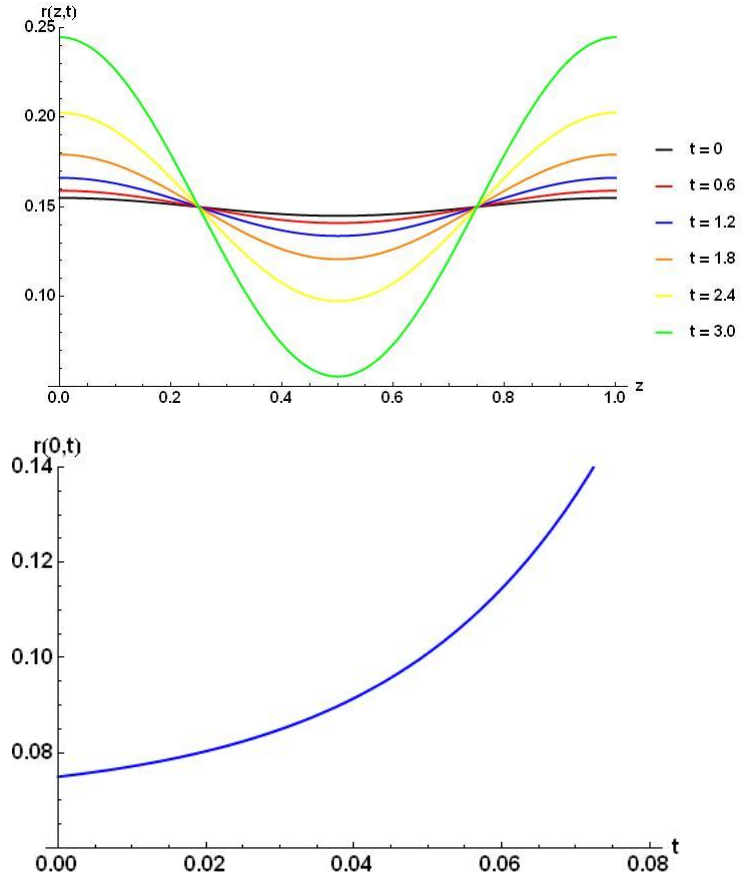

Figure 5.7: Graphs show the surface evolution of a cylindrical body with $r_0 = 0.15$ and $L = 1$ to which the perturbation (5.12) is applied. $r(z,t)$ versus z at various t is shown on right and $r(0,t)$ versus t is shown on the left.

stated as

$$\frac{r_0}{\lambda} \geq r_{cr}, \quad r_{cr} = \frac{1}{2\pi} = 0.159155. \tag{5.26}$$

Therefore, for the cylindrical body with $r_0 = 0.16$, the initial radius of the cylinder is just slightly larger than r_{cr} and, as such, the perturbation slowly decays with time.

The evolution of a perturbed cylinder with initial radius $r_0 = 0.15$ and length $L = 1$ is shown in Figure 5.7. The perturbation quickly grows in amplitude and, by $t = 3$, the body is about to degenerate into sub-particles. For $\lambda = 1$, the initial radius $r_0 < r_{cr}$ which, according to the stability criteria in (5.26), results in the growth in the amplitude of the applied perturbation and causes the cylindrical body to become

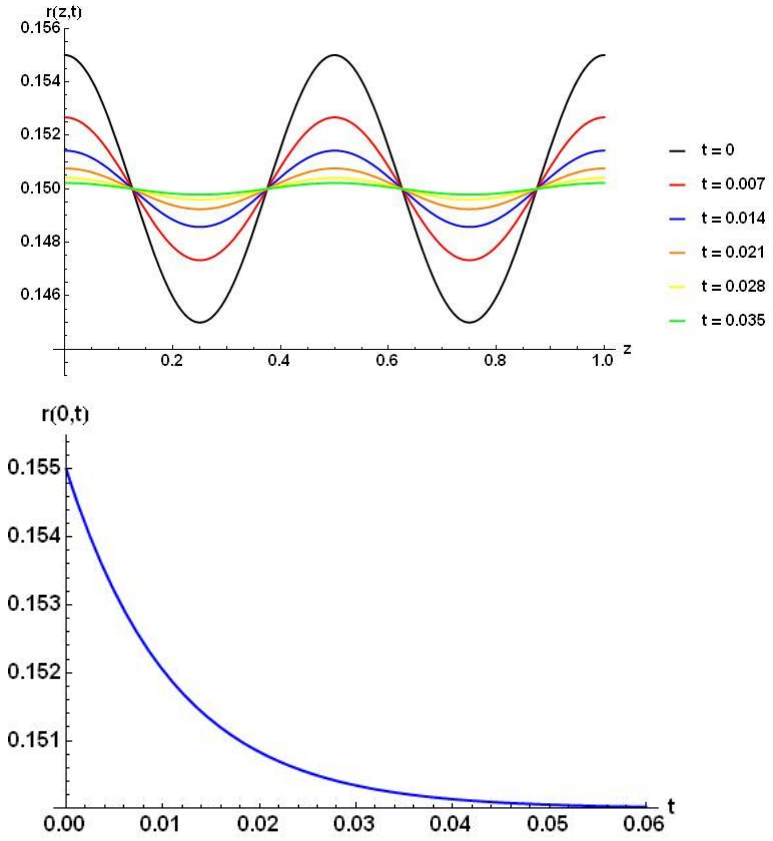

Figure 5.8: Results showing the decay of the perturbation (5.23) applied to a cylindrical body with $r_0 = 0.15$ and $L = 1$. $r(z,t)$ versus z at various t is shown on the left and $r(0,t)$ versus t is shown to the left.

unstable.

In the foregoing examples, the wavelength of the applied perturbation was kept constant and the initial radius of the body was varied. Next, using the initial cylindrical configuration of $L = 1$ and $r_0 = 0.15$, the wavelength of the applied perturbation is altered. Because $\lambda = 2\pi/k$, the wavelength is altered by changing the wavenumber of the applied perturbation. The radial coordinate of the perturbed cylindrical surface is now taken to be

$$r(z,t) = r_0 - c\epsilon(t)\cos\left(\frac{4\pi z}{L}\right). \tag{5.27}$$

The normal speed is determined from (5.13) and the mean curvature of the perturbed surface is found from the principal curvatures according to (5.8). These expressions are substituted into the transport equation (5.7). The resulting differential equation is then linearized and solved for $\epsilon(t)$ using the initial condition that $\epsilon(0) = 1$. The time dependent expression for the amplitude of the perturbation is

$$\epsilon(t) = \exp\left(\frac{16cm_s\pi^2\gamma(L^2 - 16\pi^2 r_0^2)}{L^4 r_0^2}t\right). \tag{5.28}$$

As the wavenumber has been increased to $k = 4\pi/L$, the wavelength is now reduced to $L/2$. For $r_0 = 0.15$ and $L = 1$, the ratio r_0/λ is now greater than r_{cr} and, as such, the cylindrical body should be stable under the applied perturbation. As evidenced in Figure 5.8, the perturbation is now observed to decay in amplitude.

The thermodynamic minimum wavelength λ_{min} for which the perturbation grows is not to be confused with the kinetic wavelength λ_{max} at which the rate of growth of the perturbation is fastest. As observed from Figures 5.6and 5.9, the rate of decay of the perturbation increases as the difference between r_0/λ and r_{cr} increases. Similarly, as r_0/λ is set to values that are progressively less than r_{cr}, the rate of the growth of the perturbation increases. The wavelength of the applied perturbation that maximizes the perturbation growth can be determined from the characteristic time T of the perturbation amplitude $\epsilon(t)$.

The rate of growth of the applied perturbation defined by (5.12) is controlled by the exponential amplitude function defined by (5.25). A physical quantity that has an initial value of f_0 and varies exponentially with time is represented by

$$f(t) = f_0 \exp\left(\frac{t}{T}\right), \tag{5.29}$$

where the rate of growth or decay of f is indicated by the time constant T. The

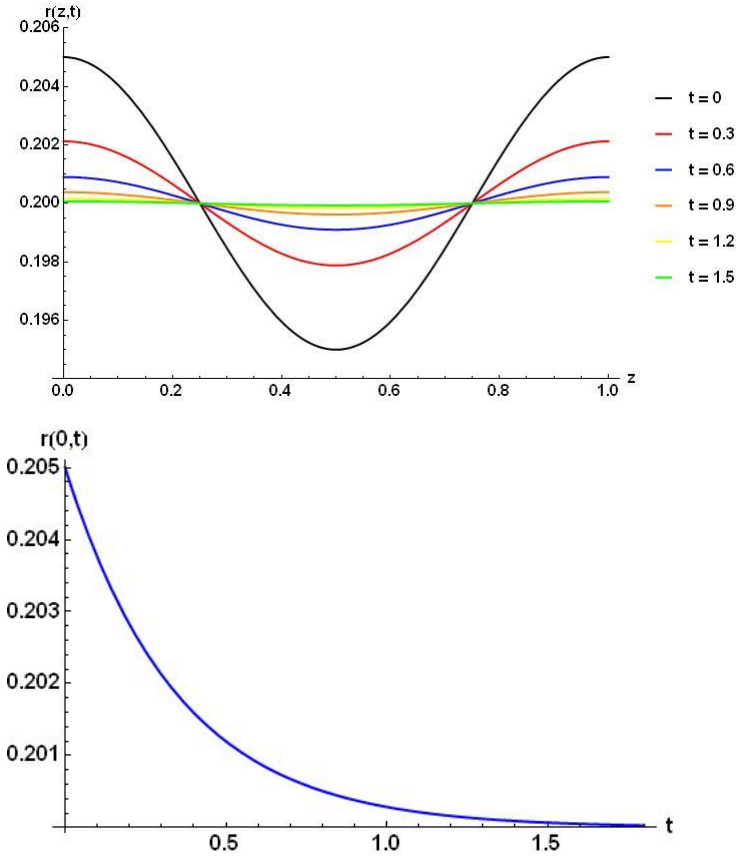

Figure 5.9: Graphs showing the decay of applied perturbation (5.12) on a cylindrical body with $r_0 = 0.2$ and $L = 1$. The graph on the left shows $r(z,t)$ versus z at various t while the curve on the right shows $r(0,t)$ versus t.

characteristic time or time constant of the exponential is the time it takes the quantity f to decay by $1/e$. The time constant for $\epsilon(t)$, given by (5.25), in terms of applied perturbation wavelength emerges as

$$T = \frac{\lambda^4 r_0^2}{4m_s\pi^2\gamma(\lambda^2 - 4\pi^2 r_0^2)}. \tag{5.30}$$

It is evident that T is a function of the wavenumber of the applied perturbation. However, regardless of the wavenumber, the wavelength that maximizes T and results

in the maximum growth rate in the perturbation amplitude, is

$$\lambda_{max} = 2\sqrt{2}\pi r_0 = \sqrt{2}\lambda_{min}. \tag{5.31}$$

Therefore if perturbations with the same initial amplitude $\epsilon(0)$ but varying wavelengths were to be applied to the cylindrical body, the perturbation with $\lambda = \lambda_{max}$ would initially increase in amplitude most quickly. While the value of λ_{min} is independent of the mass transport mechanism, the value of λ_{max} is not. As is the case for the cylindrical bodies under consideration, the expression reported in (5.31) relates to processes in which the surface diffusion is the dominant mass transport mechanism (Santala and Glaeser 2006).

According to the stability criterion presented as equation (5.26), λ_{min} and λ_{max} are characteristic quantities of linear behavior, that is, for applied perturbations with small amplitudes. Linear stability analysis focuses on the departure of the body from its current configuration and cannot accurately predict the long term behavior of the body. Nevertheless, it is still often assumed, that even for long times, the perturbation with λ_{max} would still grow in amplitude the fastest. However the stability criterion given in (5.26) involving λ_{min} does not hold for finite amplitude perturbations.

For the nonlinear perturbation analysis the nonlinear partial differential equation (5.22) is numerically integrated using the initial conditions adopted by Coleman, Falk and Moakher. The first of these axisymmetric surface shapes is given by

$$r(z,0) = 1.0 + 0.05\left(\cos(5z) + \cos\left(\frac{11z}{2}\right)\right), \tag{5.32}$$

and the solution is obtained over the interval $0 < z < L$ where $L = 4\pi$ (Coleman *et al.* 1996). The first graph in Figure 5.10 shows the initial decay of the amplitude of the perturbation from time $t = 0$ to $t = 0.01$. At this latter time, the cylindrical

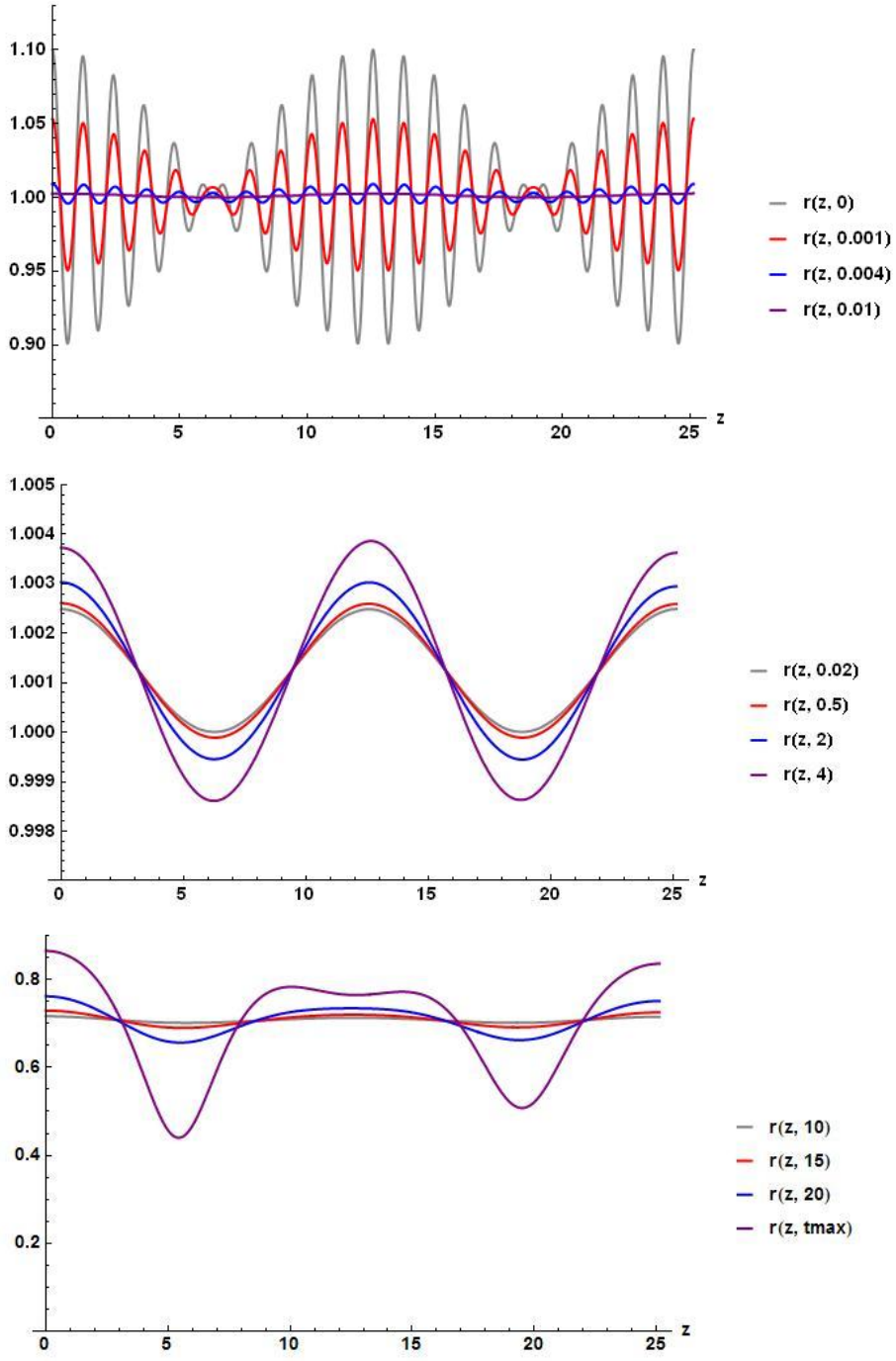

Figure 5.10: Numerical solutions of (5.22) for the initial surface (5.32). The rapid decay of the amplitude of the perturbation (5.32) is shown in the top set of curves followed by a brief dormant period captured in the middle graph. The amplitude of the perturbation is then seen to re-grow in the bottom set of curves.

surface is once again smooth. The surface remains briefly dormant until, as observed in the second graph Figure 5.10, the perturbation amplitude again begins to grow. The perturbation continues to grow until a time t_{max} at which point a singularity in the surface shape begins to develop. The volume of the body is calculated at $t = t_{max}$ and compared to the initial volume. As $V(0) = V(t_{max})$, it can be concluded that the volume of the cylindrical body is conserved throughout the evolution process.

Another multi-harmonic surface perturbation of the form

$$\begin{aligned} r(z,0) &= 1 + 0.01\left(\cos(2z) + \cos\left(\frac{13z}{6}\right) + \cos\left(\frac{7z}{3}\right) + \cos\left(\frac{5z}{2}\right)\right) \\ &+ 0.01\left(\cos\left(\frac{8z}{3}\right) + \cos\left(\frac{17z}{6}\right)\right) \end{aligned}$$

is used as the initial surface profile of the cylinder and a numerical solution is obtained over $0 < z < L$ where $L = 12\pi$ (Coleman *et al.* 1996) . The results are similar to those obtained with the previous initial shape given by (5.32). From the first graph in Figure 5.11, the amplitude of the perturbation is also observed to decay. After this initial decay, the perturbation amplitude is dormant for a brief period until about time $t = 0.5$ where, as observed in second graph Figure 5.11, the amplitude begins to revive at the edges of L. The perturbation amplitude is then observed in the last graph of Figure 5.11 to grow until the mass transport equation can no longer be solved due to the development of singularities in the solution. The volume of the cylinder is found to remain constant throughout its evolution as $V(0) = V(t_{max})$.

The observed trends in the nonlinear analysis are in agreement with the reported results of Coleman, Falk and Moakher. From the fixed time graphs of the radial coordinate, shown in Figures 5.10 and 5.11, the perturbations are observed to decay over a short period of time, followed by a period of inactivity. After this brief dormant

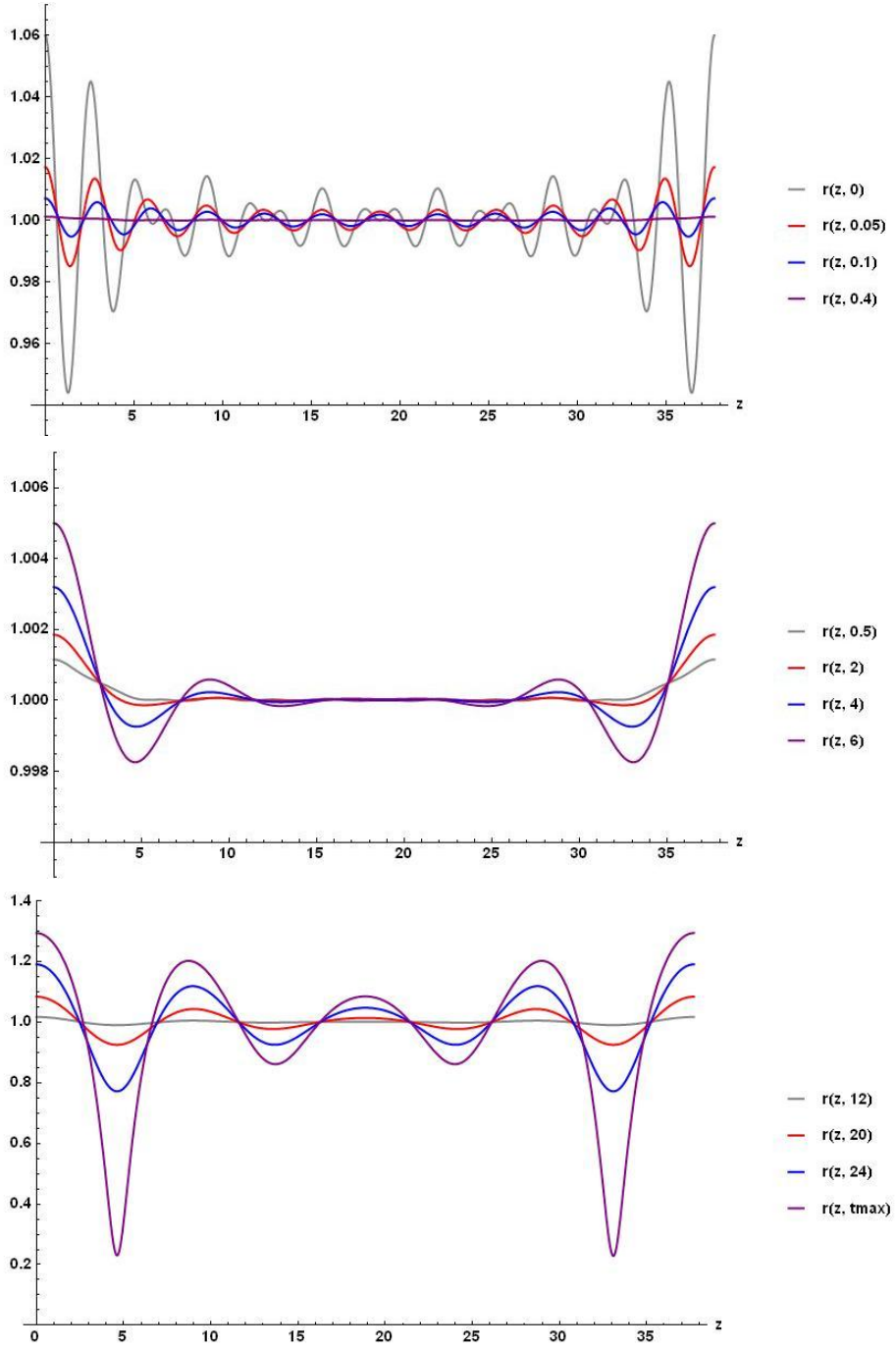

Figure 5.11: Numerical solutions of (5.22) for the initial surface (5.33). The top set of curves show the rapid decay of the amplitude of the perturbation followed by a brief dormant period in the middle set of curves. The perturbation is then seen to revive and grow in amplitude in the last set of curves.

period, the perturbations are then observed to grow in amplitude until the mass transport equation fails using the proposed method.

5.5 Conclusions on Stability of Cylindrical Bodies Evolving Due to Surface Diffusion

Linear stability analysis of an axisymmetric cylindrical body defined by (5.11) shows that, for small amplitude perturbations, there is a minimum wavelength for stability given by $\lambda_{min} = 2\pi r_0$ where r_0 is the initial cross-sectional radius. Perturbations in surface shape applied to the uniform cylindrical body with wavelengths below λ_{min} decay in amplitude and the uniform cylindrical configuration is deemed linearly stable. Conversely, applied perturbations with wavelengths above λ_{min} grow in amplitude and may cause the break up of the cylindrical body into discrete particles. This is in direct agreement with the reported results of Nichols and Mullins (1965).

The concept of instability resulting from an infinitesimal perturbation is a bit of a paradox. Essentially at some point in time during which the cylindrical body becomes unstable, the amplitude of the perturbation is large enough that the linearization of the governing equation can no longer be valid. Therefore, as the perturbation grows in amplitude, the solution is only valid during a finite time interval within which that amplitude can be considered infinitesimal.

Consequently, all stability criteria based on linear perturbation analysis are valid only for short periods of time. A reason for this has to do with the linearization of the governing equations. Neglecting the nonlinear terms does not allow for the interaction of the perturbation modes. As a result, linear analysis is simply of no use for perturbations that grow in amplitude at long times. Regardless, linear stability analysis has been successfully used to determine experimentally verified stability

criteria.

There is also a noted difference in the form of the applied perturbation from linear analysis to the nonlinear analysis. For linear analyses, the uniform cylindrical surface is perturbed by a single periodic function. On the other hand, for nonlinear analyses, the perturbing function consists of multiple periodic functions. The use of a single harmonic function for linear stability can be justified by observing the time constant T of the exponential solution such as in (5.30). The time constant of the exponential solution for an applied perturbation with a wavenumber k is given by

$$T = -c\lambda m_s k^4 t + \frac{c\lambda m_s k^2 t}{r_0^2} \tag{5.33}$$

and shows that the perturbation decays according to k^4. Therefore, higher wavenumber harmonics decay away much faster leaving the smaller wavenumber fluctuations to govern the evolution of the body. As such for linear analysis, one wavenumber is considered at a time and it is typically the one for which the growth rate is the fastest.

For the nonlinear stability analysis, the solution of the mass transport equation becomes more computationally challenging as the cylindrical surface begins to neck due to the development of singularities in the solution typically in the form of cusps in surface shape. From Figures 5.10 and 5.11, the mass transport equation fails before the actual break up of the body into sub particles. This limitation may arise from our method of fitting a curve to the numerical solution to allow for the visualization of the solution at later times. As singularities develop, it becomes increasingly difficult to fit a curve to the numerical solution. Therefore, while the numerical solution of the governing partial differential equations given by (5.7) and (5.22) may allow for the development of singularities such as occurs during pinchoff, the process of fitting a curve to the singularity solution will prevent such a solution from being observed.

Despite this, using the initial and boundary conditions reported by Coleman, Falk and Moakher (1996), we also observed that perturbations, predicted to decay in linear stability analysis, decay for a brief finite interval after which the perturbation regenerates and grows in amplitude.

In physical systems, perturbations can manifest themselves an arbitrary number of times in arbitrary fashion. Therefore, both the linear and nonlinear stability analyses conducted are limited as the applied perturbation is not an arbitrary function of the surface coordinates. The perturbations used are functions of z only and as a result surface diffusion occurs in one dimension. Perturbations with an additional rotational component, or with greater complexity in general, may present different stability criteria and different rates of growth and decay.

Also, in the mathematical formulation for solving the governing equations, the cylinder is assumed to be infinitely long. The numerical solution is obtained over a finite length L utilizing periodic boundary conditions at the ends. This however restricts the consideration of surfaces with edges or with corners. It may be of interest then to formulate the stability analysis of an axisymmetric body with finite length. A foreseen difficulty may arise if boundary conditions are to be applied to the ends of the finite body as the location of these ends vary in time. However, a mathematical study conducted by Garcke, Ito and Kohsaka (2008) on the motion of curves where the interface intersects an external boundary utilizes the Herring-Mullins transport equation (5.7) and may serve as a good starting point for such an analysis.

The formulation developed here can function as a basis for theoretical analysis of less studied axisymmetric bodies such as toroidal shapes. The results of these computational methods can also be used as a starting point in experimentally investigating the stability criteria for axisymmetric bodies with anisotropic surface energy density. Recent studies in perturbation analysis have delved into areas where the

surface energy is anisotropic. Work by Santala and Glaeser (2006) have shown that surface energy anisotropy leads to a broader spectrum of morphological behavior of materials.

Chapter 6

Concluding Remarks

This dissertation models the observed phenomena of three dimensional self assembly experiments conducted by Dean et al (2007) which show that cells self assemble into a toroidal cluster in the annular trough about a conical pillar. Some of these toroidal clusters go on to spontaneously climb the conical pillar about which it has self assembled while other clusters are sometimes observed to undergo localized thinning at cross-sections along its axial circumference. Focusing on these phenomena, models are developed to better understand the forces driving the cell cluster reorganization.

The first model presented in Chapter 3 focused on the climb of the toroidal cluster up the conical pillar. Based on the premise that the cluster climbs the conical pillar to reduce its surface area, the system free energy (3.4) comprises of a surface energy term and a gravitational potential energy term. While this is not an exhaustive list of terms that comprise the free energy, they have proven to be sufficient to provide the observed experimental behavior.

Cell to cell adhesion results in the formation of a vast intercellular network through the linking of cytoskeletal actin filaments across the adherens junctions. However, cells on the surface of the cluster are loosely bound and are free to relocate along the surface with flux $\boldsymbol{j}$ to sites that result in a lowering of the system free energy.

Surface diffusion is a dissipative process and, as such, the total dissipation at any time is a function of $\boldsymbol{j}$ and is given by (3.19). The system is isothermal and the power balance between the rate of reduction of the system free energy and the rate of dissipation of this energy is recast in the form of a variational principle. Application of this variational principle then leads to an ordinary differential equation (3.24) that is solved incrementally in time to obtain the surface shape at a time t.

Normalizing the minor radius $b(t)$ and the time t with respect to system parameters according to (3.25), the behavior implied by the differential equation depends on two nondimensional ratios κ and ω. From (3.26), the ratio κ characterizes the relative influence of the surface energy of the cluster to its gravitational potential energy and is found to influence the rate of climb of the toroidal clusters. As shown in Figures 3.9 and 3.10, all other things being equal, increasing the value of κ increases the rate of climb. Conversely, decreasing the value of κ slows the rate of climb of the cluster. This led to the discovery of a κ_{eq} value for which it is not energetically favorable for the cluster to climb the pillar.

Lowering the value of κ increases the energy penalty for configurational changes that decrease surface area. A similar effect is obtained by increasing the slope of the conical pillar with respect to the horizontal axis α. At steeper slopes, as shown by Figure 3.11, there is a slower rate of climb.

The other parameter that is observed to affect the kinetics of climb of the cluster is the surface mobility coefficient m_s of the loosely bound cells on the surface of the cluster. The value of m_s influences the rate at which the cell cluster reorganization occurs. Figure 3.12 shows that increasing the value of the m_s increases the rate of climb of the cluster. Alternately, decreasing the value of the m_s slows the rate of climb.

The influence of κ and α on the numerical results captures the energy competition

as the cluster tries to decrease its surface area by climbing the conical pillar at the expense of increasing its gravitational potential energy. The dependence of the rate of climb on m_s is a positive measure but does not prove that surface diffusion is the process by which cells in a cluster reorganize. More definitive results require experimental investigation. For example, one can observe the effects of inhibiting the mobility of the cells in the surface layer of the cluster post self assembly. If the cluster phenomena are no longer observed then it becomes more likely that cell cluster reorganization occurs by the process of surface diffusion.

The second model presented in Chapter 4 addresses clusters that do not climb the conical pillar but remain in the annular trough at its base. Such behavior recalls the Plateau-Rayleigh instability of cylindrical geometries driven by the minimization of the surface area of the body. Therefore, the aim was to conduct a linear stability analysis of the toroidal clusters to establish the geometrical features that determine their stability against small amplitude nonuniform deformations.

General linear stability analysis decides the stability of an equilibrium state by whether an applied perturbation grows in amplitude or not from its initial value. The approach implemented in Chapter 4 is novel in that the stability is decided by the effect of the applied perturbations on the free energy of the body. Perturbations that decrease the free energy of the body grow in amplitude causing the body to become unstable while perturbations that increase the free energy of the body decay in amplitude. A cluster that does not climb the conical pillar cannot change its gravitational energy significantly, so free energy is determined by surface energy alone. Therefore, if the surface energy density γ is constant everywhere on the surface of the cluster, a perturbation that decreases the surface area of the body grows in amplitude.

A small amplitude sinusoidal spatial perturbation given by (4.2) is applied to the minor radius of an initially uniform toroidal cluster. The change of the surface

area as the cluster leaves its uniform configuration $\dot{S}(0)$ is calculated to determine its stability. The first uniform toroidal cluster defined by (4.3) remains linearly stable for the particular family of sinusoidal perturbations.

An alternate perturbed cluster shape is developed for which the inner surface of the cluster conforms to the conical pillar upon application of the sinusoidal perturbation as shown in Figure 4.6. For the alternate shape, $\dot{S}(0)$ is found to be zero providing no indication of the stability of the uniform toroidal shape.

From the experiments it is known that instabilities may develop in toroidal clusters that remain at the base of the chamber. It is reiterated that conclusion of stability under one particular perturbation is by no means exhaustive. However, the inability to form unstable configurations for arbitrary wave number of the applied perturbation led to the assumption that the surface energy density is not spatially constant over the surface of the cluster.

For the simple choice of $\gamma(\theta)$, both perturbed cluster shapes considered above are shown in Figures 4.8 and 4.10 to become unstable for the applied sinusoidal perturbation at various circumferential wave numbers. Precise stability criteria could not be determined as the exact function of the surface energy density is unknown. However, Figures 4.9 and 4.11 show that the stability of the toroidal clusters depend on their initial geometry, specifically on the ratio r_0/b_0, along with the wavenumber k of the applied sinusoidal perturbation.

These results also suggest that for the family of small amplitude sinusoidal perturbation growth of unstable fluctuations cannot occur unless the surface energy density is at least spatially nonuniform. It is acknowledged that the surface energy density can also vary with time as well as with other surface coordinates. There are many possible combinations of γ varying with θ, ϕ and t along with the possibility of applying another family of perturbing functions. Of these possible combinations, it may

be of interest to begin by observing the effects of implementing either $\gamma(t)$ or $\gamma(\theta, t)$ on the linear stability of the uniform torus configuration. It may also be worthwhile to observe the effects of a more complex perturbing functions applied to clusters for which γ is spatially constant over the surface.

The goal of Chapter 5 was to reproduce reported linear and nonlinear stability criteria of cylindrical bodies which evolve in shape due to surface diffusion. The Herring-Mullins transport equation (5.7) is used to describe the evolution in shape of the bodies.

For the linear stability analysis, a small amplitude sinusoidal spatial perturbation is applied to the radius of the uniform cylindrical surface and the governing equation is linearized. Figure 5.6 shows that applied perturbations with wavelengths less than the circumference of the initial uniform cylinder $2\pi r_0$ decay in amplitude. In contrast, Figure 5.7 shows that the converse is true, in that, for perturbations with wavelengths that exceed the circumference of the uniform cylinder the configuration is unstable. These results are in agreement with the generally accepted Rayleigh-type stability criteria (1878) and with the reported results of Nichols and Mullins (1965). Comparison of Figures 5.6 and 5.9 also reveals that the rate of the growth or decay of the perturbation amplitude increases for larger values of $|\lambda - 2\pi r_0|$ and decreases for smaller values.

Next a nonlinear stability analysis is conducted in which finite amplitude multi-harmonic perturbing shapes are assumed for initially cylindrical configurations. The initial perturbing functions and the boundary conditions are taken from the reported work of Coleman Falk and Moakher (1996). Even though our method of solving the governing partial differential equation is more robust than the finite element approach used by Coleman Falk and Moakher (1996), similar results are obtained. The numerical solutions of Figures 5.10 and 5.11 show that the amplitudes of the

perturbations initially decay very rapidly. Then, following a dormant period, the amplitudes again increase and may eventually cause the break up of the body into smaller discrete particles.

Plateau-Rayleigh type instabilities have also been observed in toroidal geometries and have only recently been experimentally studied by Pairam and Fernández-Neives (2009) and by McGraw et al (2010). Therefore, the stability analysis formulated in Chapter 5 may serve as a basis for a future study of the stability of the toroidal clusters or toroidal shapes beyond the range of linear behavior.

In Chapter 3 it was noted that when constructing models involving living matter there is added uncertainty of the governing natural laws. The introductory results of these models suggest that implementing basic physical principles yield significant details of complex phenomena. The role of mathematical modeling in the biological sciences is not only hindered by the complexity of the phenomena being investigated but also by the lack of material properties available. Quantitative experiments to determine material properties and qualitative experiments to analyze the behavior of living matter are therefore necessary. Also, as was attempted in Section 3.4.1, models aimed at extracting material properties are also essential in conjunction with the experimental work.

Given more time, the methods for extracting the surface energy density γ and surface mobility coefficient m_s, outlined in Section 3.4.1, would be revisited. Especially, the extraction method based on (3.38) which was found to be particularly sensitive to errors in the experimental data. In retrospect, the cross-sectional shape of the toroidal clusters tend to be more elliptical than circular. Therefore, by reformulating the model to use toroidal shapes with elliptical cross-sections may yield more accurate results for γ and m_s with the extraction method.

The models proposed that surface area reduction is a factor that influences cell

cluster reorganization. However, with regards to toroidal stability for instances in which γ is constant everywhere on the surface, cell cluster reorganization in three dimensions is rather influenced by surface energy reduction. This broadening of perspective accounts for surface properties of the cell cluster that vary with position over the surface as well as with time.

Overall, clusters with complex geometries wish to minimize their surface energy and would do so once there is an energetically feasible pathway. The model of the climbing process of the toroidal cluster shows that clusters of cells are willing to pay an energy penalty in order to minimize their surface energy. However, for scenarios in which the energy penalty for configurational changes that decrease the surface area becomes too much, that is for clusters with $\kappa = \kappa_{eq}$, alternative pathways are explored. As a result, clusters that remain in the annular trough at the base of the chamber are observed to develop localized thinning at one or more cross-sections around the axial circumference. The toroidal stability analysis reveals that the development of local deformations also results in reduction of the surface energy of the cluster.

Therefore, both phenomena occur as a result of the toroidal clusters trying to reduce their surface energy while conserving their volume. Depending on the geometry of the cluster and the conical pillar, this is achieved this by one of two methods, resulting in the climbing and localized thinning phenomena observed. The analysis then suggests that clusters that do not exhibit either of these phenomena either have self assembled into toroidal configurations that are already at local surface energy minimum or are constrained from following any configurational pathway that would result in the reduction of its surface energy.

Bibliography

Alberts, B., Johnson, A., Lewis, J., Raff, M., Roberts, K. and Walter, P. (2002), *Molecular biology of the cell*, 4 edn, New York: Garland Science. 2.1.3, 2.1.3, 2.1.3

Baluffi, R. W., Allen, S. M. and Carter, W. C. (2005), *Kinetics of Materials*, 3 edn, Wiley. 2.2.2

Baumann, N., Joseph, D. D., Mohr, P. and Renardy, Y. (1992), 'vortex rings of one fluid in another in free fall', *Physics of Fluids A* **4**, 567 – 580. 2.2.1

Berdichevsky, V. (2009), *Variational Principles of Continuum Mechanics: II. Applications (Interaction of Mechanics and Mathematics)*, 1 edn, Springer. 2.1.4

Cahn, J. W. and Taylor, J. E. (1994), 'Surface motion by surface diffusion', *Acta metallurgica et materialia* **42**(4), 1045–1063. 2.2.2, 5.1

Carter, W. C. and Glaeser, A. M. (1987), 'The morphological stability of continuous intergranular phases: Thermodynamic considerations', *Acta Metallurgica* **35**(1), 237– 245. 2.2.4, 4.1, 5

Choy, J.-H., Hackney, S. A. and Lee, J. K. (1995), 'Nonlinear stability analysis of the diffusional spheroidization of rods', *Journal of Applied Physics* **77**(11), 5647–5654. 2.2.3

Coleman, B. D., Falk, R. S. and Moakher, M. (1995), 'Stability of cylindrical bodies in the theory of surface diffusion', *Physica D: Nonlinear Phenomena* **89**(1-2), 123–135. 2.2.1, 5

Coleman, B. D., Falk, R. S. and Moakher, M. (1996), 'Space-time finite element methods for surface diffusion with applications to the theory of the stability of cylinders', *SIAM Journal on Scientific Computing* **17**(6), 1434–1448. 2.2.1, 2.2.3, 2.2.4, 5, 5.3, 5.3, 5.4, 5.5, 6

Dean, D. M., Napolitano, A. P., Youssef, J. and Morgan, J. R. (2007), 'Rods, tori, and honeycombs: the directed self-assembly of microtissues with prescribed microscale geometries', *FASEB J.* **21**(14), 4005–4012. (document), 1, 2.1, 2.1.1, 2.2, 3, 3.1, 6

Dill, K. A. and Bromberg, S. (2003), *Molecular driving forces*, 1 edn, Garland Science New York. 3.3

Eckhaus, W. (1965), *Studies in nonlinear stability theory.*, 1 edn, Springer–Tracts in Natural Philosophy. 2.2.3, 5.2

Eggers, J. (1997), 'Nonlinear dynamics and breakup of free-surface flows', *Reviews of Modern Physics* **69**(3), 865–930. 4

Elliott, C. M. and Garcke, H. (1997), 'Existence results for diffusive surface motion laws', *Advances in Mathematical Sciences and Applications* **7**, 467–490. 5.1

Freund, L. B. and Suresh, S. (2003), *Thin film materials*, 1 edn, Cambridge University Press. 2.1.4, 2.1.4, 3.3, 3.3, 5.1

Fried, I. (1979), *Numerical Solution of Differential Equations*, 1 edn, Academic Press, Inc. 2.1.4

Garcke, H., Ito, K. and Kohsaka, Y. (2008), 'Nonlinear Stability of Stationary Solutions for Surface Diffusion with Boundary Conditions', *SIAM Journal on Mathematical Analysis* **40**(2), 491–515. 5.5

Gibbs, W. (1875,1876), 'On the Equilibrium of Heterogeneous Substances', *Transactions of the Connecticut Academy* **III**, 108–248. 5.1

Glazier, J. A. and Graner, F. (1993), 'Simulation of the differential adhesion driven rearrangement of biological cells', *Physics Review E* **47**(3), 2128–2154. 2.1.1

Herring, C. (1951), 'Surface Tension as a Motivation for Sintering', *The Physics of Powder Metallurgy* **27**(2), 143–179. 2.2.2

Herring, C. (1953), *Structure and Properties of Solid Surfaces, edited by R. Gomer and C.S. Smith*, University of Chicago Press. 2.2.2, 5.1

Holtfreter, J. (1939), 'Gewebeaffinitut, ein Mittel der embryonalen Formbildung, Revised and reprinted in English in 1964', *Arch. Exp. Zellforsch. Besonders Gewebezucht* **23**, 169–209. 2.1.1

Job, G. and Herrmann, F. (2006), 'Chemical potential;a quantity in search of recognition', *European Journal of Physics* **27**(2), 353–371. 5.1

Ko, K., Arora, P., Lee, W. and McCulloch, C. (2000), 'Biochemical and functional characterization of intercellular adhesion and gap junctions in fibroblasts', *American Journal of Physiology- Cell Physiology* **279**(1), C147–57. 2.1.3

Krendel, M., Gloushankova, N. A., Bonder, E. M., Feder, H. H., Vasiliev, J. M. and Gelfand, I. M. (1999), 'Myosin-dependent contractile activity of the actin cytoskeleton modulates the spatial organization of cell–cell contacts in cultured epitheliocytes', *Proceedings of the National Academy of Sciences* **96**(17), 9666–9670. 2.1.3

Lymn, R. W. and Taylor, E. W. (1971), 'Mechanism of adenosine triphosphate hydrolysis by actomyosin', *Biochemistry* **10**(25), 4617 – 4624. 2.1.3

Marten, K., Shariff, K., Psarakos, S. and White, D. J. (1996), 'Ring Bubbles of Dolphins', *Scientific American* **August**(4), 82–87. 2.2.1

McGraw, J. D., Li, J., Tran, D. L., Shi, A. and Dalnoki–Veress, K. (2010), 'Plateau-Rayleigh instability in a torus: formation and breakup of a polymer ring', *Soft Matter* **6**(6), 1258–1262. 2.2.1, 4, 4.5, 6

Mullins, W. W. (1957), 'Theory of Thermal Grooving', *Journal of Applied Physics* **28**(3), 333–339. 2.2.2, 5.1, 5.2

Mullins, W. W. (2001), 'Capillarity-Induced Surface Morphologies', *Interface Science* **9**(1–2), 9–20. 2.2.2

Murray, J. D. (2003), *Mathematical Biology II: Spatial Models and Biomedical Applications*, 18 edn, Springer New York. 2.1.1, 3

Nichols, F. A. and Mullins, W. W. (1965), 'Morphological Changes of a Surface of Revolution due to Capillarity-Induced Surface Diffusion', *Journal of Applied Physics* **36**(6), 1826–1835. 2.2.1, 2.2.2, 4, 5, 5.2, 5.5, 6

Pairam, E. and Fernandez-Nieves, A. (2009), 'Generation and Stability of Toroidal Droplets in a Viscous Liquid', *Physics Review Letter* **102**(23), 234–501. 2.2.1, 4, 4.5, 6

Plateau, J. (1873), 'Statique experimentale et theorique des liquide soumis aux seules forces moleculaire', *Gauthier–Villars, Paris* **ii**, 450–495. 2.2.1

Porter, D. A. and Easterling, K. E. (2000), *Phase transformations in metals and alloys*, 2 edn, CRC. 3.3

Rasband, W. (1997–2010), 'ImageJ', http://rsb.info.nih.gov/ij/. 3.1

Rayleigh, L. (1878), 'On the Instability of Jets', *Proceedings London Mathematical Society*. 2.2.1, 6

Reddy, J. N. (2002), *Energy Principles and Variational Methods in Applied Mechanics*, 2 edn, John Wiley. 2.1.4

Renardy, Y., Popinet, S., Duchemin, L., Renardy, M., Zaleski, S., Josserand, C., Drumright-Clarke, M. A., Richard, D., Clanet, C. and Quere, D. (2003), 'Pyramidal and toroidal water drops after impact on a solid surface', *Journal of Fluid Mechanics* **484**, 69 – 83. 2.2.1

Santala, M. K. and Glaeser, A. M. (2006), 'Surface-Energy-Anisotropy-Induced Orientation Effects on Rayleigh Instabilities in Sapphire', *Surface Science* **600**(4), 782 – 792. 5.4, 5.5

Steinberg, M. S. (1962), 'On the mechanism of tissue reconstruction by dissociated Cells. III: Free Energy Relations and the Reorganisation of fused, heteronomic Tissue Fragments', *Proc. Nat. Acad. Sc* **48**, 1769–1776. 2.1.1

Steinberg, M. S. (1996), 'Adhesion in Development: An Historical Overview', *Developmental Biology* **180**(2), 377 – 388. 2.1.1

Townes, P. L. and Holtfreter, J. (1955), 'Directed movements and selective adhesion of embryonic amphibian cells', *Journal of Experimental Biology* **128**(1), 53–120. 2.1.1

Turing, A. M. (1952), 'The Chemical Basis of Morphogenesis', *Philosophical Transactions of the Royal Society* **B 237**, 37–72. 2.1.1

Vale, R. D. and Milligan, R. A. (2000), 'The way things move: looking under the hood of molecular motor proteins', *Science* **288**(5463), 88–95. 2.1.3

Vilenkin, A. J. and Brokman, A. (1997), 'Shape evolution by surface diffusion', *Physical Review B* **56**(15), 9871–9873. 2.2.2

Weatherburn, C. E. (1938), *An Introduction to Riemannian Geometry and the Tensor Calculus*, 1 edn, Cambridge University Press. 3.2.2

Whitesides, G. M. and Grzybowski, B. (2002), 'Self-Assembly at All Scales', *Science* **295**(5564), 2418–2421. 3

Youssef, J., Nurse, A., Freund, L. B. and Morgan, J. R. (2010), Cell Power: Quantification of the Froces Driving Self Assembly of 3D Micro-tissues. 3.2, 4